

REPORT DOCUMENTATION PAGE			<i>Form Approved</i> OMB No. 0704-0188	
Public reporting burden for this collection of information is estimated to average 1 hour per response, including the time for reviewing instructions, searching existing data sources, gathering and maintaining the data needed, and completing and reviewing the collection of information. Send comments regarding this burden estimate or any other aspect of this collection of information, including suggestions for reducing this burden, to Washington Headquarters Services, Directorate for Information Operations and Reports, 1215 Jefferson Davis Highway, Suite 1204, Arlington, VA 22202-4302, and to the Office of Management and Budget, Paperwork Reduction Project (0704-0188), Washington, DC 20503.				
1. AGENCY USE ONLY (Leave blank)		2. REPORT DATE 2 Jul 99	3. REPORT TYPE AND DATES COVERED THESIS	
4. TITLE AND SUBTITLE CLIMATOLOGY OF WAVE BREAKING AND MIXING IN THE NORTHERN HEMISPHERE SUMMER STRATOSPHERE			5. FUNDING NUMBERS	
6. AUTHOR(S) CAPT WAGNER RICHARD E				
7. PERFORMING ORGANIZATION NAME(S) AND ADDRESS(ES) TEXAS A&M UNIVERSITY			8. PERFORMING ORGANIZATION REPORT NUMBER	
9. SPONSORING/MONITORING AGENCY NAME(S) AND ADDRESS(ES) THE DEPARTMENT OF THE AIR FORCE AFIT/CIA, BLDG 125 2950 P STREET WPAFB OH 45433			10. SPONSORING/MONITORING AGENCY REPORT NUMBER FY99-153	
11. SUPPLEMENTARY NOTES				
12a. DISTRIBUTION AVAILABILITY STATEMENT Unlimited distribution In Accordance With AFI 35-205/AFIT Sup 1			12b. DISTRIBUTION CODE	
13. ABSTRACT (Maximum 200 words)				
14. SUBJECT TERMS			15. NUMBER OF PAGES 75	
			16. PRICE CODE	
17. SECURITY CLASSIFICATION OF REPORT	18. SECURITY CLASSIFICATION OF THIS PAGE	19. SECURITY CLASSIFICATION OF ABSTRACT	20. LIMITATION OF ABSTRACT	

**CLIMATOLOGY OF WAVE BREAKING AND MIXING
IN THE NORTHERN HEMISPHERE SUMMER
STRATOSPHERE**

A Thesis

by

RICHARD EMMETT WAGNER
Captain, USAF

86 pages

MASTER OF SCIENCE

Texas A&M University

1999

Major Subject: Meteorology

DTIC QUALITY INSPECTED 2

19990805 072

**CLIMATOLOGY OF WAVE BREAKING AND MIXING
IN THE NORTHERN HEMISPHERE SUMMER
STRATOSPHERE**

A Thesis

by

RICHARD EMMETT WAGNER

Submitted to the Office of Graduate Studies of
Texas A&M University
in partial fulfillment of the requirements for the degree of

MASTER OF SCIENCE

August 1999

Major Subject: Meteorology

CLIMATOLOGY OF WAVE BREAKING AND MIXING
IN THE NORTHERN HEMISPHERE SUMMER
STRATOSPHERE

A Thesis

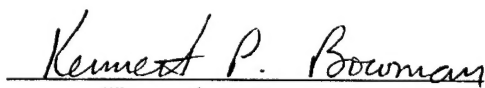
by

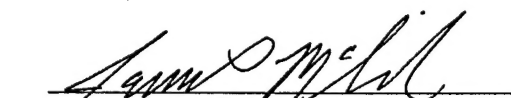
RICHARD EMMETT WAGNER

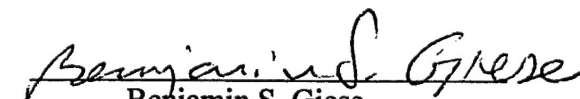
Submitted to Texas A&M University
in partial fulfillment of the requirements
for the degree of

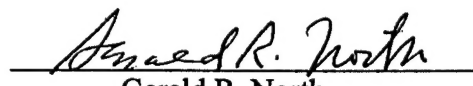
MASTER OF SCIENCE

Approved as to style and content by:


Kenneth P. Bowman
(Chair of Committee)


James P. McGuirk
(Member)


Benjamin S. Giese
(Member)


Gerald R. North
(Head of Department)

August 1999

Major Subject: Meteorology

ABSTRACT

Climatology of Wave Breaking and Mixing in the Northern

Hemisphere Summer Stratosphere. (August 1999)

Richard Emmett Wagner, B.S., Oregon State University

Chair of Advisory Committee: Dr. Kenneth P. Bowman

The cause of large zonal ozone variations observed by POAM II (Polar Ozone and Aerosol Measurement II) in the Northern Hemisphere (NH) summer stratosphere between 55°N-65°N and ~20-30 km is investigated using the United Kingdom Meteorological Office stratospheric data set with time-mean anomalies removed. This study tests the hypothesis from *Hoppel et al.* [1999] that breaking of westward-propagating planetary waves in the region of maximum ozone variance (RMV) induces substantial meridional transport which is responsible for the observed ozone variance.

EP-flux vectors show that wave activity propagates vertically from source regions in the lower midlatitude troposphere into the stratosphere and RMV during the NH summer. In the RMV, EP-flux divergence is clearly nonzero, which means the zonal-mean zonal flow is forced by waves in this region. Close examination of individual zonal wavenumber contributions to the climatological monthly-mean EP-flux divergence shows that wavenumbers 1-5 generally account for over 90% of the forcing of the zonal-mean flow in the RMV from June to August.

Forcing of the zonal-mean flow in the RMV is shown to be driven largely by dissipation of waves breaking at critical levels in the region. Power spectra clearly show that breaking waves in the RMV are westward-propagating waves 1-5.

EP flux divergence, meridional transport, and ozone variance in the RMV all decrease from June to July and increase in August. Amplitudes of zonal waves 1-5 do the same, further connecting the meridional transport (which induces the observed ozone variance) to breaking westward-propagating waves 1-5, lending credibility to the hypothesis in *Hoppel et al.* [1999].

DEDICATION

I would like to dedicate this thesis to my Lord God, my wife Karen, and my father. They were the three who encouraged me to do this, provided loving and steadfast support every step of the way, and will be the most proud when they see I got it done.

ACKNOWLEDGEMENTS

I owe many heartfelt thanks to my advisor, Dr. Kenneth P. Bowman, for keeping his promise and driving me to finish on time. Thanks also go out to Dr. James P. McGuirk and Dr. Benjamin S. Giese for serving on my committee and offering valuable advice and suggestions regarding this thesis. A special thanks to Karl W. Hoppel for providing insight and the necessary ozone gradient data to carry on a portion of the research he, Dr. Bowman, and Dr. Richard M. Bevilacqua initiated.

I am grateful to Dr. Kwang-Yul Kim for his kind and dedicated attention to helping me troubleshoot my EP-flux divergence and other IDL programs; Kyong-Hwan Seo for his friendship and patient mentorship during my struggles to digest *Charney and Drazin* [1961], EP-flux divergence, and traveling-wave power spectra; Gordon Carrie for providing me the fundamentals to start programming in IDL; and Neil Smith for teaching me to use UNIX and for fixing loads of computer server and ATM problems.

I would also like to thank Frank Leahy for his friendship, programming skills, and ability to look at scientific problems from a different angle; Mac Harris, my office mate, for grinding through the past two years with me, helping me troubleshoot programs, and being religiously devoted to the "hack break"; Michele Nordeen for her cat stories and teaching me the fundamentals of NCDF files; and Neil Sanger for tag-teaming Statistics 651 with me and encouraging me to renew my relationship with God. To my friends Dong-Heon Lee, Hye-Kyung Cho, Steve Nesbitt, Clay Blankenship, and Dave Wolff, thanks for all the hours dedicated to nailing down the fundamentals of atmospheric dynamics. Thanks to Greg Markowski for his help with late-night FTP/printer problems.

Finally, I would like to thank my wife, Karen, for her valuable graphic design inputs to this thesis in addition to her unlimited patience, love, understanding, and dedication to "keeping it all going" the past two years; my father for helping "turn on the light" of understanding when my first-semester dynamics and physics studies ground to a halt; and Kyle Bellue, his wife Luz, and my little brother Randy for shooting pool with me 'til dawn when things got a little too frantic.

This work was funded by the Air Force Institute of Technology, Wright Patterson Air Force Base, OH.

TABLE OF CONTENTS

	Page
ABSTRACT.....	iii
DEDICATION.....	iv
ACKNOWLEDGEMENTS.....	v
TABLE OF CONTENTS.....	vi
LIST OF FIGURES.....	vii
LIST OF TABLES	x
CHAPTER	
I INTRODUCTION AND BACKGROUND.....	1
1.1. Introduction.....	1
1.2. Previous Studies.....	6
1.3. Objectives	9
II DATA DESCRIPTION.....	10
III METHODS.....	29
3.1. Wave Amplitudes.....	29
3.2. Space-Time Power Spectra.....	29
3.3. Effective Meridional Diffusion Coefficients.....	30
3.4. Eliassen-Palm Flux and Flux Divergence	30
IV RESULTS.....	33
4.1. Characteristics of the Zonal-Mean u and T Fields in the NH Summer Stratosphere	33
4.2. Characteristics of Planetary-Scale and Medium-Scale Waves in the NH Summer Stratosphere.....	35
4.3. Meridional Mixing of Ozone in the NH Summer Stratosphere.....	49
4.4. EP-Flux and Flux Divergence in the NH Summer Stratosphere	52
V SUMMARY AND CONCLUSIONS	67
REFERENCES.....	73
VITA.....	75

LIST OF FIGURES

FIGURE		Page
1	Zonal-mean zonal wind for January 1998 and July 1998	3
2	Monthly-mean meridional wind amplitude for the sum of zonal waves 1-3 for January 1998 and July 1998	4
3	Altitude structure of zonal ozone standard deviation in the summertime stratosphere	5
4	Hovmoller plot of the unmodified UKMO unfiltered meridional wind For 1 June 1998 – 31 August 1998	12
5	Hovmoller plot of the modified UKMO unfiltered meridional wind For 1 June 1998 – 31 August 1998	13
6	Hovmoller plots of the unmodified UKMO meridional wind by zonal wavenumber for 1 June 1998 – 31 August 1998	14
7	Hovmoller plots of the modified UKMO meridional wind by zonal wavenumber for 1 June 1998 – 31 August 1998	17
8	Percent reduction in wave amplitude of the UKMO climatological monthly-mean meridional wind for June 1992-1998	21
9	Percent reduction in wave amplitude of the UKMO climatological monthly-mean meridional wind for July 1992-1998	23
10	Percent reduction in wave amplitude of the UKMO climatological monthly-mean meridional wind for August 1992-1998	25
11	UKMO climatological monthly-mean zonal-mean u and T meridional cross sections for June, July, and August 1992-1998 in the extratropical NH	34
12	UKMO climatological monthly-mean wave-amplitude meridional cross sections for individual waves 1-8 and combined waves 1-8 in terms of the meridional wind for June 1992-1998 in the extratropical NH	36
13	UKMO climatological monthly-mean wave-amplitude meridional cross sections for individual waves 1-8 and combined waves 1-8 in terms of the meridional wind for July 1992-1998 in the extratropical NH	38

FIGURE		Page
14	UKMO climatological monthly-mean wave-amplitude meridional cross sections for individual waves 1-8 and combined waves 1-8 in terms of the meridional wind for August 1992-1998 in the extratropical NH	40
15	Climatological monthly-mean v -amplitude plotted as a function of zonal wavenumber	44
16	Space-time power spectra of the climatological monthly-mean meridional wind for June, July, and August 1992-1998	46
17	Climatological monthly-mean meridional diffusivity and zonal-mean zonal wind cross sections for the extratropical NH summer 1992-1998.	48
18	Climatological monthly-mean meridional diffusivities meridionally averaged over the latitudinal width of the RMV for June, July, and August 1992-1998	50
19	Climatological monthly-mean scaled EP-flux and flux divergence for June 1992-1998 in the extratropical NH	53
20	Climatological monthly-mean scaled EP-flux and flux divergence for July 1992-1998 in the extratropical NH	54
21	Climatological monthly-mean scaled EP-flux and flux divergence for August 1992-1998 in the extratropical NH	55
22	Climatological monthly-mean total scaled EP-flux divergence meridionally averaged over the latitudinal width of the RMV for June, July, and August 1992-1998	56
23	Climatological monthly-mean scaled EP-flux divergence meridionally averaged over the latitudinal width of the RMV for June 1992-1998	58
24	Climatological monthly-mean scaled EP-flux divergence meridionally averaged over the latitudinal width of the RMV for July 1992-1998	59
25	Climatological monthly-mean scaled EP-flux divergence meridionally averaged over the latitudinal width of the RMV for August 1992-1998.	60
26	Absolute value of scaled EP-flux divergence in the middle stratosphere plotted on a \log_{10} scale with a linear fit for June, July, and August 1992-1998	65

FIGURE		Page
27	Composite of Figure 26 highlighting the decrease in negative D from June to July and subsequent increase in August in the lower half of the RMV	66
28	Location of particle tracers (initialized on 1 July 1996) around latitude circle at 5-day intervals in NH	70
29	Plot of MLS ozone vs. latitude on potential temperature levels for NH summer 1994	72

LIST OF TABLES

TABLE		Page
1	Standard UARS pressure levels converted to equivalent $\log p$ and potential temperature levels	11
2	Range of percent reduction in wave amplitudes of the climatological monthly-mean UKMO meridional wind resulting from removal of seasonal time-means	28
3	Range of climatological monthly-mean v amplitudes in the RMV ...	43
4	Percent contribution by wavenumber to the total climatological monthly-mean scaled EP-flux divergence for June, July, and August 1992-1998	61
5	Climatological monthly-mean scaled EP-flux divergence by zonal wavenumber for June, July, and August 1992-1998	62

CHAPTER I

INTRODUCTION AND BACKGROUND

1.1. Introduction

In the wintertime Northern Hemisphere (NH) extratropical stratosphere (December-February), the zonal-mean zonal winds are westerly throughout the layer, increasing with altitude into the polar-night jet (Figure 1, top). In the summertime NH extratropical stratosphere (June-August), on the other hand, the zonal-mean zonal winds are predominantly easterly with only a shallow layer of westerlies below roughly 20 km (Figure 1, bottom).

The planetary-scale wave-characteristics of the stratosphere are also very different in the two seasons. In the winter, planetary wave amplitudes are large, while summer wave amplitudes are generally weak. Figure 2 illustrates this seasonal variation for January and July 1998. Wave amplitudes are plotted in terms of the meridional wind (v) for the sum of zonal waves 1–3.

Comparing Figure 2 to Figure 1, large amplitude waves can readily be seen in regions of westerly zonal-mean zonal flow in both January and July. However, in the summertime stratospheric easterlies (Figure 2, bottom), large amplitude waves are conspicuously absent.

These observations are consistent with *Charney and Drazin* [1961], who showed that the summertime easterly zonal-mean flow, \bar{u} , in the upper stratosphere effectively prevents vertical propagation of stationary planetary-scale waves. The Charney-Drazin theorem states that only waves satisfying the relationship

$$0 < \bar{u} - c < \bar{u}_c \quad (1)$$

(where c is the intrinsic phase speed of the wave) can propagate vertically (details below). That is, the Doppler-shifted phase speed of the wave, $\bar{u} - c$, must be positive (eastward) but less than a critical value, \bar{u}_c . Stationary waves ($c = 0$), for example, can

The journal model for this thesis is the *Journal of Geophysical Research*.

only propagate vertically into regions where the winds are westerly and less than \bar{u}_c . During the summer, stationary planetary-scale waves can propagate only into the lower stratosphere. Above the zero wind line, the waves become evanescent with height. Traveling waves can propagate vertically into easterly winds only if they have zonal phase speeds faster (more negative) than \bar{u} . There is evidence of westward-propagating waves in the summer stratosphere [Muench, 1968].

The relative weakness of large-scale waves in the summer stratosphere suggests that most atmospheric quantities should be nearly zonally symmetric. Hoppel *et al.* [1999], in their study of NH summer ozone variability observed by POAM II (Polar Ozone and Aerosol Measurement II), however, showed considerable zonal variations of ozone in the lower stratosphere between 55°-65°N latitude and ~20-30 km (Figure 3). They described the zonal ozone variance as “persistent large-scale ozone patterns that move approximately with the zonal-mean wind.” Their trajectory calculations indicated that the zonal variance is a result of meridional transport. Hoppel *et al.* [1999] further suggested that this meridional transport might be caused by breaking of westward-propagating planetary-scale waves at critical levels in the stratospheric easterlies. The waves would become evanescent above their critical levels, consistent with the theory of Charney and Drazin [1961]. They suggested that these waves have sufficient amplitude in the lower stratospheric easterlies to produce weak critical layers and substantial meridional transport.

This study investigates the hypothesis in Hoppel *et al.* [1999] that breaking of stationary or westward-propagating planetary-scale waves in the NH summertime stratospheric easterlies induces the meridional transport that is responsible for the large zonal ozone variance observed by POAM II in the region between 55°-65°N and ~20-30 km (hereafter called the RMV, region of maximum ozone variance).

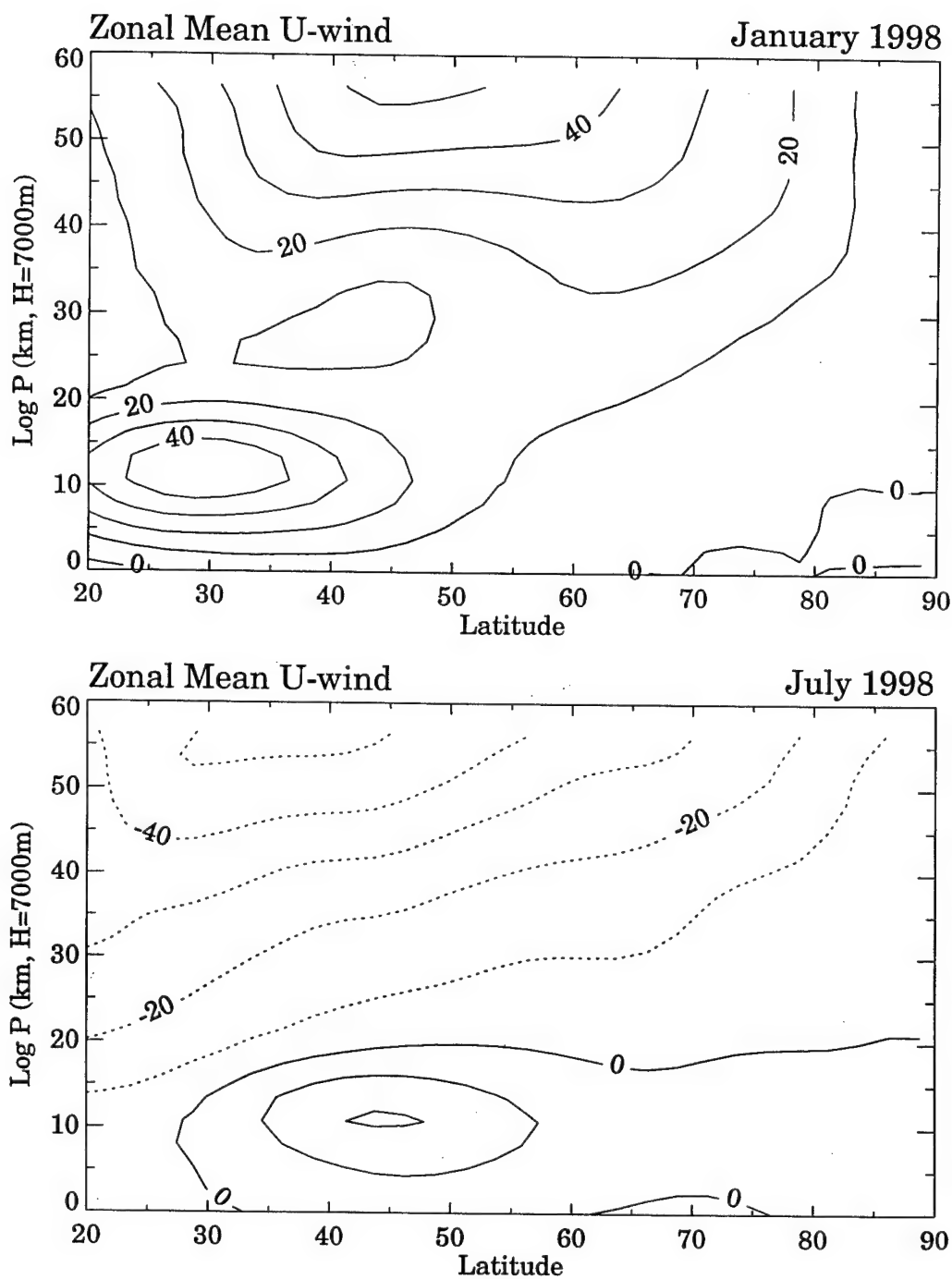


Figure 1. Zonal-mean zonal wind (m s^{-1}) for January 1998 and July 1998. Solid contours indicate westerly flow whereas dotted contours indicate easterlies.

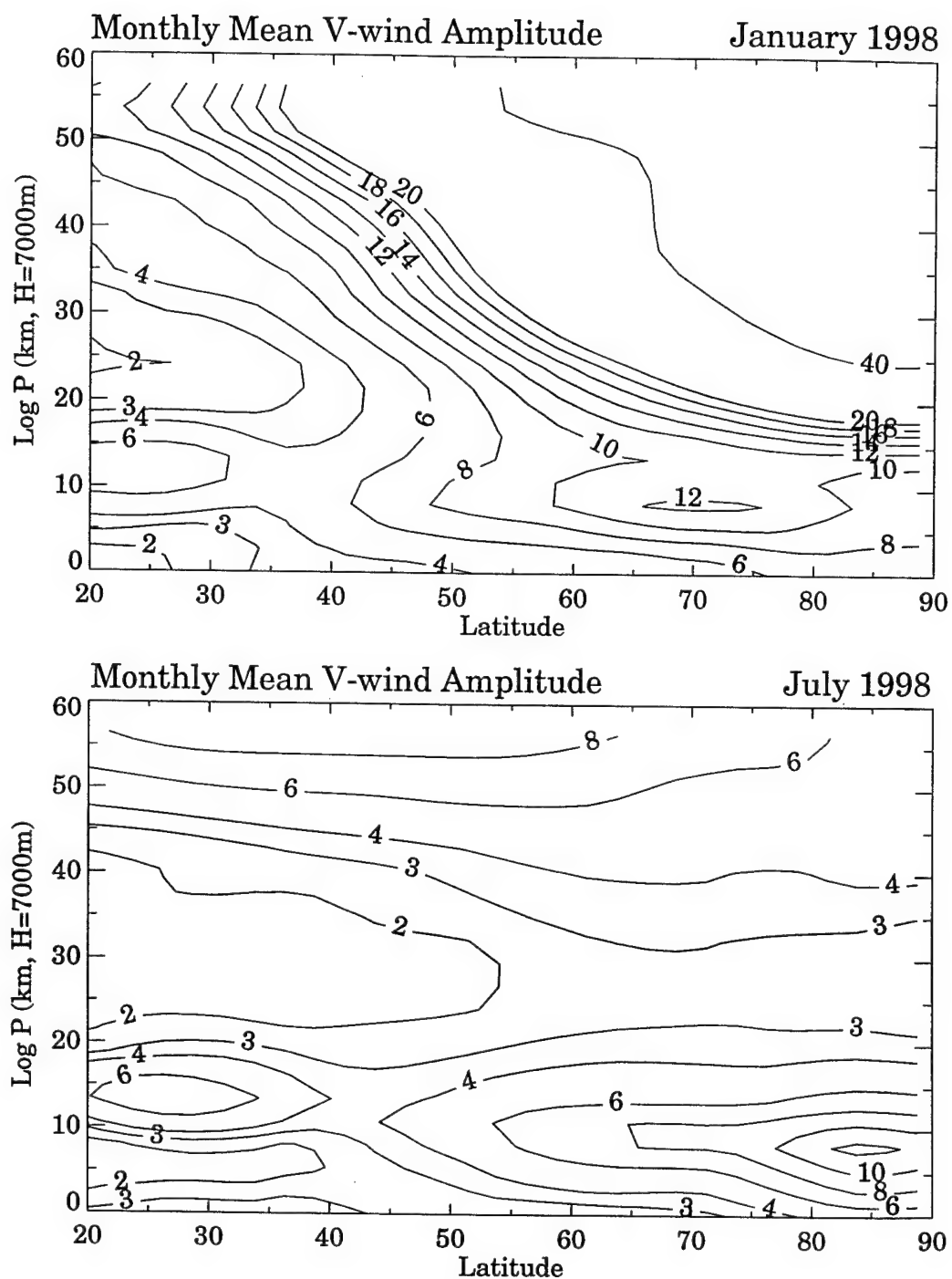


Figure 2. Monthly-mean meridional wind amplitude (m s^{-1}) for the sum of zonal waves 1-3 for January 1998 and July 1998.

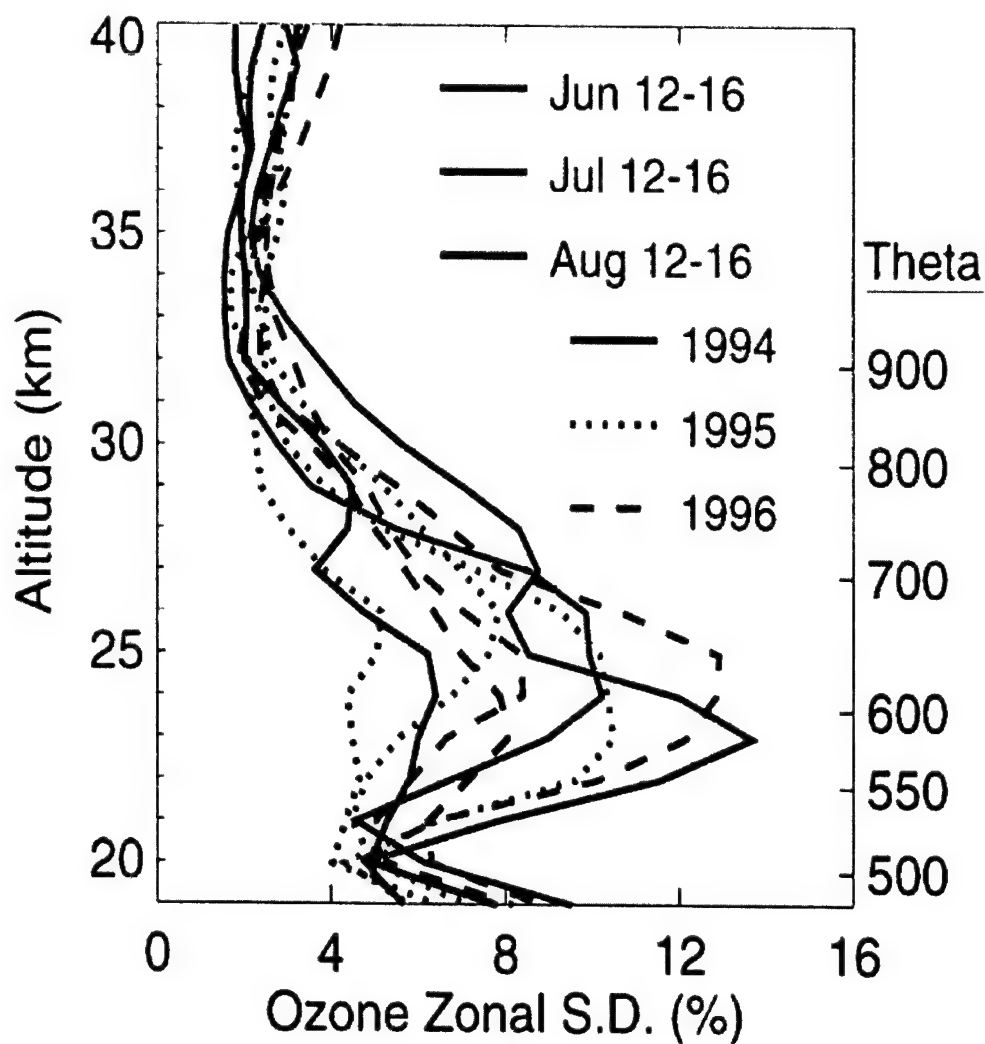


Figure 3. Altitude structure of zonal ozone standard deviation in the summertime stratosphere. Altitude profiles are shown for the middle of June, July, and August for all three years. Ozone variance is highest in the 20-30 km (~57-14 hPa) altitude region (from Hoppel *et al.* [1999], used by permission).

1.2. Previous Studies

A number of studies have focused on trying to understand the possible sources and lifecycle characteristics of traveling planetary waves in the summertime stratosphere. *Charney and Drazin* [1961] showed that propagation of planetary-scale wave disturbances from the troposphere into the stratosphere is analogous to the transmission of electromagnetic radiation in heterogeneous media. Using this analogy, they determined that the effective index of refraction for planetary waves depends primarily on the distribution of the zonal-mean zonal wind with height. In the case of a planetary wave that propagates both vertically and zonally (e.g., a westward and vertically propagating Rossby wave), the criteria for the wave to be able to propagate vertically is

$$0 < \bar{u} - c < \bar{u}_c \equiv \beta / \{ (k^2 + l^2) + f_0^2 / 4 H^2 N^2 \}, \quad (2)$$

where \bar{u} is the zonal-mean zonal wind, c is the intrinsic phase speed of the wave, and \bar{u}_c is the critical velocity or limiting speed beyond which the wave can no longer propagate in the vertical [Andrews *et al.*, 1987]. The Doppler-shifted phase speed ($\bar{u} - c$) must be greater than zero and less than the limiting speed, \bar{u}_c , which is dependent upon the static stability (N^2), Coriolis parameter (f_0), $\beta \equiv \partial f / \partial y$, scale height (H), and the zonal and meridional wavenumbers (k, l) of the wave in question. It is particularly important to note the dependence of \bar{u}_c on k and l . The smaller the wavenumber, the larger the limiting speed of the wave. Since zonal wind speeds in the stratosphere generally increase with height, planetary-scale waves (wavenumbers 1-3) can propagate higher into the stratosphere than smaller-scale waves because \bar{u}_c is larger for the planetary waves. Most of the smaller-scale waves (wavenumber ≥ 4) have such small \bar{u}_c that $\bar{u} - c > \bar{u}_c$ before they enter the stratosphere and so become evanescent (trapped). This is the reason for the dominance of planetary-scale waves in the winter stratosphere.

For example, referring back to Figure 1 (top panel), the wintertime stratospheric zonal-mean zonal wind is westerly ($\bar{u} > 0$). Therefore, all westward-propagating ($c < 0$) planetary waves can propagate vertically into the stratosphere until they reach their respective critical levels (where $\bar{u} - c = 0$) or limiting levels (where $\bar{u} - c = \bar{u}_c$), if such levels exist. Beyond these points the waves become evanescent.

Figure 1 (bottom) shows the summertime stratospheric zonal-mean zonal wind to be easterly above roughly 20 km (~ 57 hPa). In this case $\bar{u} < 0$. Therefore, only planetary-scale waves that propagate westward more rapidly than the zonal-mean zonal current will be able to propagate vertically into the stratospheric easterlies. All other waves will become evanescent in the stratospheric easterlies.

For the purpose of this study, the most important conclusion drawn by *Charney and Drazin* [1961] is that the summertime easterly zonal-mean zonal flow in the upper stratosphere effectively prevents stationary or quasi-stationary planetary-scale waves from propagating vertically into the upper stratosphere. However, stationary planetary-scale waves can still exist in the lower stratosphere in the westerlies below the zero-wind line.

Muench [1968] used high-level balloon data spanning the region from eastern Asia across North America to western Europe to investigate disturbances in the summertime stratosphere from 27-36 km. He discovered traveling planetary waves at these altitudes (in the stratospheric easterlies), propagating westward at 30° of longitude per day. The waves were detected as periodic oscillations in the u -wind component, with amplitudes up to 4 m s^{-1} extending from 25° - 45° N and from 25-45 km in the vertical. The cause of these westward-propagating long waves is unknown but *Muench* [1968] speculated that they receive their energy from outside the stratosphere.

Analysis of ozone observations from the Limb Infrared Monitor of the Stratosphere (LIMS) [*Miles et al.*, 1994], Microwave Limb Sounder (MLS) [*Elson et al.*, 1994], and Halogen Occultation Experiment (HALOE) [*Park and Russell*, 1994] revealed that the largest stratospheric ozone variability is confined to a distinct region between 20 km and 30 km in altitude, and 50° - 75° in latitude during the NH and SH summers. Several hypotheses have been proposed for the source of the summertime stratospheric zonal ozone variation:

Hess and Holton [1985] used balloon observations of long-lived tracers to suggest that patterns of high and low tracer values were created during the spring breakdown of the anticyclonic circumpolar vortex. The authors proposed that the tracer values were frozen into the mean summertime flow.

Randel [1993] documented westward-propagating Rossby normal-mode planetary waves in stratospheric ozone data using Solar Backscatter Ultraviolet (SBUV) satellite measurements. His "ozone waves" had maxima in high latitudes of the middle stratosphere (due to transport) and over midlatitudes in the upper stratosphere (due to photochemistry). These global modes were observed to occasionally exhibit large amplitudes in the summertime stratosphere suggesting that they may contribute substantially to the overall variance there. He concluded that constituent oscillations associated with normal modes provide a mechanism for summertime stratospheric variability that complements the mechanism proposed in *Hess and Holton* [1985].

Miles et al. [1994] concluded that wavenumber 1 ozone variance in the SH summer was at least partly dynamical in origin, forced by stationary and westward propagating wavenumber 1 disturbances. In *Park and Russell* [1994], observed HALOE summer ozone variance was found to be anti-correlated with the variations of HCl and NO, but uncorrelated with the tracer species HF and CH₄. This observation suggests that the ozone patterns may be caused by local NO_x chemistry. *Luo et al.* [1997] showed that these species are not very sensitive indicators of isentropic transport by virtue of the fact that their mixing ratio isopleths are very nearly parallel to isentropes poleward of 60°N during the summer. *Natarajan and Callis* [1997] and *Luo et al.* [1997] analyzed selected days of HALOE data during August in the NH and found that regions of high and low ozone mixing ratio correlate reasonably well with the meridional transport histories obtained by trajectory calculations.

Hoppel et al. [1999] analyzed observations of ozone variance obtained by POAM II for the 1994, 1995, and 1996 NH summers. POAM II provides a continuous time series of measurements with high vertical resolution in a narrow latitude band, 55°-65°N, near the center of the region of maximum ozone variability observed by LIMS, MLS, and HALOE (50°-75°N). Like the previous studies, *Hoppel et al.* [1999] also found considerable zonal variations of ozone in the lower stratosphere between ~20-30 km. They described the zonal variance as "persistent large-scale ozone patterns that move approximately with the zonal-mean wind." Trajectory calculations indicated that the zonal variance was a result of meridional transport. Effective meridional diffusivity

(K_{yy}) calculations [Bowman, 1996] indicated significant meridional dispersion and mixing of air parcels in the stratospheric easterlies between the 550 K and 800 K isentropic surfaces (approximately 21-29 km). Examination of the zonal-wave amplitudes and phases of UKMO winds corrected for stationary anomalies [Bowman, 1998] revealed that westward-propagating, large-scale waves (zonal wavenumbers 1-5) were present intermittently throughout the NH summer. To determine if these waves played any role at all in causing the zonal ozone variance, Hoppel *et al.* [1999] filtered all westward-propagating wave-modes from the UKMO wind field. This caused the meridional mixing, which was present in their previous K_{yy} calculations (using unfiltered UKMO winds), to disappear almost entirely. Therefore, Hoppel *et al.* [1999] hypothesized that the meridional transport inducing the zonal ozone variance was caused by breaking of these westward-propagating planetary-scale waves at critical levels in the easterlies. The waves would become evanescent above their critical levels, consistent with the theory of Charney and Drazin [1961]. Though evanescent, these waves would have sufficient amplitude in the lower stratospheric easterlies to produce weak critical layers and substantial meridional transport.

1.3. Objectives

The primary goal of this study is to analyze the structure and characteristics of the planetary-scale waves in the summertime stratosphere and to determine the relationship between these waves and the zonal ozone variability observed by POAM II in the NH summer stratosphere.

CHAPTER II

DATA DESCRIPTION

Dynamical data are taken from the United Kingdom Meteorological Office (UKMO) stratospheric data set. The UKMO data are 3-dimensional assimilated fields provided by the UKMO as their contribution to the Upper Atmosphere Research Satellite (UARS) project. The data spans the period from 1 Nov 1991 to 30 Nov 1998 and so includes 7 NH summers (June-August).

The data set consists of wind fields of zonal wind (u), meridional wind (v), and omega (ω). It also includes thermodynamic fields of temperature (T) and geopotential height (Z). All fields are contained on the 22 standard UARS pressure levels listed in Table 1. The UARS pressure levels extend from 1000 hPa to 0.316 hPa [at intervals of approximately 2.69 km of $\log p$ height ($H = 7000$ m)] and on 2.5° latitude by 3.75° longitude global staggered grids. The latitude grid for the thermodynamic variables (T, Z) extends from -90° to 90° at intervals of 2.5° . The longitude grid for the thermodynamic variables extends from 0° to 356.25° at intervals of 3.75° . The latitude grid for the wind variables (u, v, ω) extends from -88.75° to 88.75° at intervals of 2.5° . The longitude grid for the wind variables extends from 1.875° to 358.125° at intervals of 3.75° .

The analyses are generated through continuous assimilation of operational meteorological observations (e.g., NOAA satellite temperature profiles and radiosonde data) into a general circulation model (GCM) using the Analysis Correction Data Assimilation Scheme [Lorenc *et al.*, 1991]. The data assimilation system is a development of the scheme used at the UKMO for operational weather forecasting, which has been extended to cover the stratosphere. For further details, see Swinbank and O'Neill [1994]. The primary product is a daily analysis at 1200 UTC.

Bowman *et al.* [1998] showed that a number of NH meteorological data sets, including the UKMO data set, contain stationary anomalies in the summertime stratosphere that are inconsistent with Charney and Drazin [1961] in that stationary

Table 1. Standard UARS pressure levels converted to equivalent $\log p$ and potential temperature (θ) levels. Values of θ are estimated at 60°N for the NH summer. Shaded pressure levels represent the RMV.

p (hPa)	log p (km)	Theta (K)
0.32	56.4	2640
0.46	53.7	2390
0.68	51.0	2150
1.00	48.4	1960
1.47	45.6	1770
2.15	42.9	1550
3.16	40.3	1370
4.64	37.6	1190
6.81	34.9	1040
10.00	32.2	900
14.70	29.6	800
21.50	26.9	700
31.60	24.2	610
46.40	21.5	550
68.10	18.8	490
100.00	16.1	440
147.00	13.4	390
215.00	10.7	350
316.00	8.1	330
464.00	5.4	315
681.00	2.7	300
1000.00	0	< 300

waves should be very weak (evanescent) in easterly-wind regimes. Figure 4 is a Hovmoller plot of the NH summertime UKMO total (unfiltered) v field at approximately 27 km and 61.25°N latitude (in the middle of the RMV, well above the zero-wind line and in the summertime stratospheric easterlies). The stationary wave anomalies are clearly visible as vertical structures that do not change longitude position for the duration of the NH summer. Because these stationary (or time-mean) anomalies are large with respect to the relatively weak flow in the summertime stratosphere, they can have

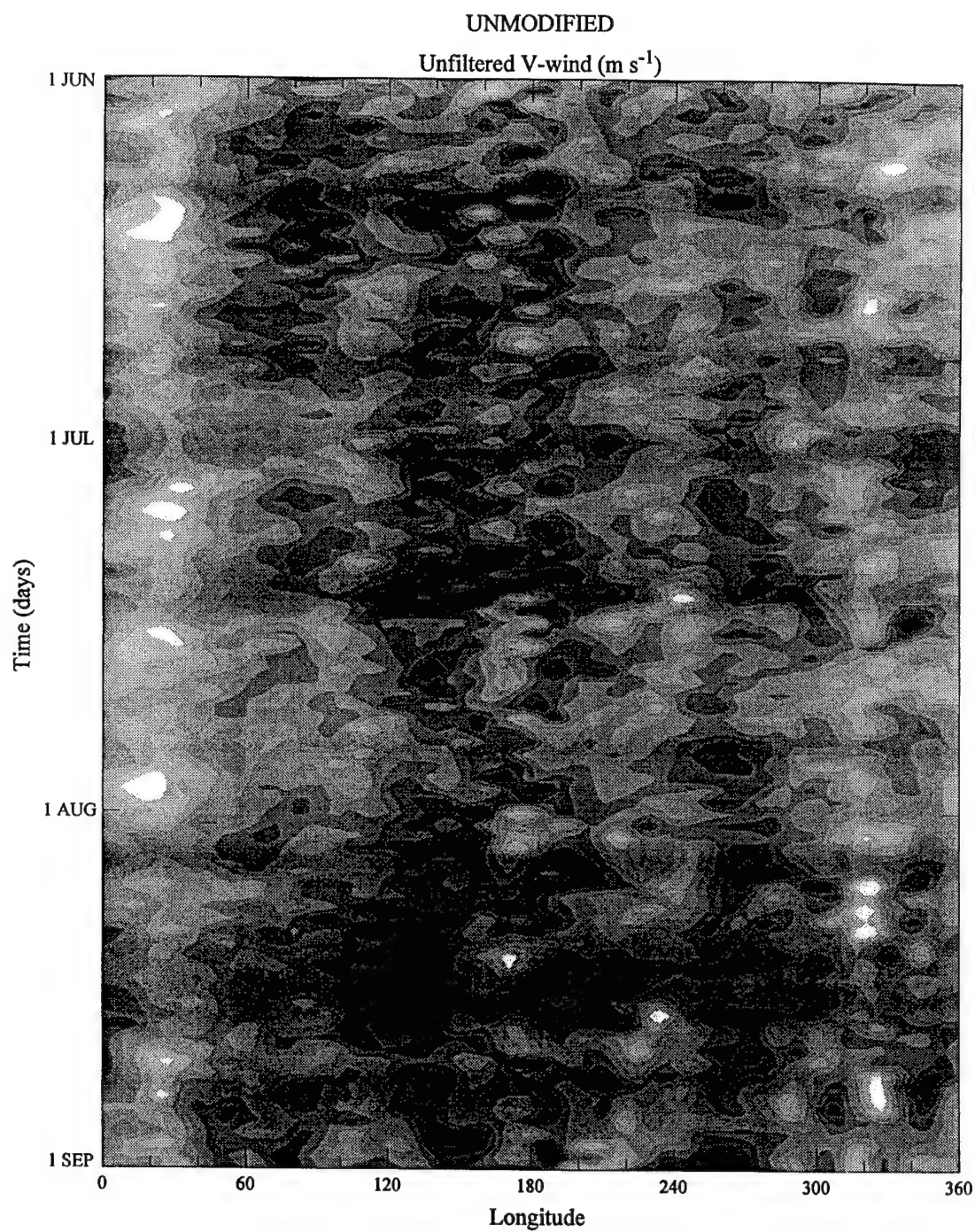


Figure 4. Hovmoller plot of the unmodified UKMO unfiltered meridional wind (v) for 1 June 1998 - 31 August 1998. Pressure level = 21.5 hPa, Latitude = 61.25°N .

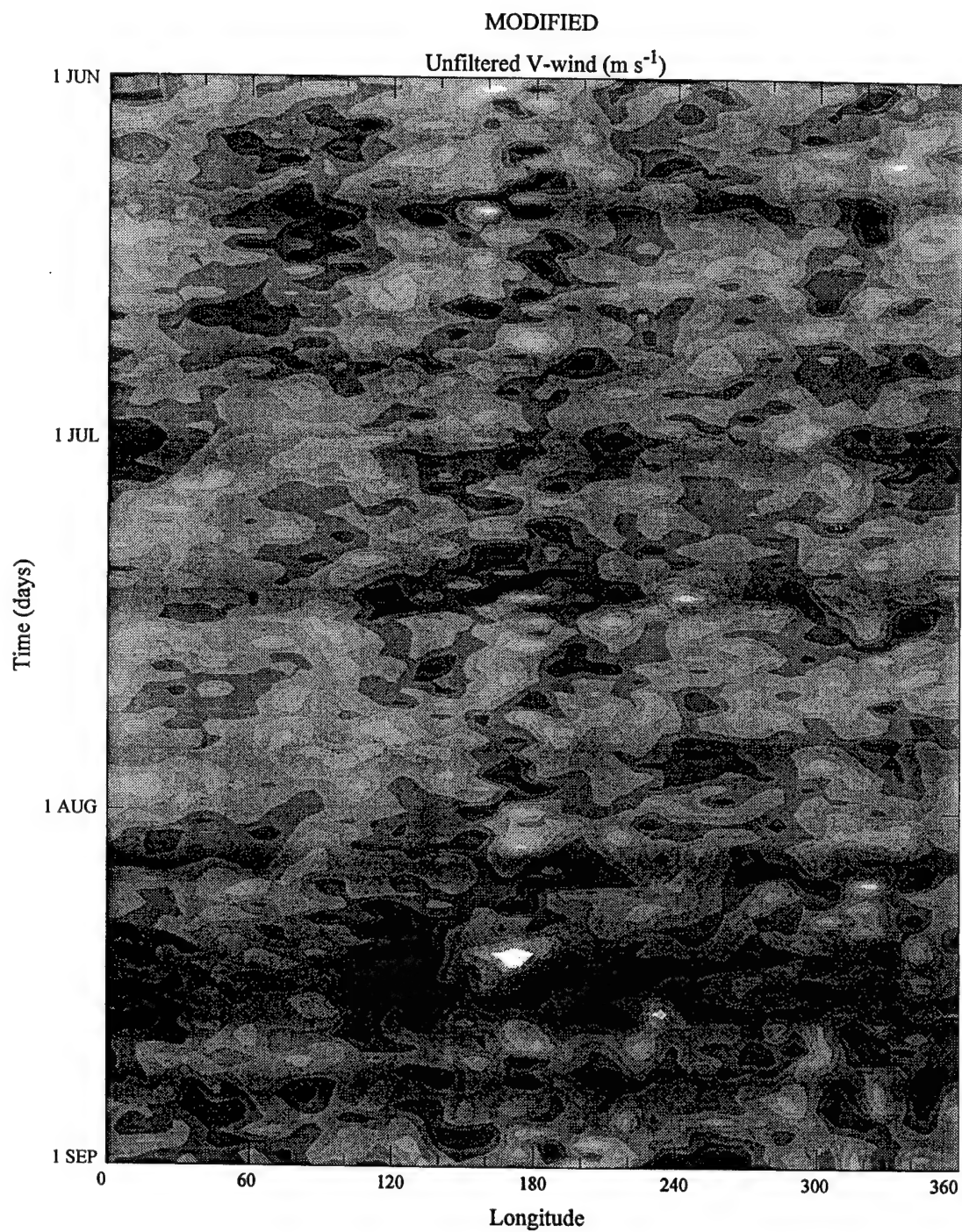


Figure 5. Hovmoller plot of the modified UKMO unfiltered meridional wind (v) for 1 June 1998 - 31 August 1998. Pressure level = 21.5 hPa, Latitude = 61.25°N.

UNMODIFIED

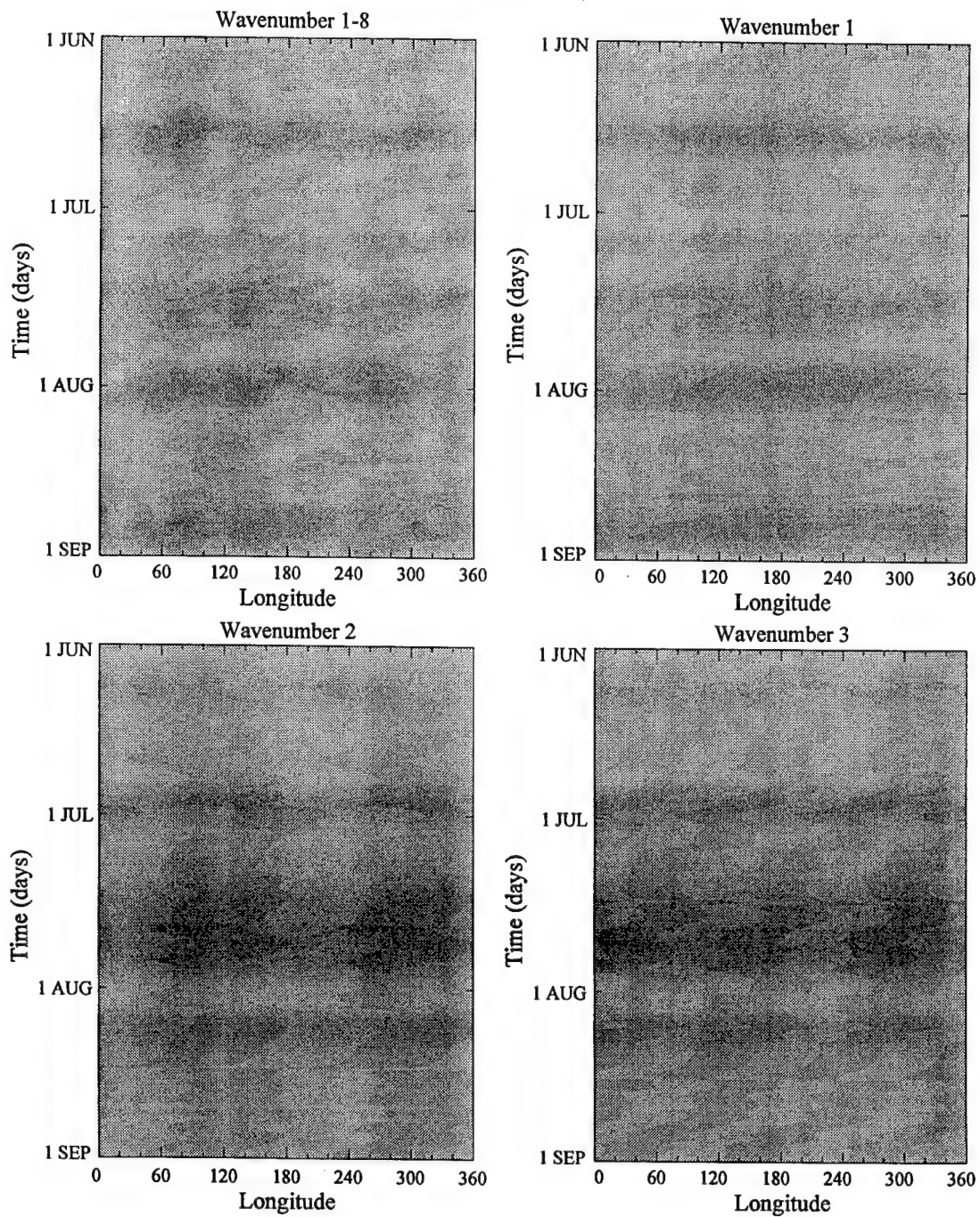


Figure 6. Hovmöller plots of the unmodified UKMO meridional wind (v) by zonal wavenumber for 1 June 1998 - 31 August 1998. Pressure level = 21.5 hPa, Latitude = 61.25°N.

UNMODIFIED

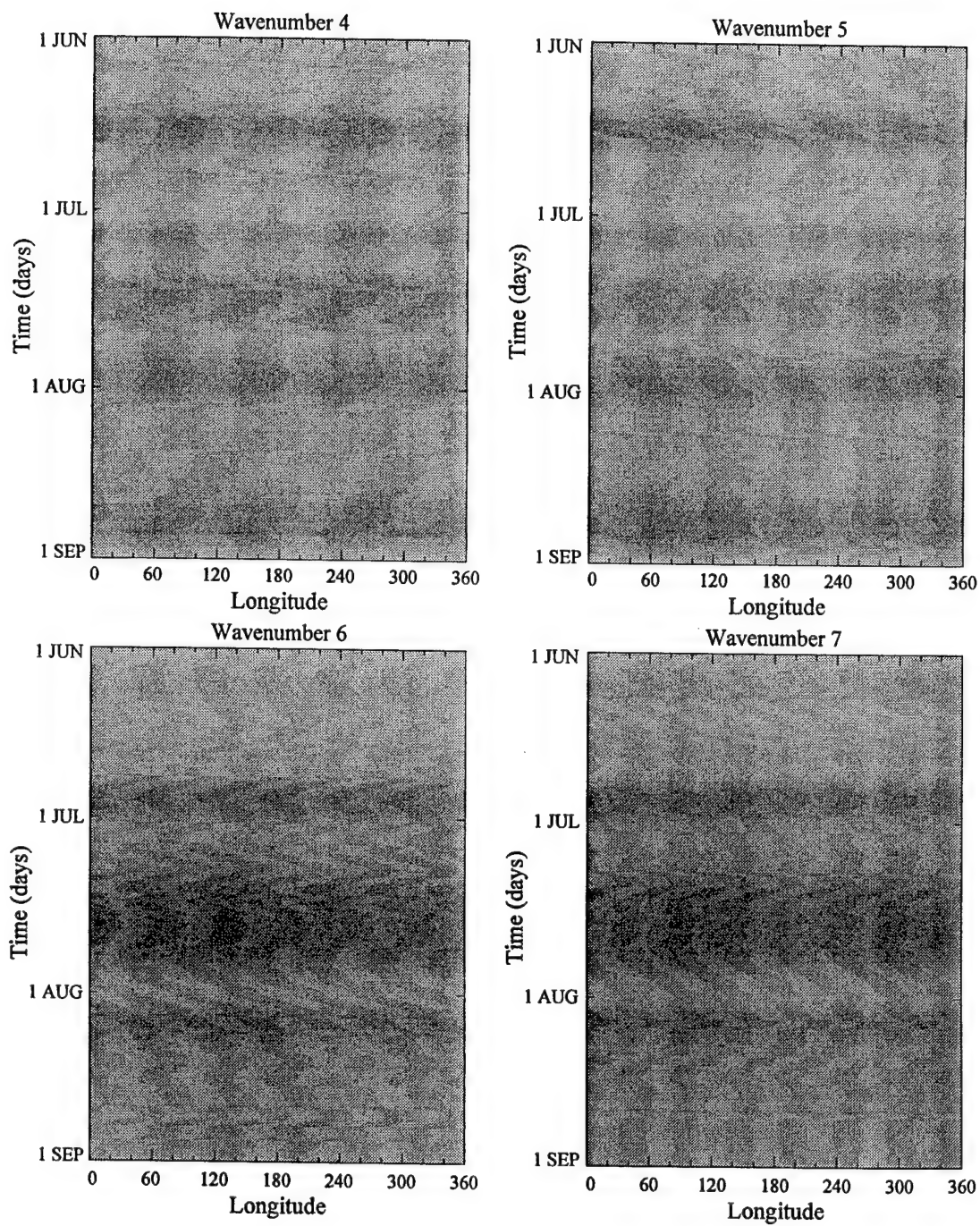


Figure 6. Continued.

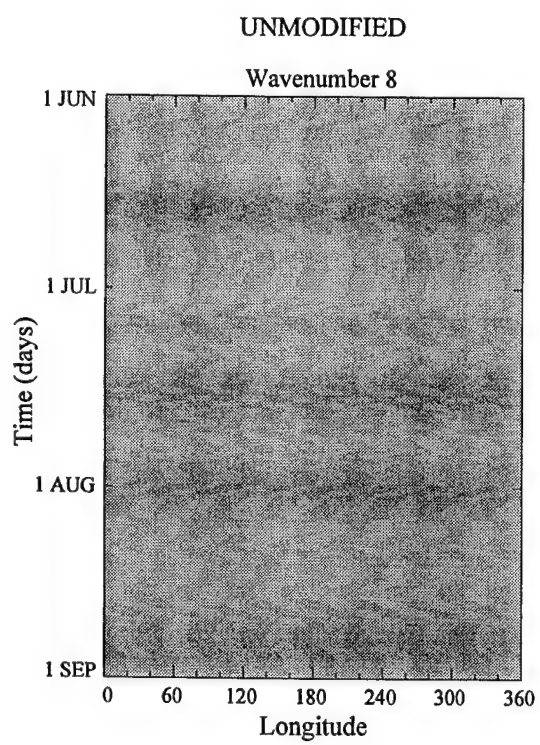


Figure 6. Continued.

MODIFIED

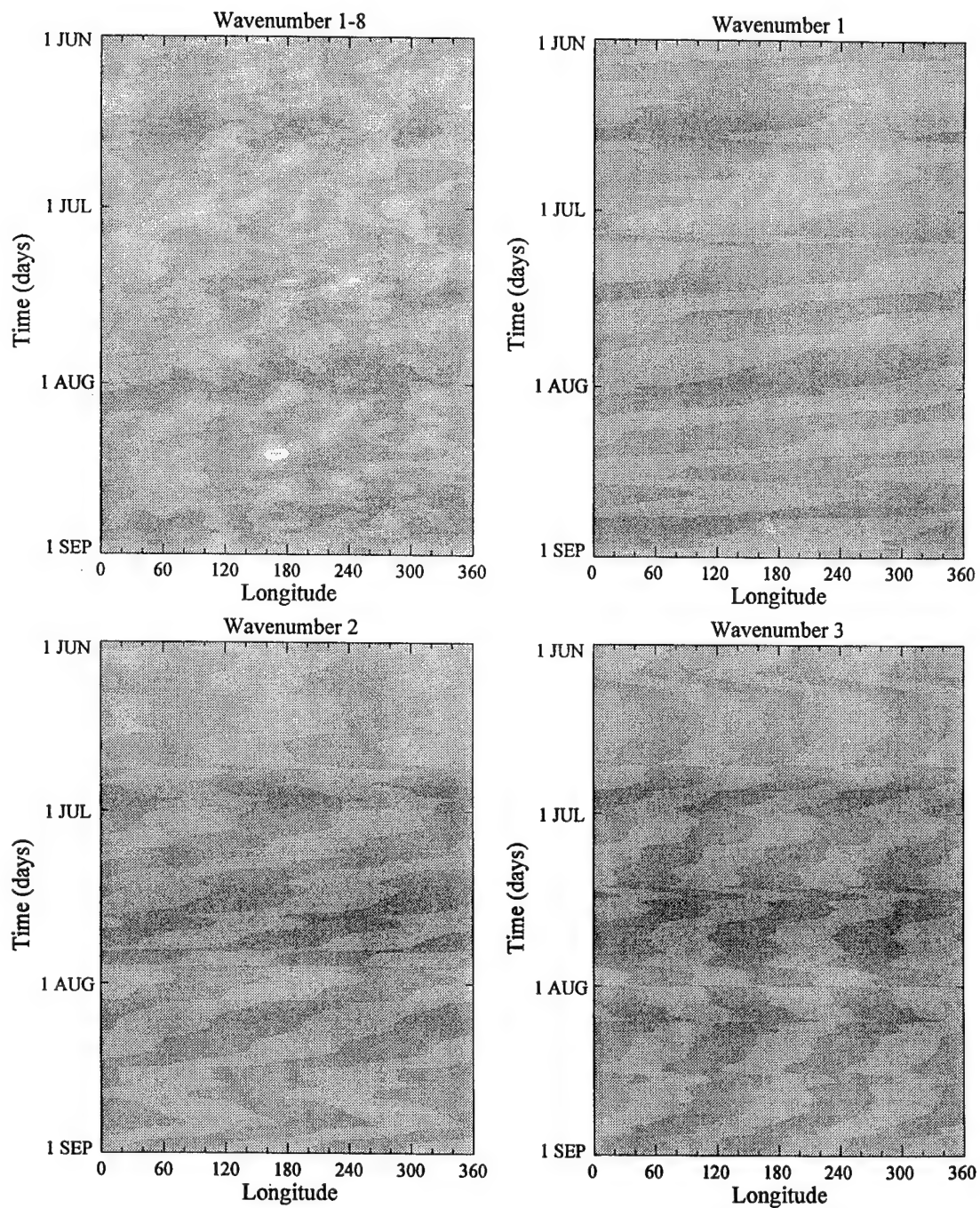
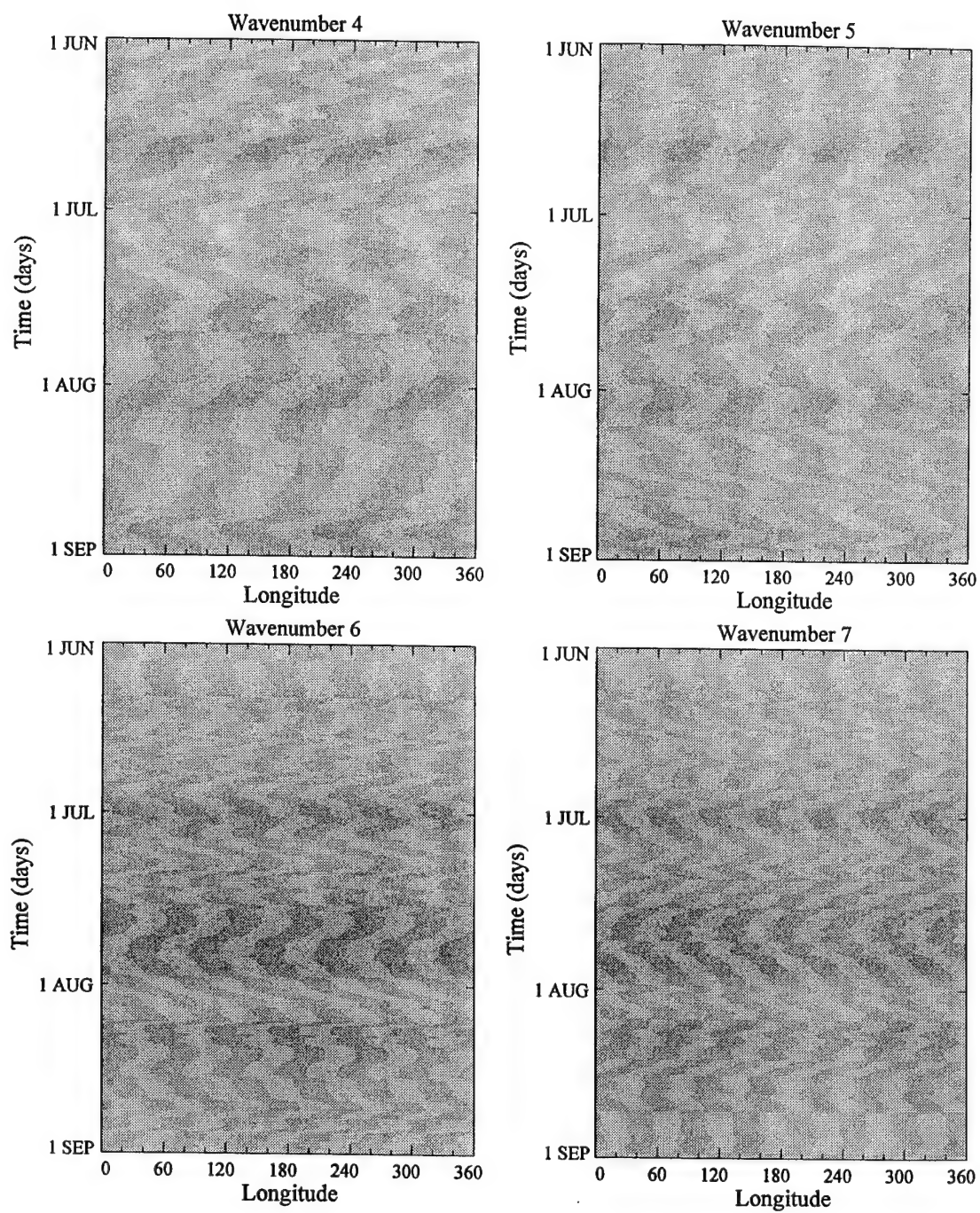


Figure 7. Hovmöller plots of the modified UKMO meridional wind (v) by zonal wavenumber for 1 June 1998 - 31 August 1998. Pressure level = 21.5 hPa, Latitude = 61.25°N.

MODIFIED

**Figure 7. Continued.**

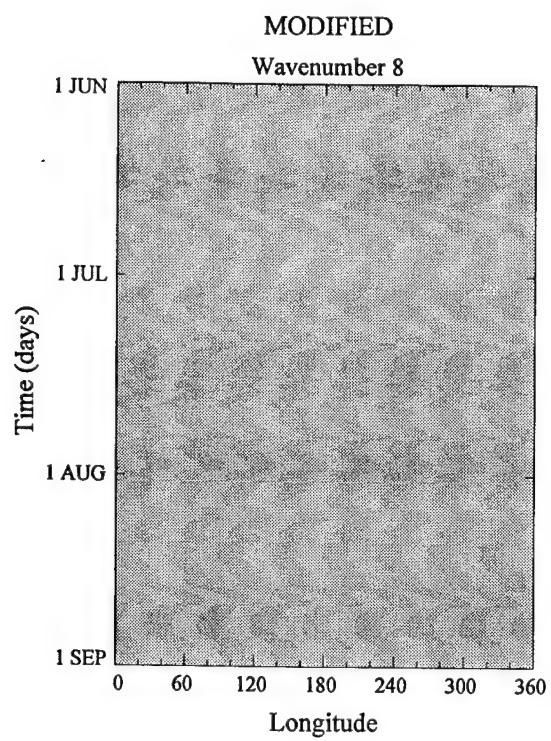


Figure 7. Continued.

significant impacts on many applications of the data. Therefore, an effort has been made to remove these anomalies from the data. NH June-August time-means have been calculated for each UKMO variable used in this study and removed from each field accordingly. Figure 5 shows a Hovmoller plot of the NH summertime total (unfiltered) UKMO v field modified by the removal of the summer time-mean. The stationary anomalies are no longer the dominant feature, which is more consistent with *Charney and Drazin* [1961].

Figure 6 shows Hovmoller plots of the unmodified UKMO v field for individual waves 1-8 and combined waves 1-8. Again, stationary wave anomalies are clearly visible in each panel. Figure 7 shows Hovmoller plots of the NH summertime modified UKMO v field where each wavenumber has had its respective summer time-mean removed. The stationary anomalies are no longer the dominant feature, which is in better agreement with planetary-wave theory.

Removal of the stationary anomalies does have the effect of removing some real stationary planetary-scale waves, especially in and above the subtropical jet. Figures 8-10 show percent reduction in wave amplitude (in terms of the climatological monthly-mean UKMO meridional wind, v) in the NH summertime (June-August 1992-1998) stratosphere for individual waves 1-8 as well as combined waves 1-8. In the top two panels of figures 8-10, wave 1 (top left) and 2 (top right) amplitudes are reduced 40-70% in and above the area of the NH subtropical jet (between approximately 10°N-40°N and 10-30 km). The stationary waves removed here are most likely real in that the removed stationary parts appear to intrude into the stratosphere from the maximum in the area of the subtropical jet. However, in each month there are also 40-70% reductions in wave 1 amplitude above 30 km that extend down into the middle stratosphere from maxima in the lower mesosphere. Since at such high altitudes the zonal-mean zonal flow is easterly, it is hard to believe that stationary waves in this region are real [*Charney and Drazin*, 1961]. The stationary anomalies removed here are probably, in part, diurnal tides aliased to zero frequency by once-daily sampling and are, therefore, most likely artifacts of the data.

June 1992-1998

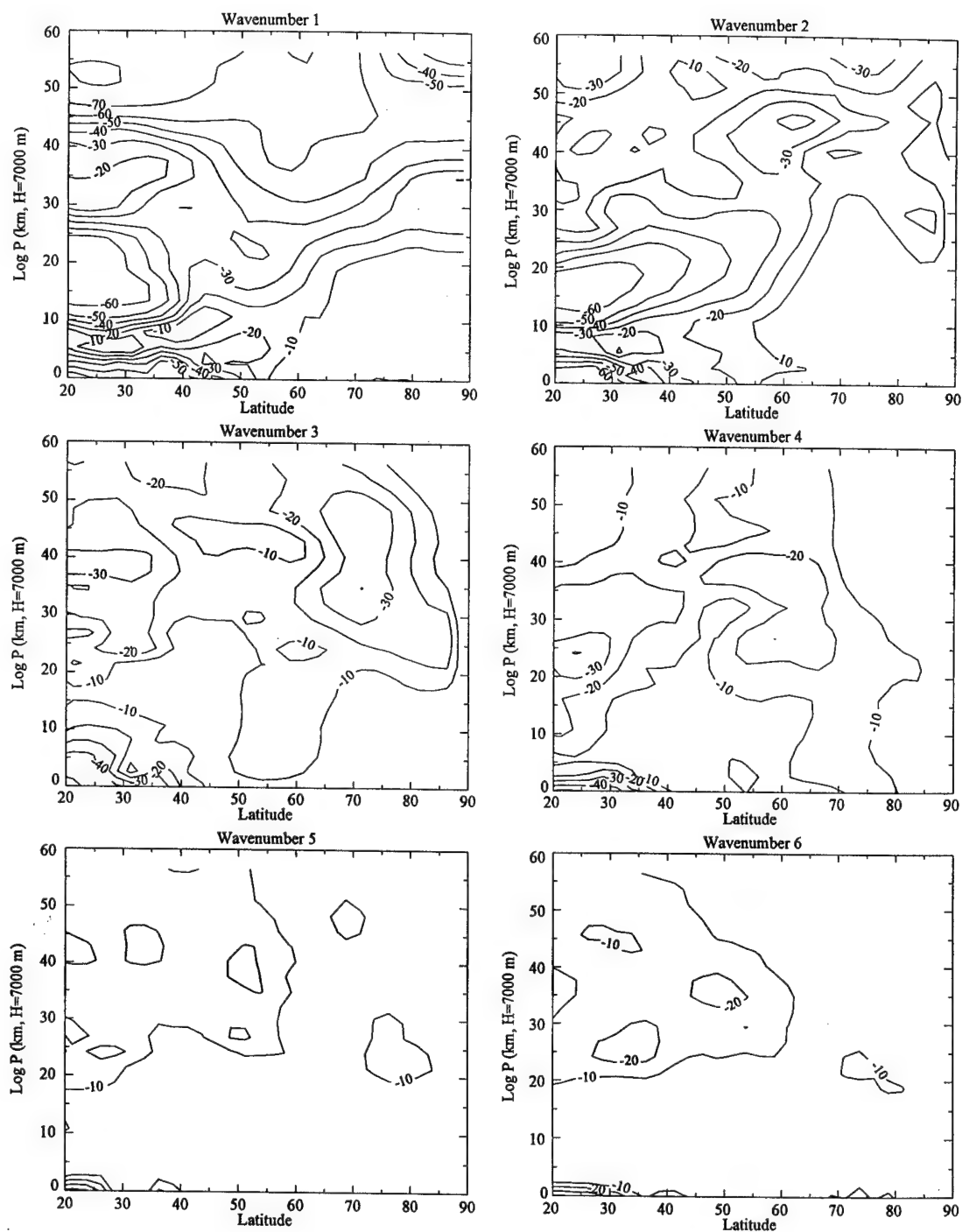


Figure 8. Percent reduction in wave amplitude of the UKMO climatological monthly-mean meridional wind (v) for June 1992-1998. Percent reduction was calculated as $[(\text{MODIFIED} - \text{UNMODIFIED})/\text{UNMODIFIED}] \times 100$.

June 1992-1998

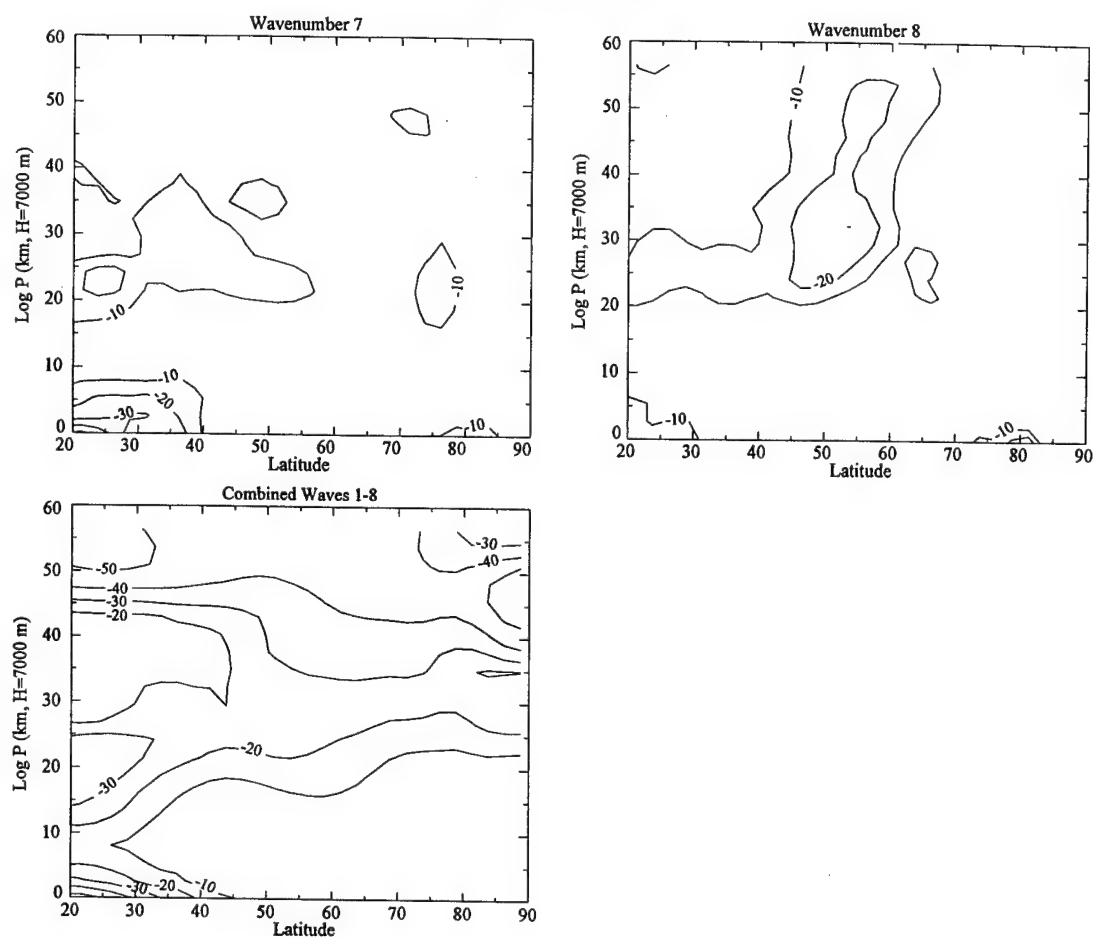


Figure 8. Continued.

July 1992-1998

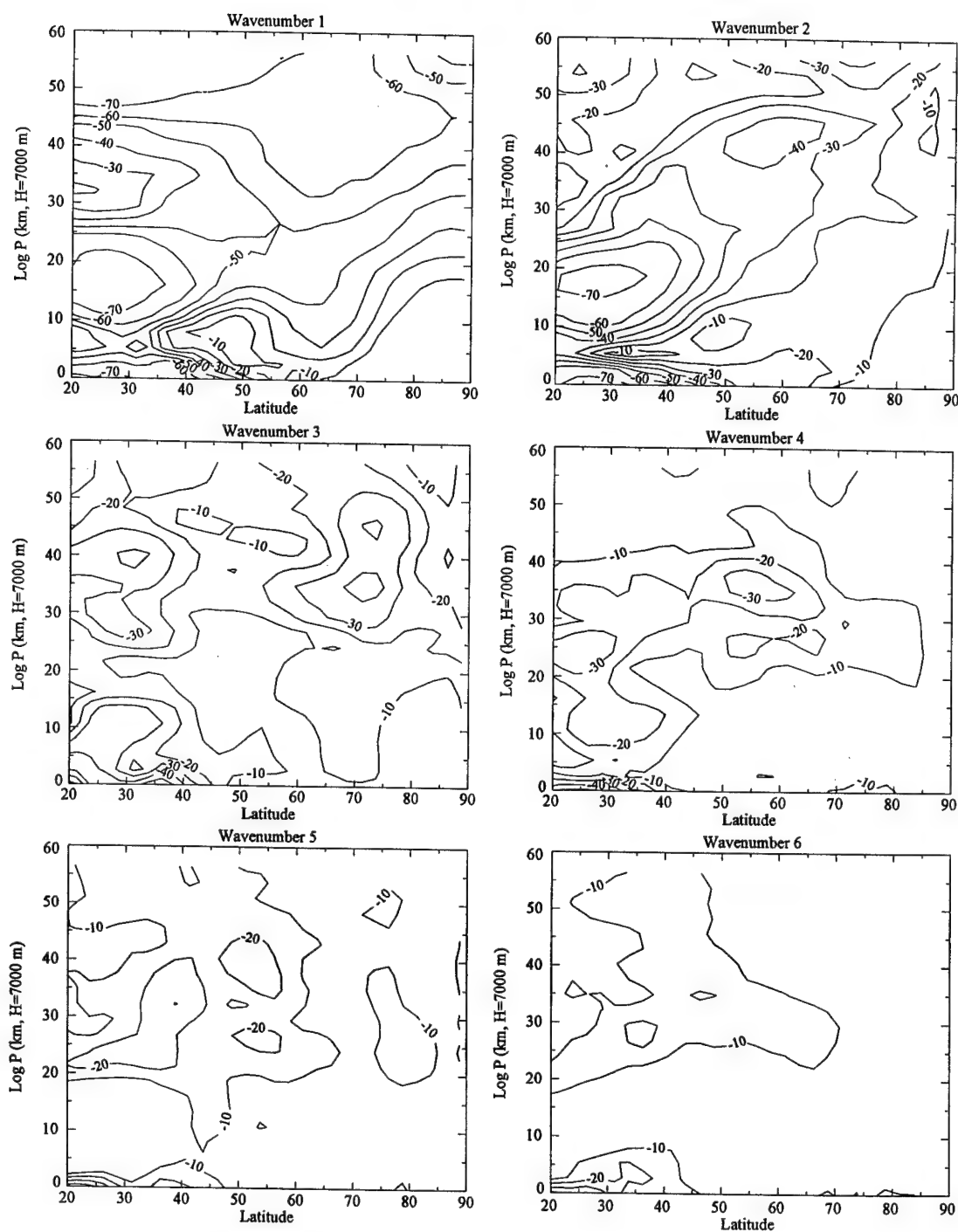


Figure 9. Percent reduction in wave amplitude of the UKMO climatological monthly-mean meridional wind (v) for July 1992-1998. Percent reduction was calculated as $[(\text{MODIFIED} - \text{UNMODIFIED})/\text{UNMODIFIED}] \times 100$.

July 1992-1998

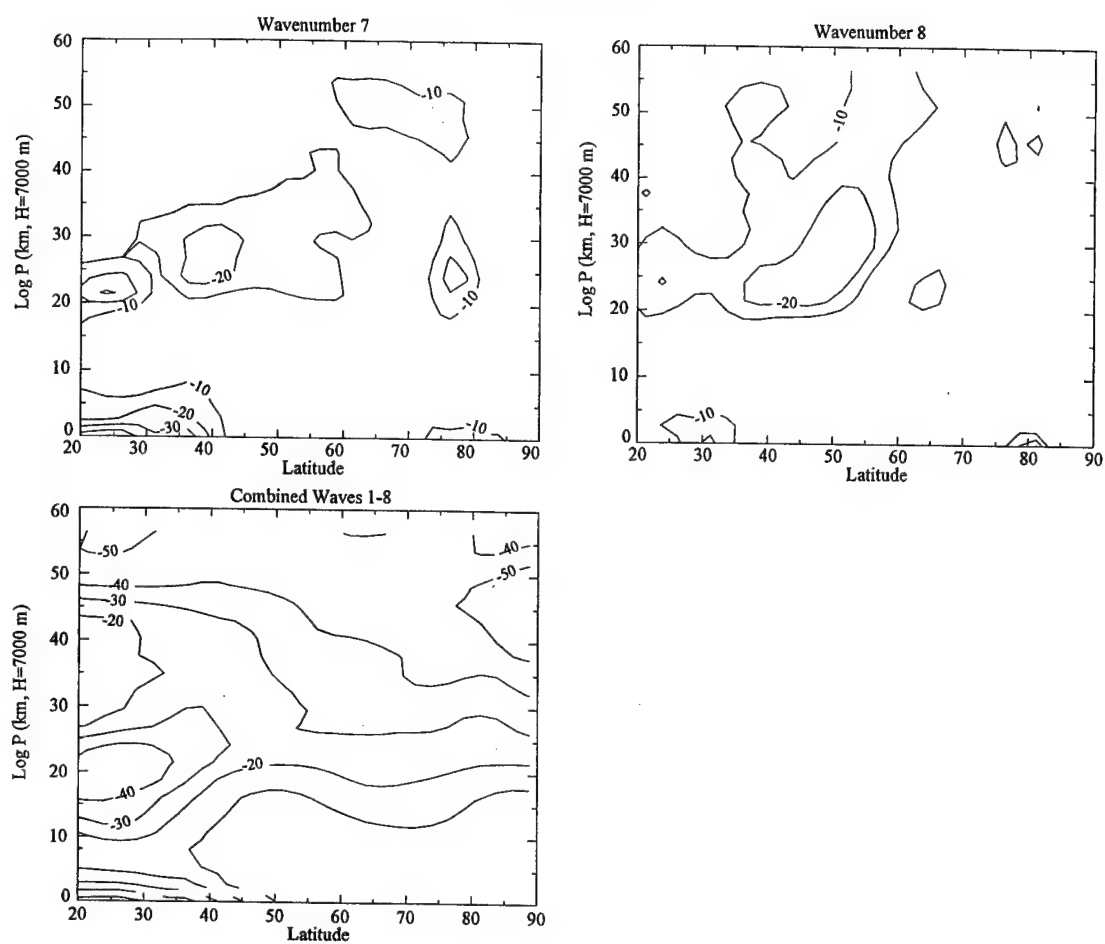


Figure 9. Continued.

August 1992-1998

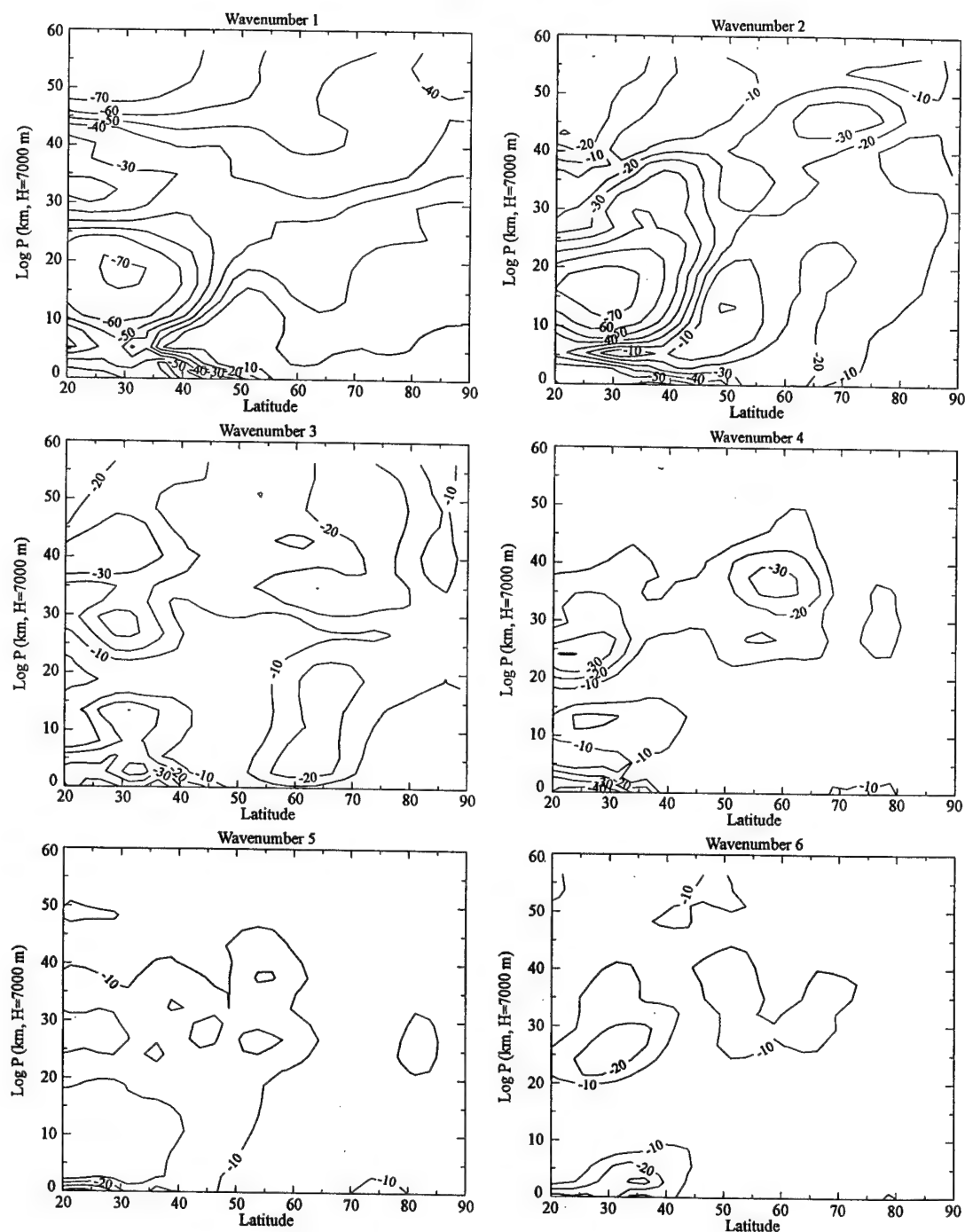


Figure 10. Percent reduction in wave amplitude of the UKMO climatological monthly-mean meridional wind (v) for August 1992-1998. Percent reduction was calculated as $[(\text{MODIFIED} - \text{UNMODIFIED})/\text{UNMODIFIED}] \times 100$.

August 1992-1998

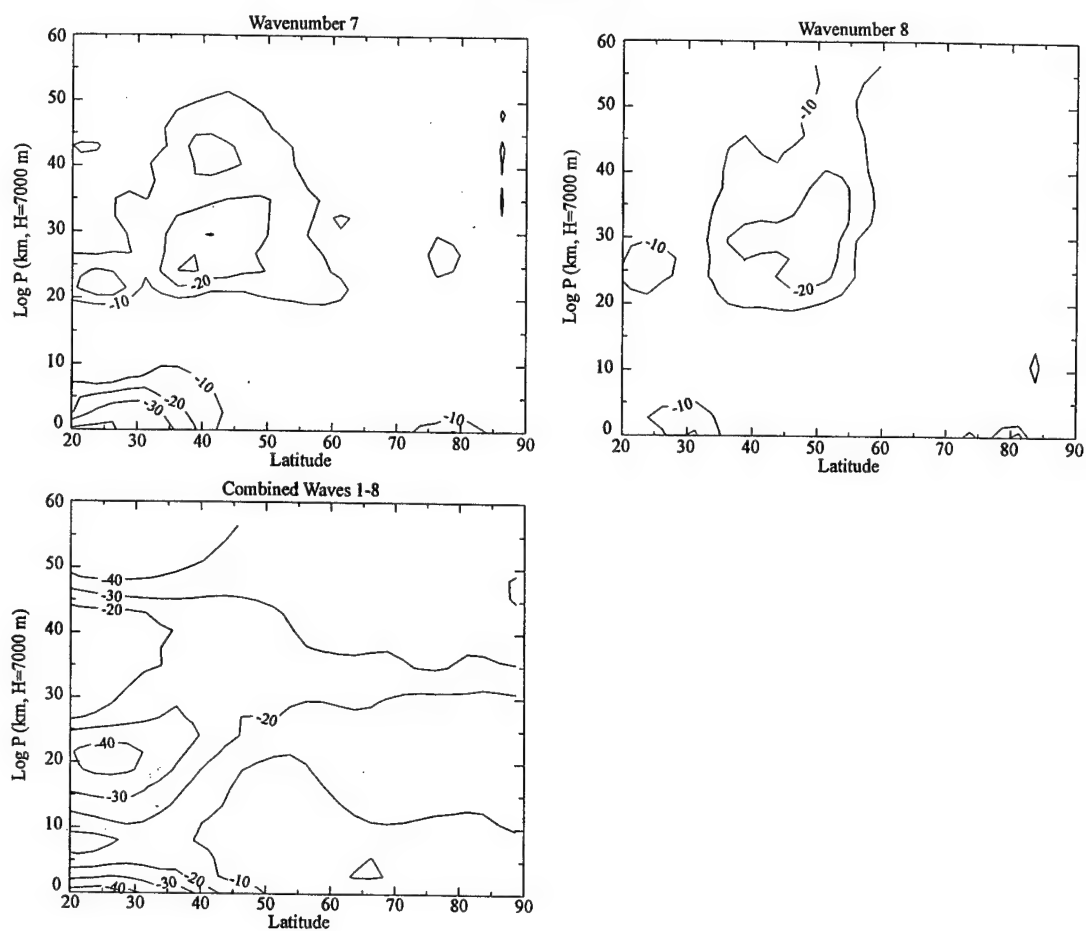


Figure 10. Continued.

Wave 3 shows 20-40% amplitude reductions in the troposphere and lower stratosphere around the subtropical jet. The stationary components removed here are probably largely real stationary waves. However, waves 3-8 in figures 8-10 consistently show 20-30% amplitude-reduction maxima in the middle stratosphere that appear to be unconnected to large amplitude-reduction maxima in the troposphere and lower stratosphere. It is reasonable to assume that the stationary anomalies removed in these panels are actual artifacts of the data as it seems unlikely to have medium-scale stationary waves present in easterly flow in the middle stratosphere [*Charney and Drazin, 1961*].

Percent reductions in amplitude for the June, July, and August 1992-1998 combined waves 1-8 (Figures 8-10, second page, last panel) are dominated by wave 1 and wave 2 amplitude reductions. Therefore, explanations for the areas of maximum amplitude reduction for the combined waves 1-8 mirror explanations for waves 1 and 2.

In our region of interest (RMV), the mean flow is generally easterly, so stationary waves here are also assumed to be artifacts of the data. Table 2 summarizes the range of percent reductions in climatological monthly-mean UKMO v -amplitudes in the RMV for individual wavenumbers 1-8 and combined waves 1-8.

All calculations in this study are computed using the modified UKMO data set with stationary anomalies removed.

Table 2. Range of percent reduction in wave amplitudes of the climatological monthly-mean UKMO meridional wind (v) resulting from removal of seasonal time-means. The RMV extends from 55°N-65°N and ~20-30 km.

Zonal Wave Number	% Reduction of UKMO V-Wind Wave Amplitude in the RMV					
	June		July		August	
	min	max	min	max	min	max
1	15	47	43	58	24	36
2	6	35	28	38	12	22
3	8	26	5	32	1	22
4	15	30	8	24	3	21
5	0.6	12	5	22	3	22
6	3	14	1	19	2	16
7	1	11	1	14	2	14
8	1	24	3	20	0.3	10
Combined Waves 1-8	11	27	21	38	11	22

CHAPTER III

METHODS

3.1. Wave Amplitudes

Some quantities are computed directly from the gridded UKMO data. In other cases it is useful to expand the UKMO data in zonal Fourier sine and cosine series of the form

$$X(\lambda_i) = \sum_k (S_k \sin k\lambda_i + C_k \cos k\lambda_i), \quad (3)$$

where X is the UKMO variable, λ_i is the longitude of each grid point in radians, and k is the zonal wavenumber. The complex Fourier coefficients, S_k and C_k , are defined as follows:

$$S_k = \frac{1}{\pi} \int_0^{2\pi} X(\lambda) \sin(k\lambda) d\lambda, \quad (4)$$

$$C_k = \frac{1}{\pi} \int_0^{2\pi} X(\lambda) \cos(k\lambda) d\lambda. \quad (5)$$

The Fourier coefficients are computed using fast Fourier transforms. In this study only waves 1-8 are retained. The amplitudes of individual wave components are

$$A_k = \sqrt{(S_k^2 + C_k^2)}. \quad (6)$$

3.2. Space-Time Power Spectra

Traveling-wave power spectra for the NH summertime stratosphere are computed following *Bowman* [1996]. The UKMO meridional wind, v , is expanded in a space-time Fourier series as follows:

$$v(\lambda_i, t_s) = \sum_k \sum_v v_{k,v} e^{i(k\lambda - vt)}, \quad (7)$$

where v is the meridional wind, t_s is the daily time samples, k and v are discrete spatial and temporal frequencies (k is still the zonal wavenumber), and $v_{k,v}$ is the complex amplitude of each wave. The complex two-dimensional spectrum, $v_{k,v}$, is computed

using fast Fourier transforms. The actual quantity plotted in the power spectra diagrams is $v_{k,v} v_{k,v}^*$, where $v_{k,v}^*$ is the complex-conjugate of $v_{k,v}$.

Climatological monthly-mean power spectra are computed for waves 1-8 for 7 NH summers (June-August) from 1992 to 1998.

3.3. Effective Meridional Diffusion Coefficients

In this study, ozone mixing in the NH summertime stratosphere will be measured by way of effective meridional diffusion coefficients, K_{yy} . Lagrangian trajectories are calculated from modified UKMO winds on isentropic surfaces using a standard fourth-order Runge-Kutta scheme [Bowman, 1993]. From these trajectories, meridional particle dispersion, $\langle \eta'^2 \rangle$, an indicator of meridional mixing, is computed to establish the rate of change of the latitudinal variance for an ensemble of particles initially located around a latitude circle. Here, η is latitude, η' is the deviation from the Lagrangian mean ($\eta' = \eta - \langle \eta \rangle$), and angle brackets represent the mean over an ensemble of particles. Effective meridional diffusion coefficients (K_{yy}) are then estimated from $\langle \eta'^2 \rangle$ for each month as outlined in Schoeberl *et al.* [1992] and Bowman [1993]. K_{yy} will be used in this study as the indicator of meridional mixing and transport of ozone.

3.4. Eliassen-Palm Flux and Flux Divergence

Eliassen-Palm flux (\bar{F}), referred to as the EP flux, and the divergence of the EP flux ($\nabla \cdot \bar{F}$) are used as diagnostic tools to determine the forcing of the zonal-mean zonal flow by wave disturbances. \bar{F} is a vector quantity lying in a meridional plane, consisting of components of northward eddy heat flux ($F_{(z)}$) and northward eddy momentum flux ($F_{(\phi)}$). In the case of spherical geometry with $z = -H \ln(p/p_0)$ as the vertical coordinate, \bar{F} is given by

$$\bar{F} = \{F_{(\phi)}, F_{(z)}\}, \quad (8)$$

where

$$F_{(\phi)} = \rho_0 r_0 \cos \phi (\bar{u}_z \bar{v}' \theta' / \bar{\theta}_z - \bar{v}' u'), \quad (9)$$

$$F_{(z)} = \rho_0 r_0 \cos \phi \left\{ \left[f - (r_0 \cos \phi)^{-1} (\bar{u} \cos \phi)_\phi \right] \bar{v}' \theta' / \bar{\theta}_z - \bar{w}' u' \right\}. \quad (10)$$

Here, ϕ is latitude; u , v , and w are zonal, meridional, and vertical velocities (respectively) in m s^{-1} ; θ is potential temperature in K; r_0 is the mean radius of the earth in meters; ρ_0 is basic state density in kg m^{-3} ; and $f = f(\phi)$ is the Coriolis parameter in rad s^{-1} [Andrews *et al.*, 1987]. Overbars denote zonal means, primes denote departures from the zonal mean, and subscripts without parentheses denote partial differentiation (e.g., $\bar{\theta}_z$ is the partial derivative of the zonal-mean potential temperature with respect to z). The divergence of the EP flux is defined under the same conditions as

$$\nabla \cdot \bar{F} = \frac{1}{r_0 \cos \phi} \left(F_{(\phi)} \cos \phi \right)_\phi + \left(F_{(z)} \right)_z. \quad (11)$$

\bar{F} and $\nabla \cdot \bar{F}$ are calculated from the Transformed Eulerian Mean (TEM) set of equations for spherical coordinates in Andrews *et al.* [1987],

$$\bar{u}_t - \bar{v}^* \left[(r_0 \cos \phi)^{-1} (\bar{u} \cos \phi)_\phi - f \right] + \bar{w}^* \bar{u}_z - \bar{X} = (\rho_0 r_0 \cos \phi)^{-1} \nabla \cdot \bar{F}, \quad (12)$$

$$\bar{u} (f + \bar{u} r_0^{-1} \tan \phi) + r_0^{-1} \bar{\Phi}_\phi = G, \quad (13)$$

$$\bar{\Phi}_z - H^{-1} R \bar{\theta} e^{-\kappa z/H} = 0, \quad (14)$$

$$(r_0 \cos \phi)^{-1} (\bar{v}^* \cos \phi)_\phi + \rho_0^{-1} (\rho_0 \bar{w}^*)_z = 0, \quad (15)$$

$$\bar{\theta}_t + r_0^{-1} \bar{v}^* \bar{\theta}_\phi + \bar{w}^* \bar{\theta}_z - \bar{Q} = -\rho_0^{-1} \left[\rho_0 (\bar{v}' \bar{\theta}' / r_0 \bar{\theta}_z + \bar{w}' \bar{\theta}') \right]_z, \quad (16)$$

where R is the specific gas constant for dry air in $\text{J kg}^{-1} \text{K}^{-1}$, H is scale height ($H = 7000$ m), κ is the specific gas constant for dry air, Φ is geopotential in $\text{m}^2 \text{s}^{-2}$, and \bar{v}^* and \bar{w}^* are the meridional and vertical components (respectively) of the residual meridional circulation. These last two components are defined as follows:

$$\bar{v}^* = \bar{v} - \rho_0^{-1} \left(\rho_0 \frac{\bar{v}' \bar{\theta}'}{\bar{\theta}_z} \right)_z, \quad (17)$$

$$\bar{w}^* = \bar{w} + \frac{1}{r_0 \cos \phi} \left(\frac{\bar{v}' \bar{\theta}'}{\bar{\theta}_z} \cos \phi \right)_\phi. \quad (18)$$

The \bar{X} and \bar{Q} terms in (12) and (16) represent frictional dissipation and diabatic heating, respectively. G in (13) represents all the terms that lead to a departure from gradient-wind balance between \bar{u} and $\bar{\Phi}$. For our purposes, G is negligible.

Following Edmon *et al.* [1980] and Andrews *et al.* [1987] and neglecting smaller order terms, (9) and (10) take the form:

$$F_{(\phi)} = -\rho_0 r_0 \cos \phi (\overline{v'u'}), \quad (19)$$

$$F_{(z)} = f \rho_0 r_0 \cos \phi (\overline{v'\theta'}/\bar{\theta}_z). \quad (20)$$

Equations (19) and (20) will be the form used to compute and plot the vectors representing $F_{(\phi)}$ and $F_{(z)}$. Likewise, for plotting purposes, (11) will be multiplied by $(\rho_0 r_0 \cos \phi)^{-1}$:

$$\frac{1}{\rho_0 r_0 \cos \phi} [\nabla \cdot \bar{F}] = \frac{1}{\rho_0 r_0 \cos \phi} \left[\frac{1}{r_0 \cos \phi} (F_{(\phi)} \cos \phi)_{\phi} + (F_{(z)})_z \right]. \quad (21)$$

so that contoured values of EP flux divergence will be in units of acceleration and directly represent the right side of (12). This way, acceleration of the zonal-mean zonal flow $[\bar{u}_t$ on left-hand side of (12)] can be deduced directly from the values generated by (21).

CHAPTER IV

RESULTS

4.1. Characteristics of the Zonal-Mean u and T Fields in the NH Summer Stratosphere

Figure 11 shows the NH climatological monthly-mean zonal-mean u and T fields for June, July, and August 1992-1998. In the zonal-mean zonal wind (\bar{u}) cross sections (left column of Figure 11), solid contours represent westerly flow and dotted contours represent easterlies.

In June (Figure 11, top left panel), the tropospheric zonal-mean jet is westerly with a 20 m s^{-1} maximum centered at 38°N latitude and approximately 12 km (midlatitude tropopause) in height. The zero-wind line is located at approximately 20 km poleward of 30°N . In the stratosphere, winds are westerly below the zero-wind line. Above the zero wind line, \bar{u} is easterly. Easterly wind speeds increase with height to a maximum of greater than -40 m s^{-1} above 50 km between 20° - 40°N . Stratospheric zonal wind speeds are strongest near 30°N and weaken with increasing latitude to the pole.

Temperatures (Figure 11, top right panel) at the equatorial tropopause ($\sim 16 \text{ km}$) are about 200 K and increase approximately 2 K km^{-1} up to the stratopause ($\sim 45 \text{ km}$). Poleward of 20°N the increase is more gradual and doesn't achieve the equatorial vertical gradient until approximately 30 km. At the stratopause, T is a maximum at the pole ($>280\text{K}$) and decreases meridionally to the equator.

In July (Figure 11, middle left panel) and August (bottom left panel), the tropospheric subtropical jet core has the same magnitude and direction as in June, but is narrower and shifted poleward approximately 5° of latitude. The zero-wind line still sits at approximately 20 km in the lower midlatitudes for both months. Poleward of 50°N , however, the zero-wind line rises to 25 km at the pole in July and 30 km at the pole in August. The maximum stratospheric winds maintain roughly the same position as in June for both months, but increase in speed in July and then decrease in August. Of the 3 months, stratospheric easterlies are weakest in August.

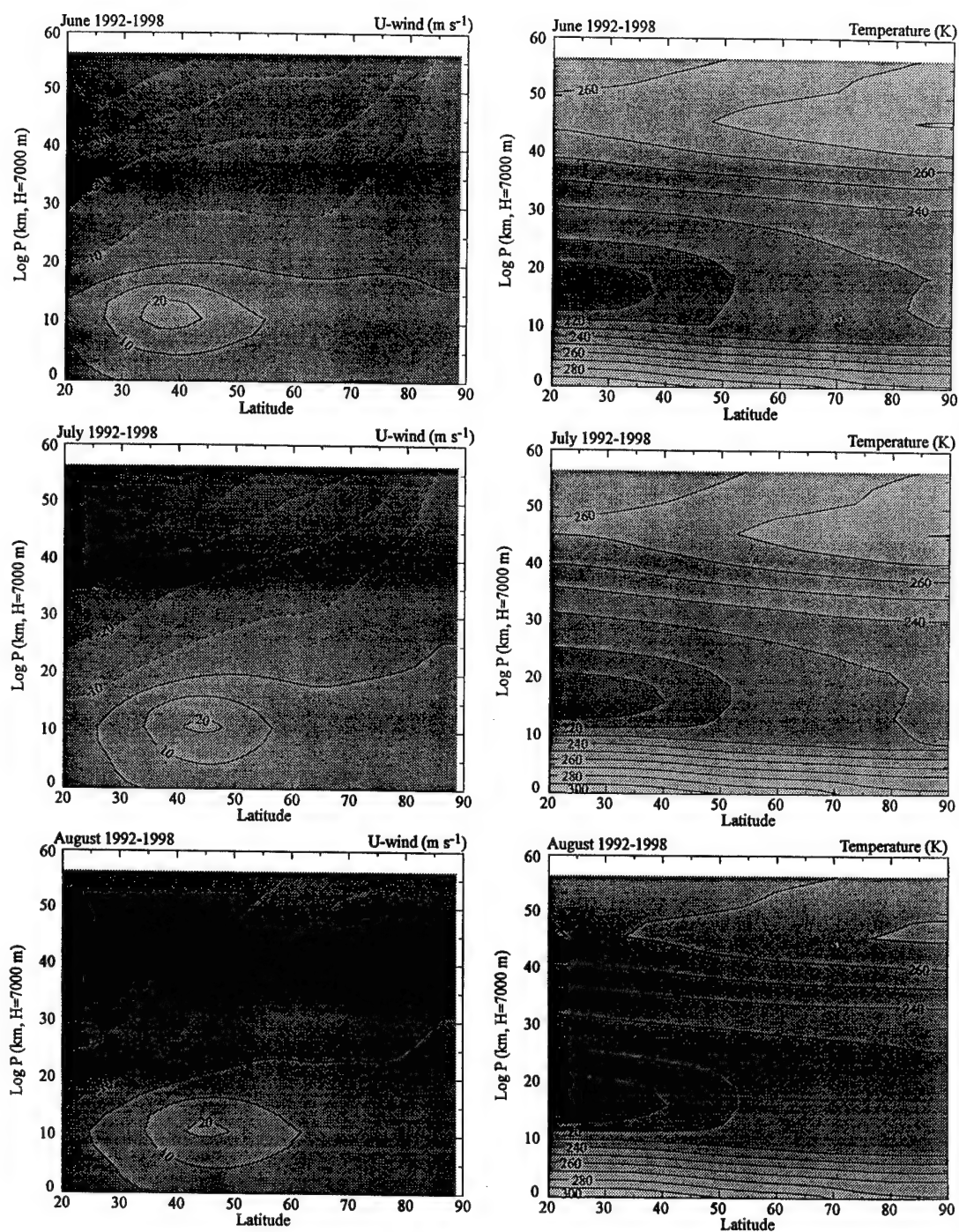


Figure 11. UKMO climatological monthly-mean zonal-mean u and T meridional cross sections for June, July, and August 1992-1998 in the extratropical NH.

July temperatures (Figure 11, middle right panel) in the stratosphere are nearly identical to June. In August (Figure 11, bottom right panel), however, the vertical temperature gradient near the pole weakens as maximum insolation from the sun begins to move equatorward. Above 30 km, the vertical temperature gradient weakens somewhat, as does the equator-to-pole temperature gradient at the stratopause. The equatorial upper stratosphere warms to greater than 260 K and the polar upper stratosphere cools to less than 280 K. This and thermal-wind balance explain the weakening of the stratospheric easterlies in August.

4.2. Characteristics of Planetary-Scale and Medium-Scale Waves in the NH Summer Stratosphere

4.2.1. Wave Amplitudes

Figures 12-14 show NH summertime climatological monthly-mean latitude vs. $\log p$ height cross sections of UKMO modified wave amplitudes (in terms of v) for June, July, and August 1992-1998, respectively. Planetary-scale waves 1-3, medium-scale waves 4-8, and combined waves 1-8 are depicted in each figure. The zonal-mean v (wavenumber 0) is also depicted for reference.

In June (Figure 12) over the pole, wave 1 decreases from a maximum of 7 m s^{-1} at 8 km in the upper troposphere to 2 m s^{-1} at about 40 km in the upper stratosphere. Meridionally, wave 1 decreases from the pole along the tropopause ($\sim 8\text{-}12 \text{ km}$) to a weak $1\text{-}2 \text{ m s}^{-1}$ maximum centered at 30°N . Between approximately 12-40 km in the vertical and equatorward of about 60°N , wave-1 amplitudes are generally less than 1 m s^{-1} . Above 40 km, wave 1 increases again from 1 m s^{-1} to weaker maxima of approximately 3 m s^{-1} at around 55 km near equator and pole. Wave 1 in July (Figure 13) is virtually identical to June, except that the polar maximum is slightly broader and the weak maximum at 30°N is smaller and has shifted 5° of latitude poleward. In August (Figure 14), the wave 1 maximum at the tropopause increases to 10 m s^{-1} and decreases less rapidly with height. Meridionally, wave 1 diminishes more rapidly along the tropopause than in June and July so that the weak maximum near 30°N is practically nonexistent.

June 1992-1998

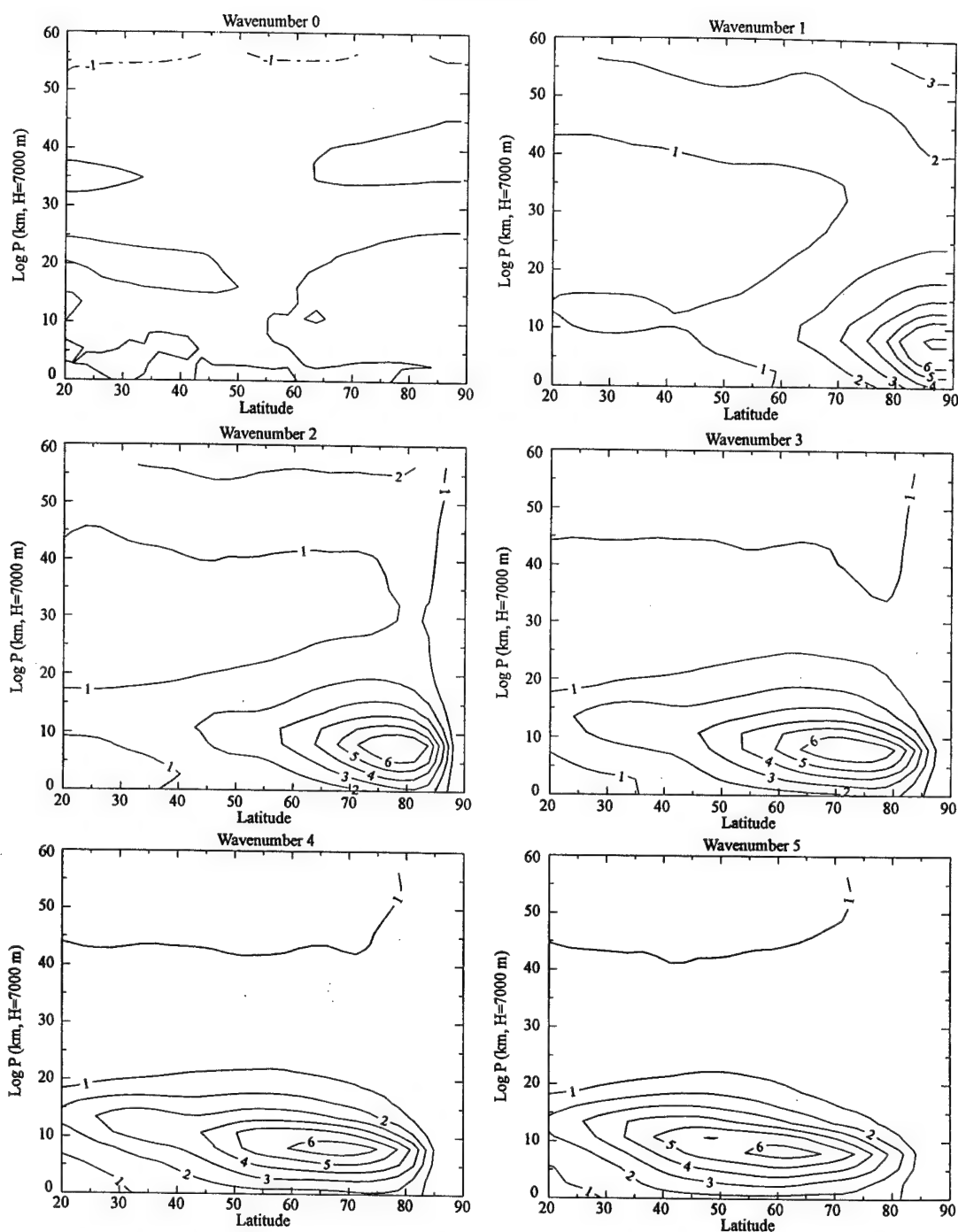


Figure 12. UKMO climatological monthly-mean wave-amplitude meridional cross sections for individual waves 1-8 and combined waves 1-8 in terms of the meridional wind, v (m s^{-1}) for June 1992-1998 in the extratropical NH. Wavenumber 0 represents the zonal mean.

June 1992-1998

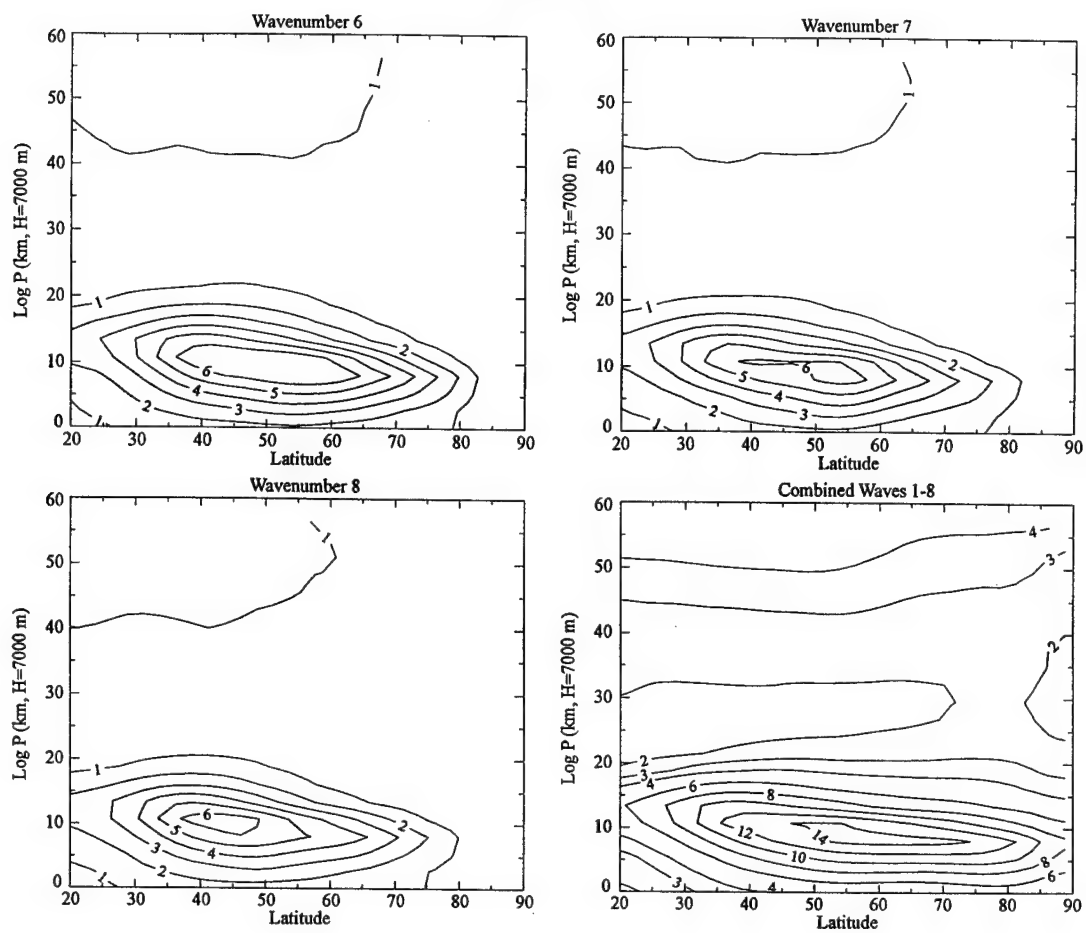


Figure 12. Continued.

July 1992-1998

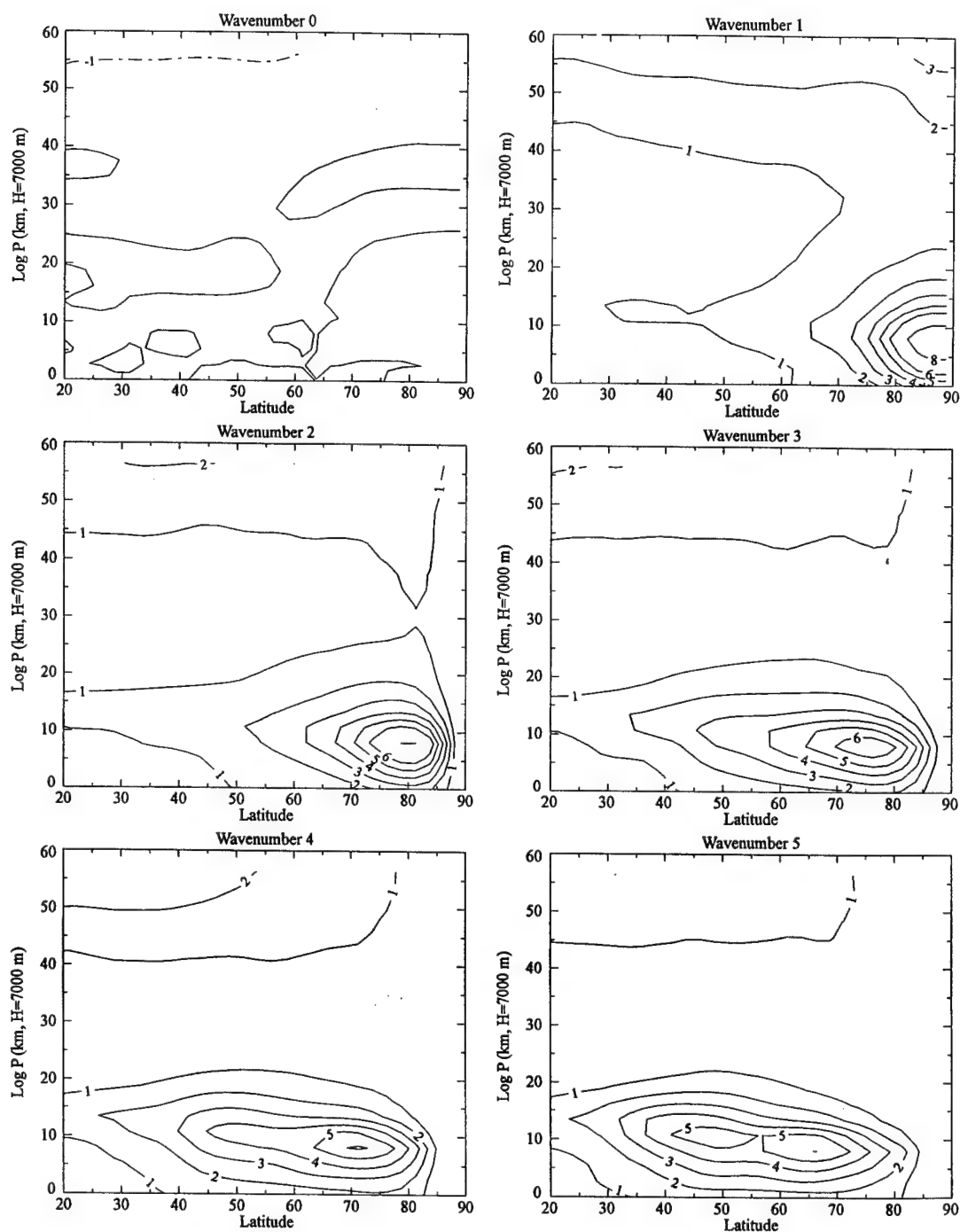


Figure 13. UKMO climatological monthly-mean wave-amplitude meridional cross sections for individual waves 1-8 and combined waves 1-8 in terms of the meridional wind, v (m s^{-1}) for July 1992-1998 in the extratropical NH. Wavenumber 0 represents the zonal mean.

July 1992-1998

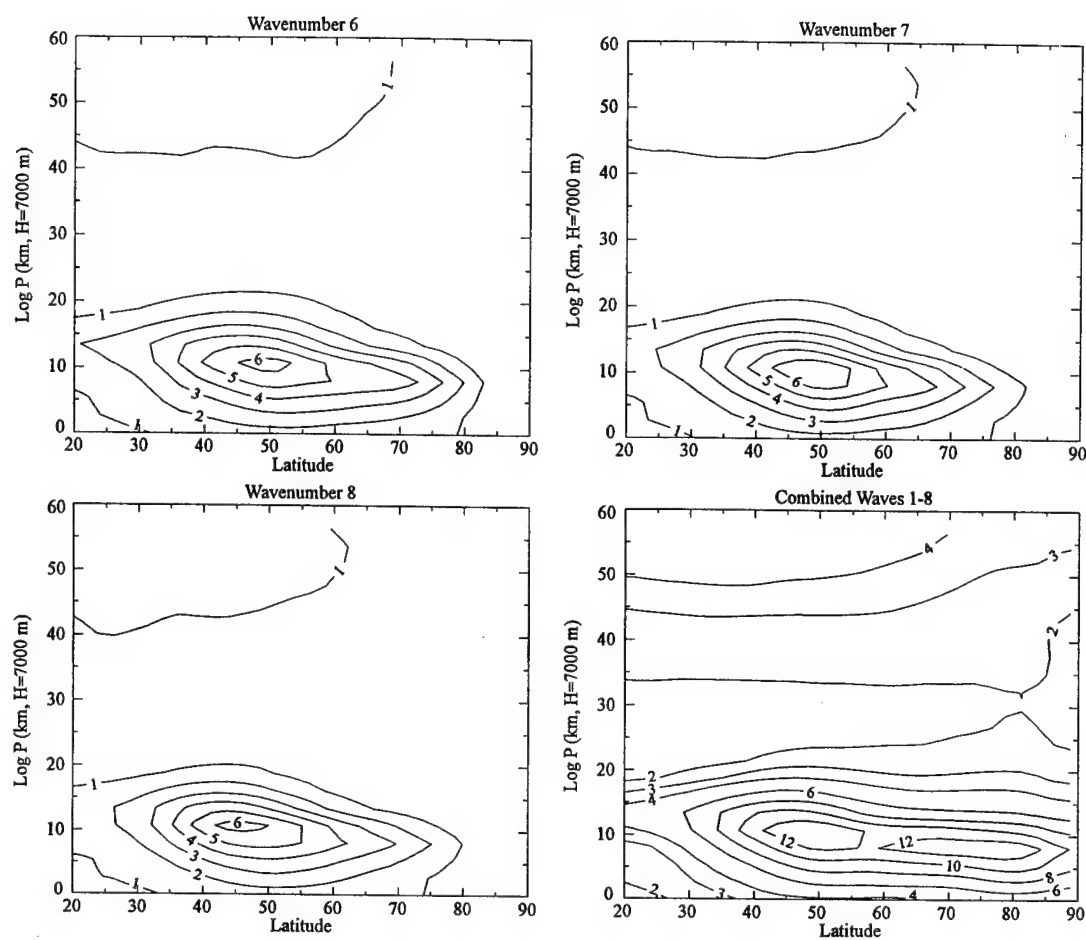


Figure 13. Continued.

August 1992-1998

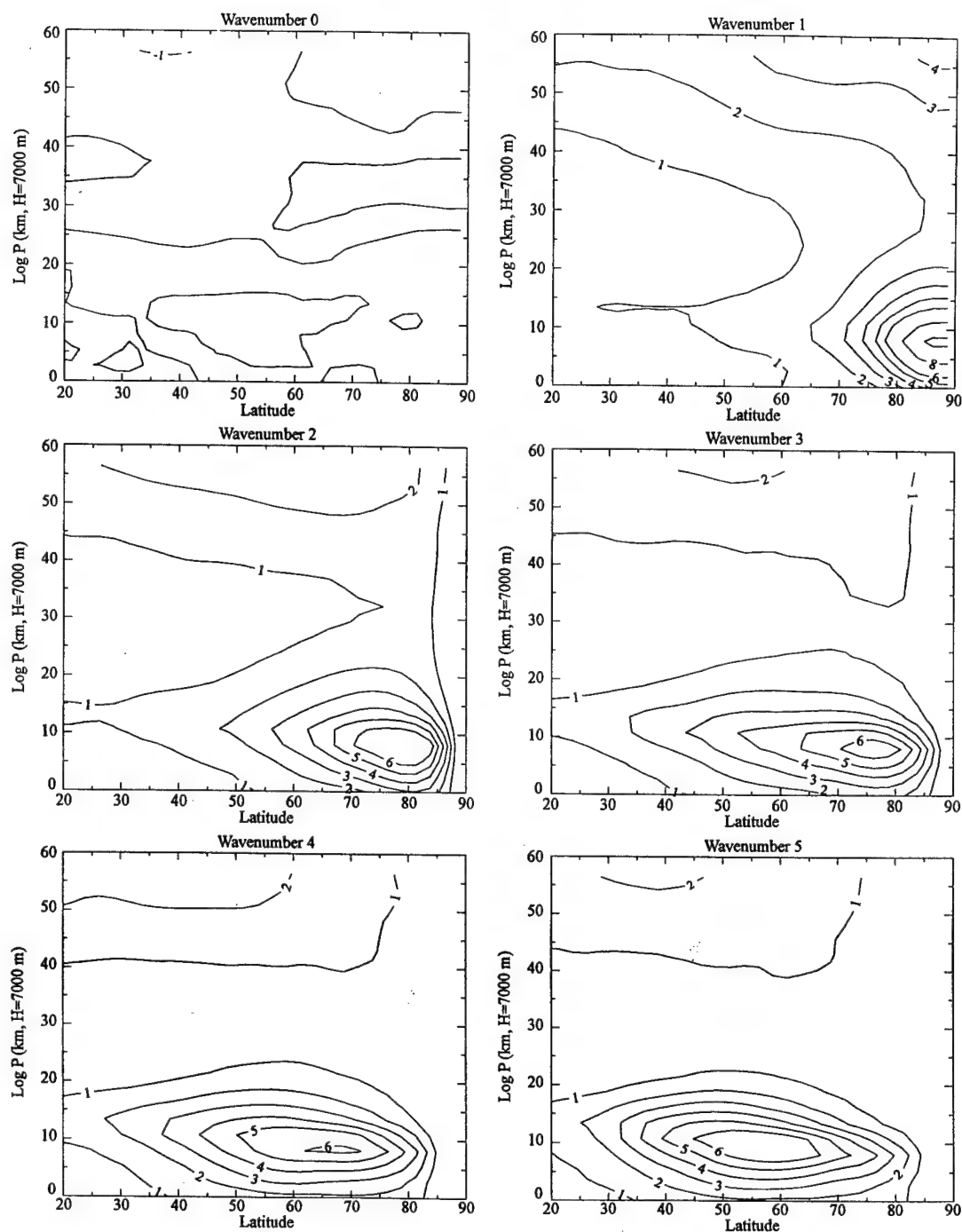


Figure 14. UKMO climatological monthly-mean wave-amplitude meridional cross sections for individual waves 1-8 and combined waves 1-8 in terms of the meridional wind, v (m s^{-1}) for August 1992-1998 in the extratropical NH. Wavenumber 0 represents the zonal mean.

August 1992-1998

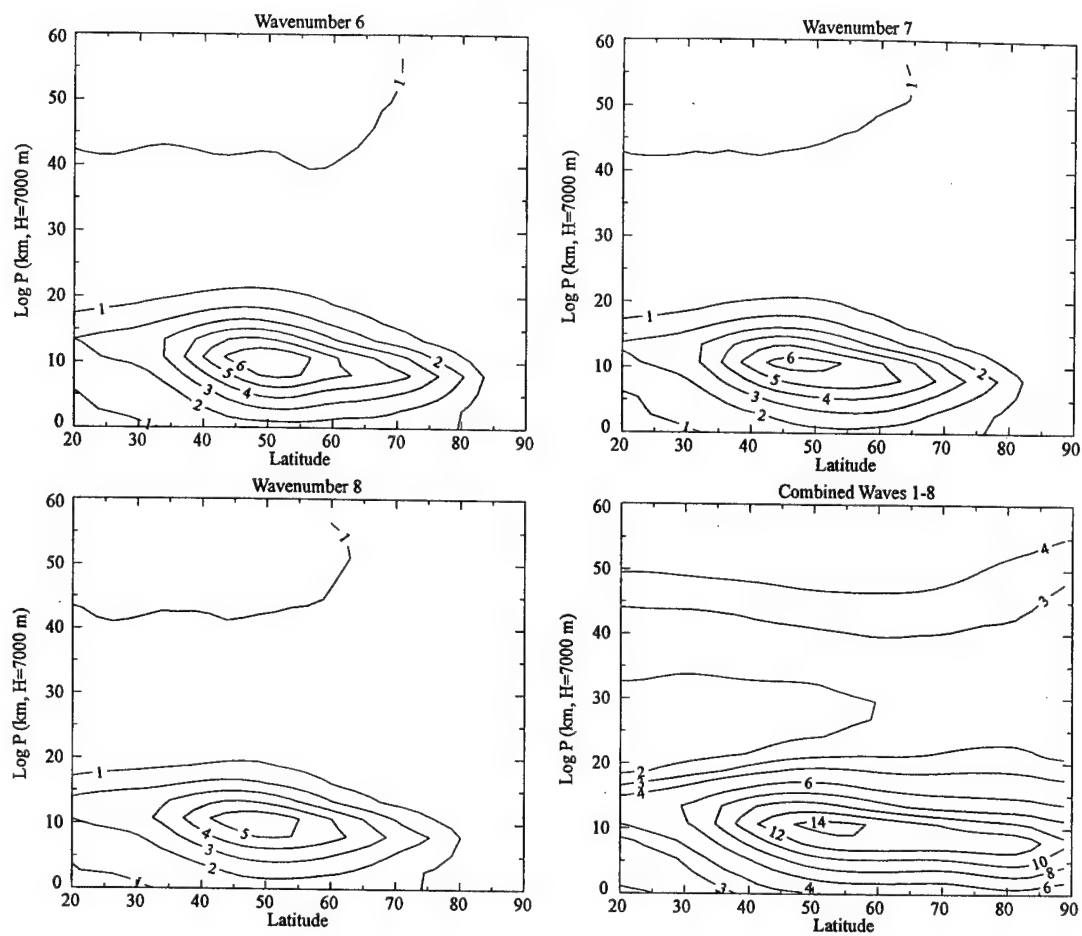


Figure 14. Continued.

Wave 2, in June (Figure 12), has a maximum amplitude of 6 m s^{-1} between 5-10 km and 70° - 80° N. Amplitude decreases vertically to less than 2 m s^{-1} above 20 km. Equatorward of the maximum, wave 2 decreases to between 1 and 2 m s^{-1} at the equator. Like wave 1, in the lower-to-middle stratosphere wave 2 is very small. However, above about 40 km, wave 2 increases slightly in amplitude from 1 to 2 m s^{-1} at 55 km. July (Figure 13) is about the same, except that the maximum near the pole has increased to 8 m s^{-1} and the broad area of very weak wave 2 in the lower-to-middle stratosphere has broadened 5 km vertically and several degrees poleward. In August (Figure 14), this area shrinks considerably in the vertical and back toward the equator. The tropospheric maximum also weakens back to 6 m s^{-1} but now penetrates deeper into the lower stratosphere.

Wave 3, in June (Figure 12), has a broad maximum of $\sim 6 \text{ m s}^{-1}$ at 6-10 km between 65° - 80° N. From there, amplitude decreases to less than 1 m s^{-1} at 25 km and then increases only very slightly again into the upper stratosphere and lower mesosphere. Meridionally, wave 3 decreases rapidly to less than 1 m s^{-1} at the pole and decreases less rapidly along the tropopause to between 1 m s^{-1} and 2 m s^{-1} at 20° N. Most of the middle-to-upper stratosphere above 20 km is less than 2 m s^{-1} . Like wave 2, wave 3 is less than 1 m s^{-1} in the entire atmospheric column directly over the pole. July and August (Figures 13 and 14) are virtually the same.

Waves 4-8, in June (Figure 12), look very similar with a broad maximum of approximately 6 m s^{-1} at 6-10 km. The only difference is that the maximum shifts further equatorward with increasing wavenumber. July and August behave in very much the same way, except that July (Figure 13) amplitude maxima between roughly 6-10 km are weaker by about 1 m s^{-1} for wavenumbers 4 and 5. The lower mesosphere maximum also increases from 1 m s^{-1} to 2 m s^{-1} for the same wavenumbers.

Combined waves 1-8, in June (Figure 12), have a maximum amplitude of 14 m s^{-1} at 8 km between 47° - 75° N. From there amplitude decreases vertically to between 2 m s^{-1} and 3 m s^{-1} at 30 km above which amplitude increases more gradually to a weaker maximum of 4 m s^{-1} near the pole at around 55 km. Meridionally, the amplitude of the combined wave decreases along the tropopause to between 3 m s^{-1} and 4 m s^{-1} at

20°N. The combined wave amplitude is a minimum between 20-30 km equatorward of 70°N. This amplitude minimum broadens in July (Figure 13) and then shrinks again in August (Figure 14) as the mesospheric and tropospheric amplitude maxima penetrate deeper into the middle stratosphere. The upper-tropospheric maximum decreases to 12 m s^{-1} from June to July and then returns to a much narrower maximum of 14 m s^{-1} between 50°N-60°N in August.

Figure 15 shows the relative contribution of wavenumbers 1-8 to the total climatological monthly-mean v amplitude in the RMV for June, July, and August 1992-1998. It is clear that waves 1-5 have the largest magnitudes and the most variation in magnitude from month to month. Amplitudes of waves 1-5 decrease noticeably from June to July and then increase again in August. Wave 3 is a maximum in June and wave 2 is a maximum in August. Table 3 shows the range of climatological monthly-mean v amplitudes for individual waves 1-8 and combined waves 1-8 in the RMV.

Table 3. Range of climatological monthly-mean v amplitudes in the RMV. Maximum values are at the lower boundary of the RMV and minimum values are at the upper boundary.

Zonal Wave Number	UKMO V-Wind Wave Amplitudes (m/s) in the RMV					
	June		July		August	
	min	max	min	max	min	max
1	0.71	1.25	0.69	1.16	0.74	1.18
2	0.73	1.46	0.63	1.25	0.71	1.78
3	0.68	1.45	0.60	1.21	0.69	1.38
4	0.58	1.07	0.56	1.02	0.62	1.29
5	0.52	1.05	0.49	1.01	0.57	1.17
6	0.48	0.84	0.49	0.88	0.48	0.84
7	0.40	0.65	0.40	0.69	0.41	0.7
8	0.32	0.59	0.33	0.55	0.38	0.63
Combined Waves 1-8	1.83	2.71	1.67	2.5	1.87	2.94

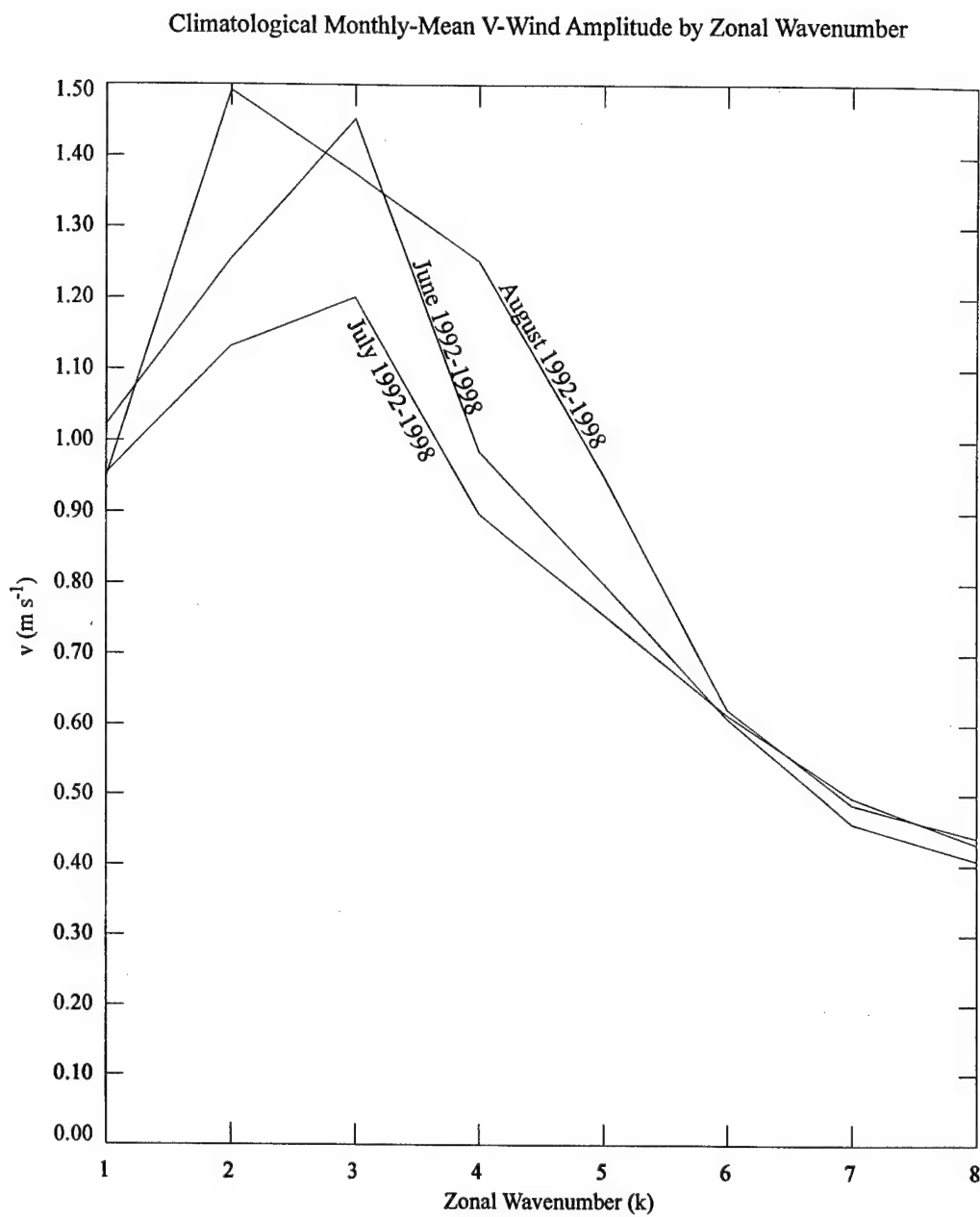


Figure 15. Climatological monthly-mean v -amplitude (meridionally averaged over the latitudinal width of the RMV) plotted as a function of zonal wavenumber. Data represents the bottom level of the RMV (46.4 hPa).

4.2.2. Space-Time Power Spectra

Climatological monthly-mean traveling-wave power spectra for June, July, and August 1992-1998 are shown in Figure 16 for the modified UKMO v -wind at 61.25°N and 215 hPa, 46 hPa, 31 hPa, 21 hPa, and 14 hPa. The 215 hPa level represents wave spectra in the upper troposphere; the remaining 4 pressure levels represent the four levels within the RMV that are available from the UKMO data set. Stationary wave components (infinite period) lie along the abscissa. Wavenumber 0 represents the zonal mean. The dotted lines indicate the zonal phase speeds for the waves relative to the ground at 61.25°N. The climatological monthly-mean zonal-mean wind (\bar{u}) is plotted as a heavy solid line.

In the upper troposphere (215 hPa), the spectra are broad. The largest components are stationary and quasi-stationary waves 3 and 4 in June, stationary waves 1, 3, and 5 in July, and stationary waves 2-5 in August. There is significant eastward-propagating power at phase speeds less than \bar{u} in all 3 months.

In June at 46 hPa, which is at the bottom of the RMV, \bar{u} is -3.1 m s^{-1} and maximum power is greater in the westward propagating waves, indicating filtering of eastward propagating waves as they propagate vertically into the stratospheric easterlies in accordance with (1). From (1), waves that have easterly phase speeds slower than \bar{u} (solid line) should be evanescent in the vertical, whereas waves with westward phase speeds faster than \bar{u} can propagate higher into the RMV. Further filtering of the spectrum is evident at successively higher levels as wave power shifts toward faster negative phase speeds. At 31 hPa the highest power in waves with westward phase speeds faster than \bar{u} is in waves 1-4 with maximum power in waves 2 and 3. The same is basically true at 21 hPa. At the top of the RMV, waves with westward phase speeds faster than \bar{u} appear to have the highest power in planetary waves 1-3.

July is similar to June with somewhat greater power in wave 1 at periods of approximately 5 and 10 days. In August \bar{u} is more westerly throughout the layer. The wind at higher levels is only weakly easterly, so less filtering of westward-propagating waves is apparent.

June 1992-1998

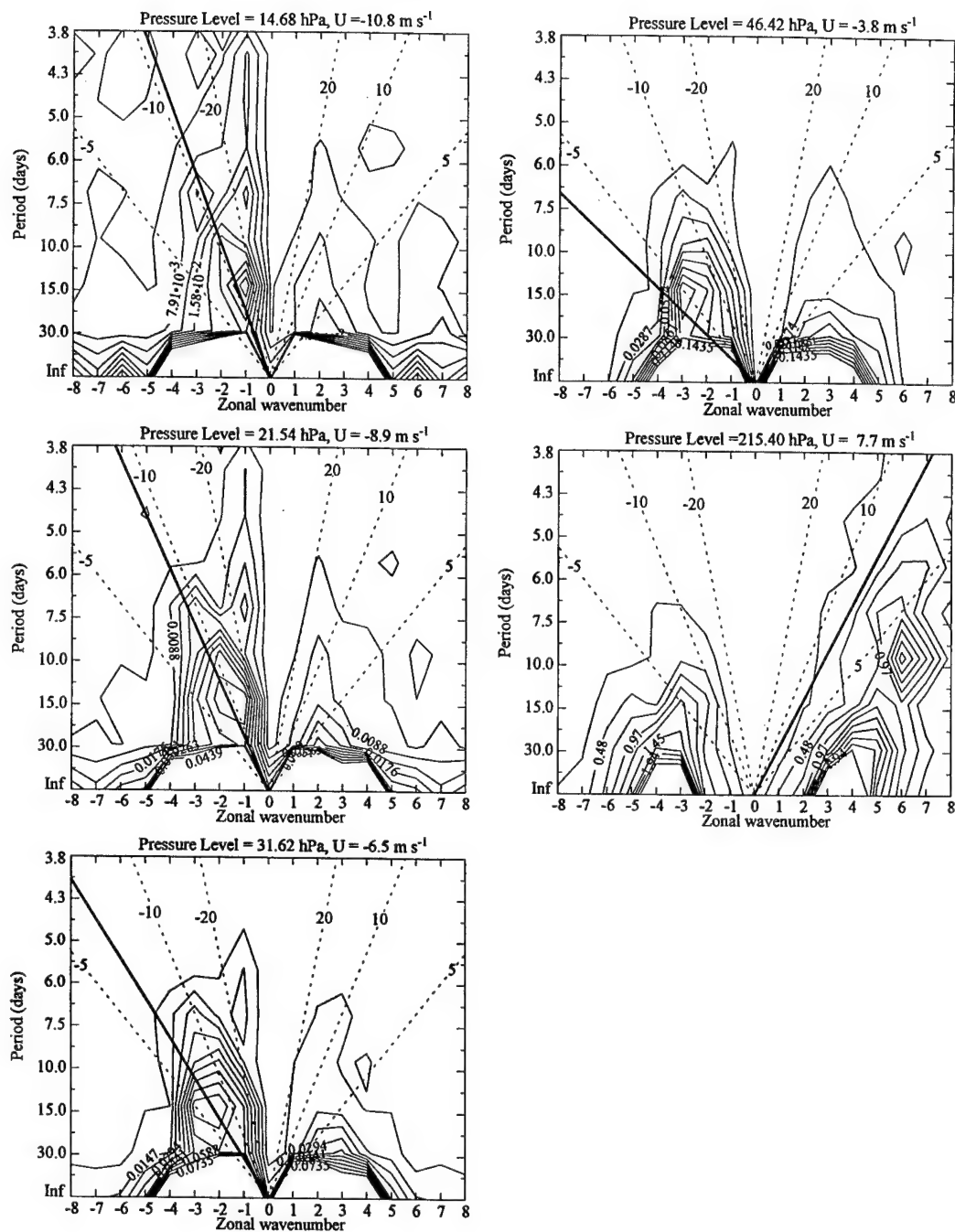


Figure 16. Space-time power spectra of the climatological monthly mean meridional wind for June, July, and August 1992-1998. Phase speeds (dashed lines) are in m s^{-1} and are relative to the ground at 61.25°N .

July 1992-1998

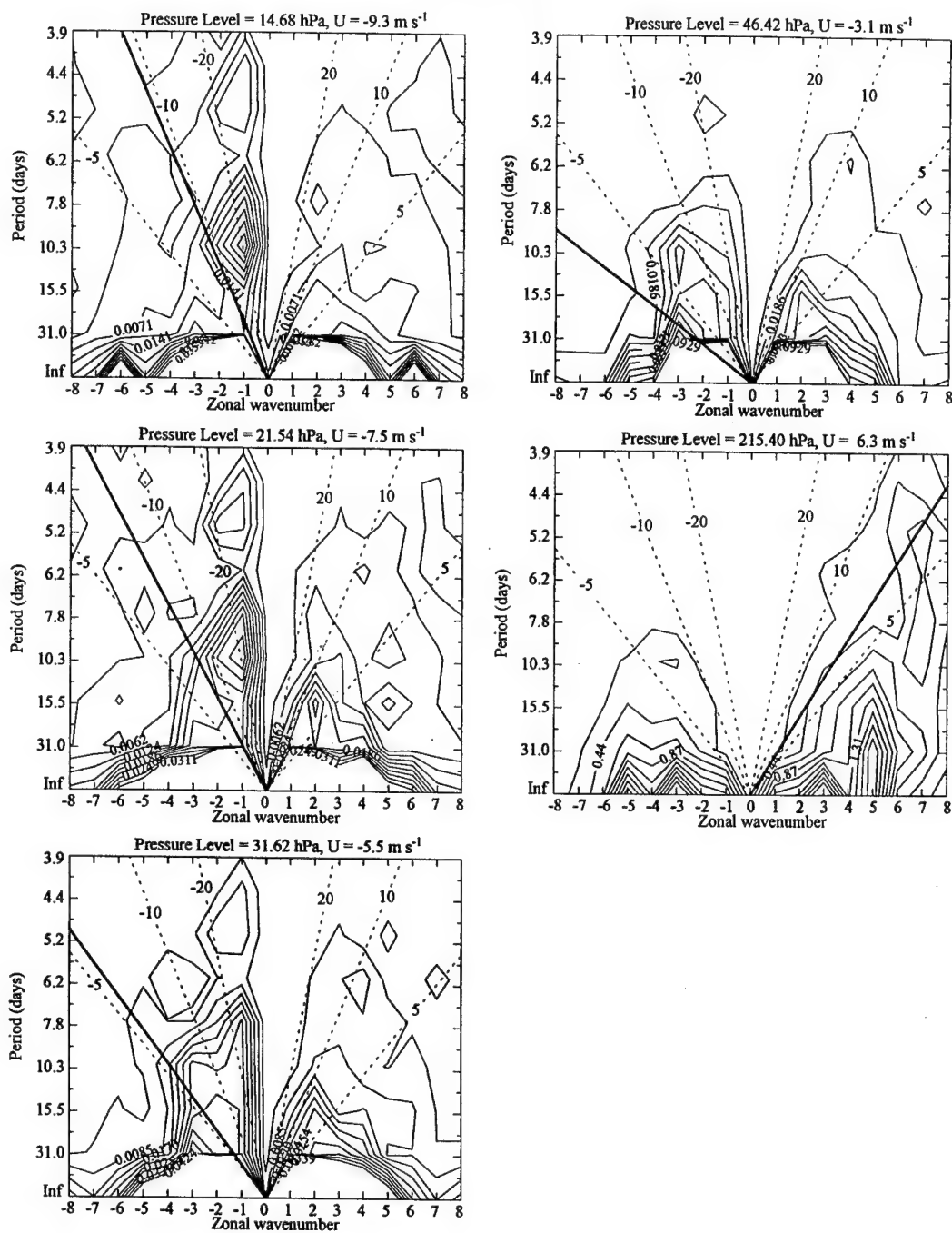


Figure 16. Continued.

August 1992-1998

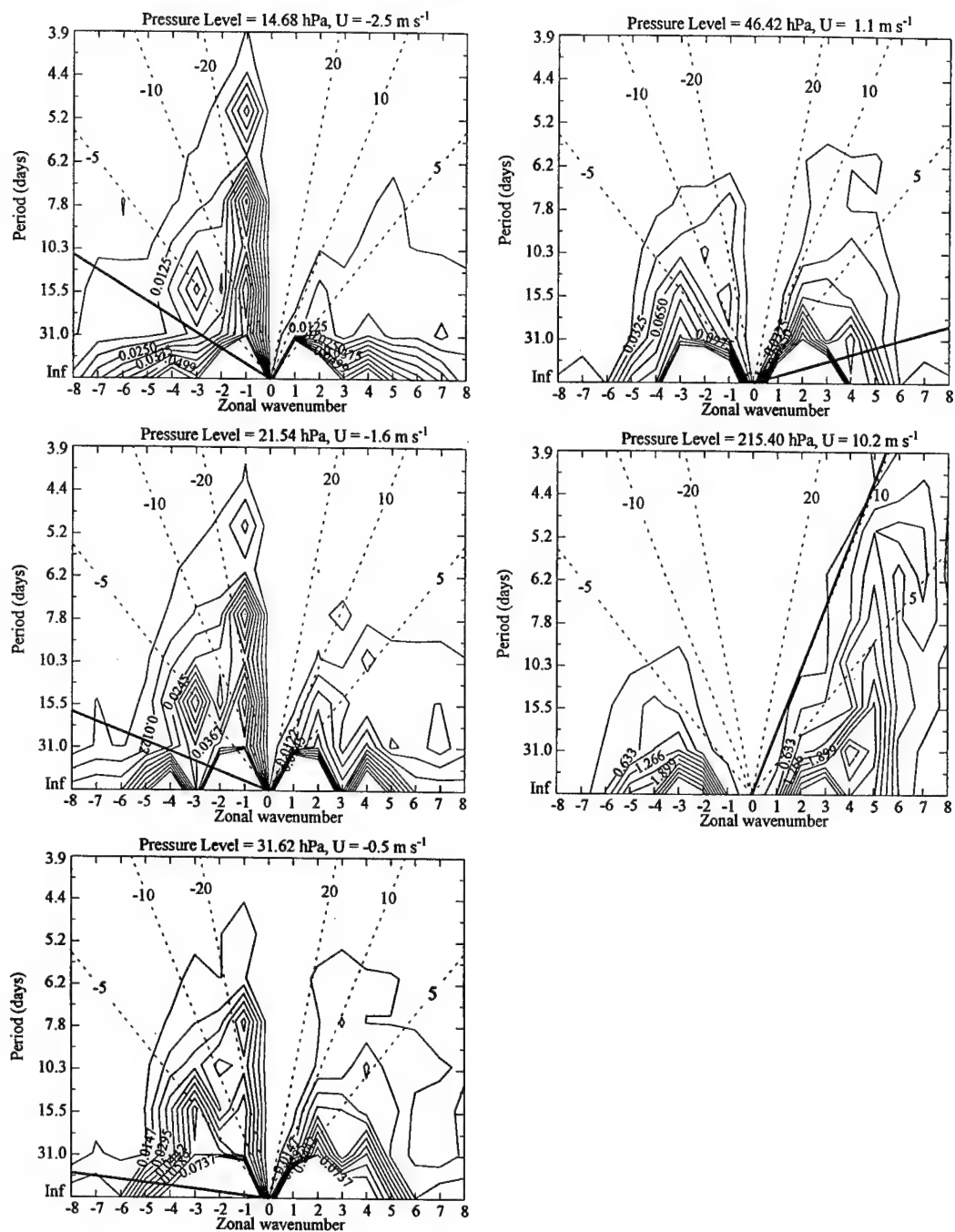


Figure 16. Continued.

4.3. Meridional Mixing of Ozone in the NH Summer Stratosphere

4.3.1. The NH in General

Figure 17 shows latitude vs. θ cross sections of climatological monthly-mean effective meridional diffusion coefficients (K_{yy} , $\cdot 10^5 \text{ m}^2 \text{ s}^{-2}$) in the extratropical NH stratosphere for June, July, and August 1992-1998. K_{yy} is represented by dashed lines. The zonal-mean zonal wind, \bar{u} (in m s^{-1}), is also plotted in Figure 17 for reference. Thin solid contours represent westerly flow and dotted contours represent easterlies. The heavy solid line represents the zero-wind line.

In all three panels, the most obvious feature is that K_{yy} decreases rapidly with increasing altitude up to approximately 550 K. Values of K_{yy} above 550 K are generally less than $3 \cdot 10^5 \text{ m}^2 \text{ s}^{-2}$. Therefore, the strongest meridional mixing (transport) is confined to the troposphere and lower stratosphere below roughly 550 K.

In August (Figure 19, bottom panel), values of K_{yy} between $2 \cdot 10^5 \text{ m}^2 \text{ s}^{-2}$ and $3 \cdot 10^5 \text{ m}^2 \text{ s}^{-2}$ penetrate all the way up to 950 K ($\sim 34 \text{ km}$).

4.3.2. The RMV

Figure 18 shows plots of climatological monthly-mean K_{yy} (meridionally averaged over the latitudinal width of the RMV) vs. θ for June, July, and August 1992-1998. The K_{yy} profiles are plotted on a logarithmic scale for comparison. K_{yy} values in the RMV decrease from June to July and then increase again in August. This trend closely mirrors the July reduction and August increase in climatological monthly-mean v amplitudes at the base of the RMV in Figure 15.

The e -folding depth of K_{yy} is calculated by assuming an exponential decay rate of the form

$$K = K_0 e^{-\frac{z}{H_e}}. \quad (22)$$

The profiles are approximately linear between 350 K and 750 K. A simple linear fit to the profiles in that region yields e -folding depths of 9 km, 11 km, and 18 km for June, July, and August respectively.

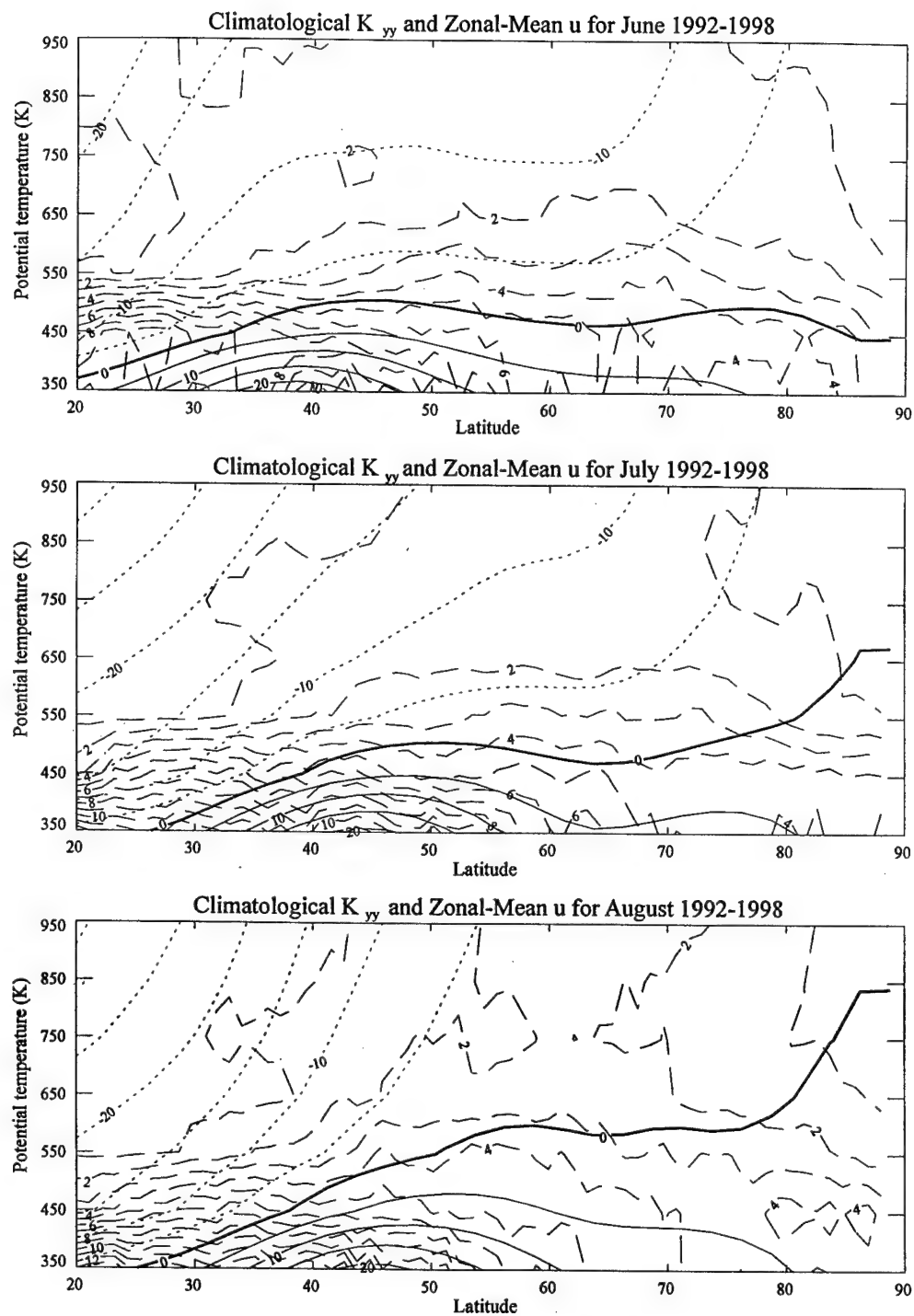


Figure 17. Climatological monthly-mean meridional diffusivity (K_{yy}) and zonal-mean zonal wind cross sections for the extratropical NH summer 1992-1998. Dashed contours represent K_{yy} , solid contours represent westerlies, and dotted contours represent easterlies.

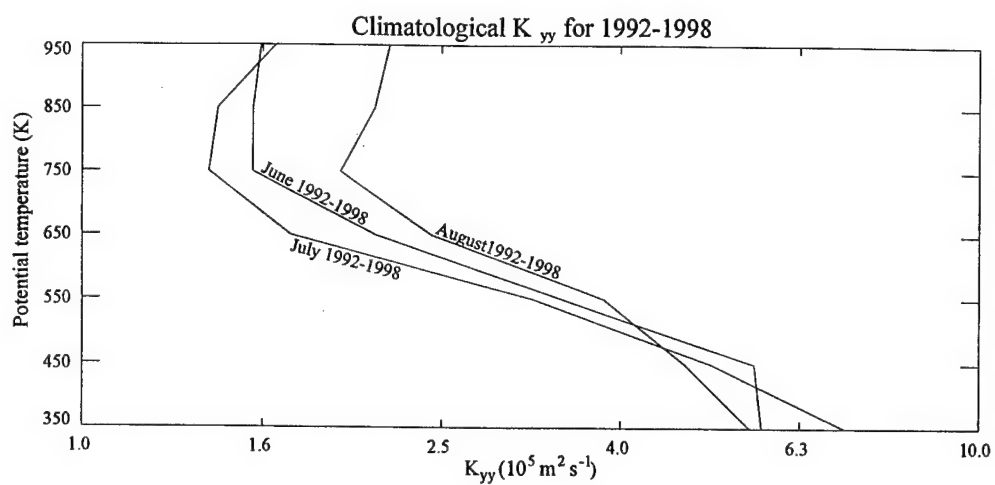


Figure 18. Climatological monthly-mean meridional diffusivities (K_{yy}) meridionally averaged over the latitudinal width of the RMV for June, July, and August 1992-1998.

4.4. EP-Flux and Flux Divergence in the NH Summer Stratosphere

4.4.1. The NH in General

Figures 19-21 present meridional cross sections of climatological monthly-mean unfiltered EP-flux vectors and contours of unfiltered EP-flux divergence for June, July, and August 1992-1998. Important to note is that the contours actually represent a scaled EP-flux divergence of the form

$$D = (\rho_0 r_0 \cos \phi)^{-1} \nabla \cdot \bar{F} \quad (23)$$

so that contour values are in units of acceleration (m s^{-2}) and directly represent the right-hand side of (12). The \bar{F} arrows have been normalized to overcome the typical rapid decrease in magnitude with increasing height. Therefore, they no longer accurately represent the magnitudes of the contributions of eddy momentum and eddy heat fluxes to the total EP-flux divergence, but they do give representation of the direction of propagation of “wave-activity”.

The most important characteristics of the EP-flux are that, for the entire NH summer, wave activity in the midlatitudes generally propagates upward from source regions in the lower troposphere. D in the stratosphere is almost entirely negative (convergent) from the subtropics to roughly 80°N . D is a convergent maximum in the upper troposphere and lower stratosphere below 20km.

4.4.2. Total EP-Flux Divergence in the RMV

To show the effects of removing the time-mean waves on D , we plot both modified and unmodified climatological monthly-mean D meridionally averaged over the latitudinal width of the RMV in Figure 22. Dotted horizontal lines represent the lower and upper boundaries of the RMV. In the RMV, differences between the modified and unmodified D are visible, but the characteristics of the curve are maintained, suggesting that removal of the time-mean anomalies has a relatively small impact on the data in our particular region of interest. It is important to note, however, that a similar plot latitudinally averaged around the area of the subtropical jet would not show similar good agreement between both data sets because large-amplitude (most likely real)

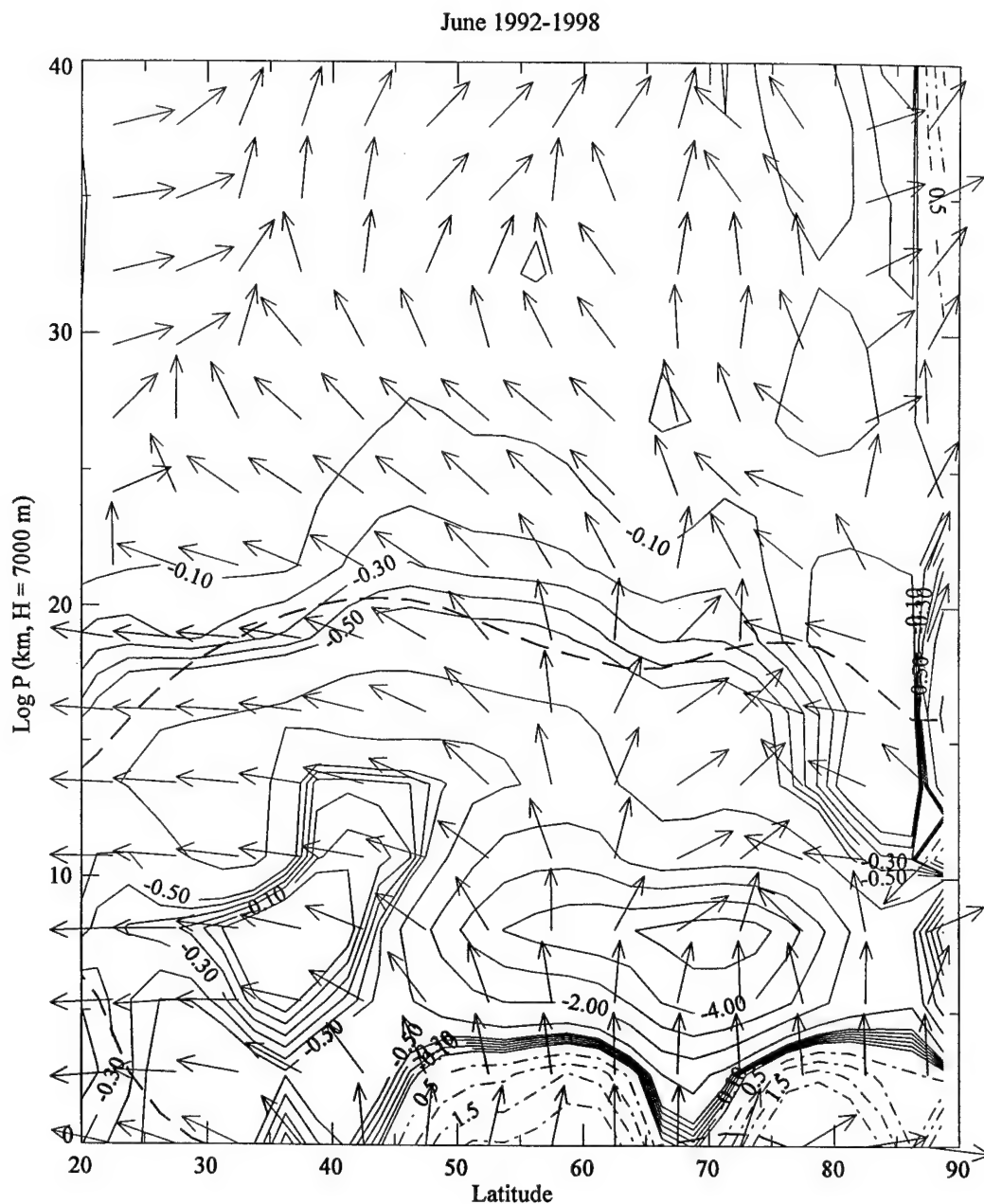


Figure 19. Climatological monthly-mean scaled EP-flux (arrows) and flux divergence (D , contours) for June 1992-1998 in the extratropical NH. Solid contours represent negative D and dashed contours represent positive D . Units of D are 10^{-5} m s^{-2} .

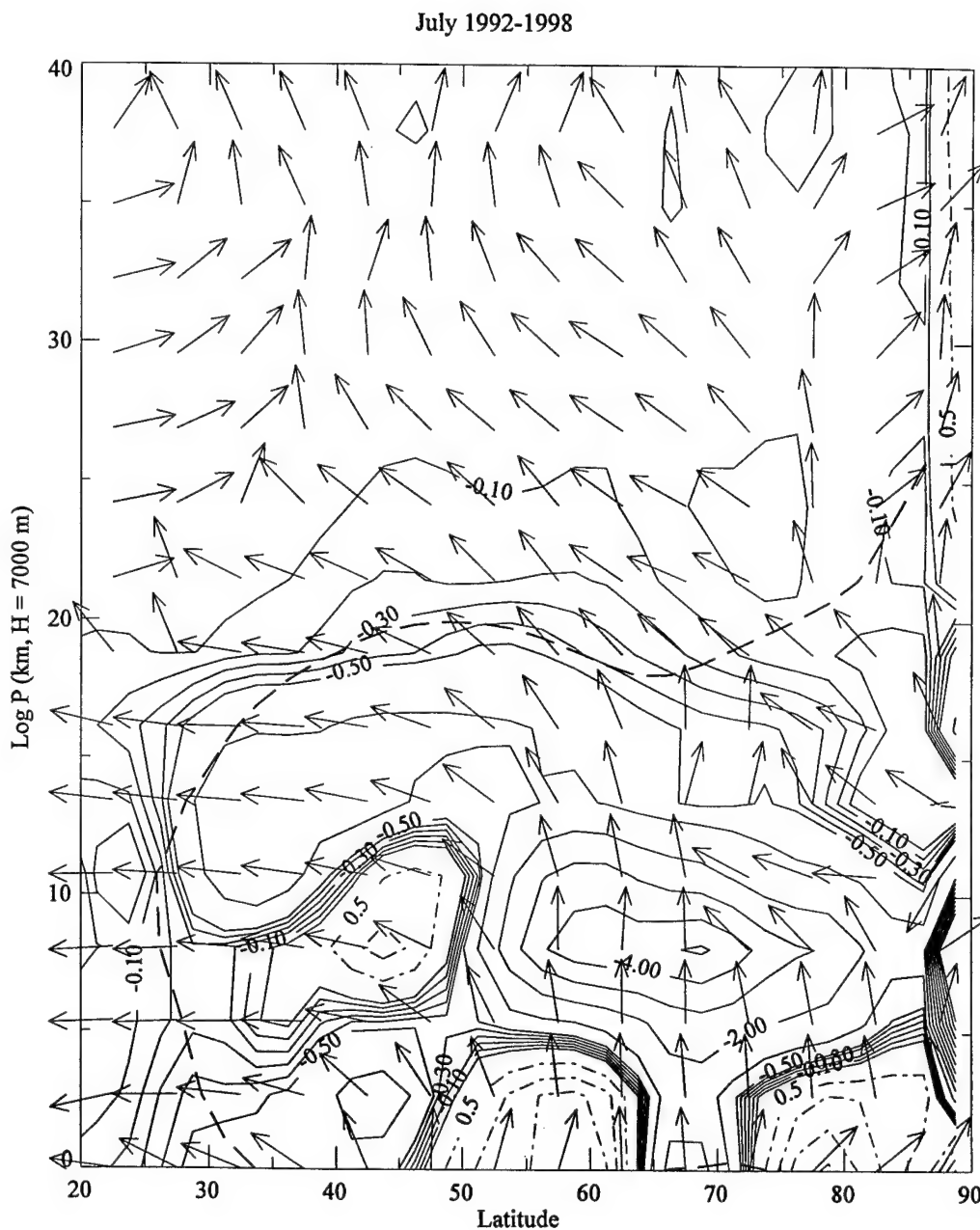


Figure 20. Climatological monthly-mean scaled EP-flux (arrows) and flux divergence (D , contours) for July 1992-1998 in the extratropical NH. Solid contours represent negative D and dashed contours represent positive D . Units of D are 10^{-5} m s^{-2} .

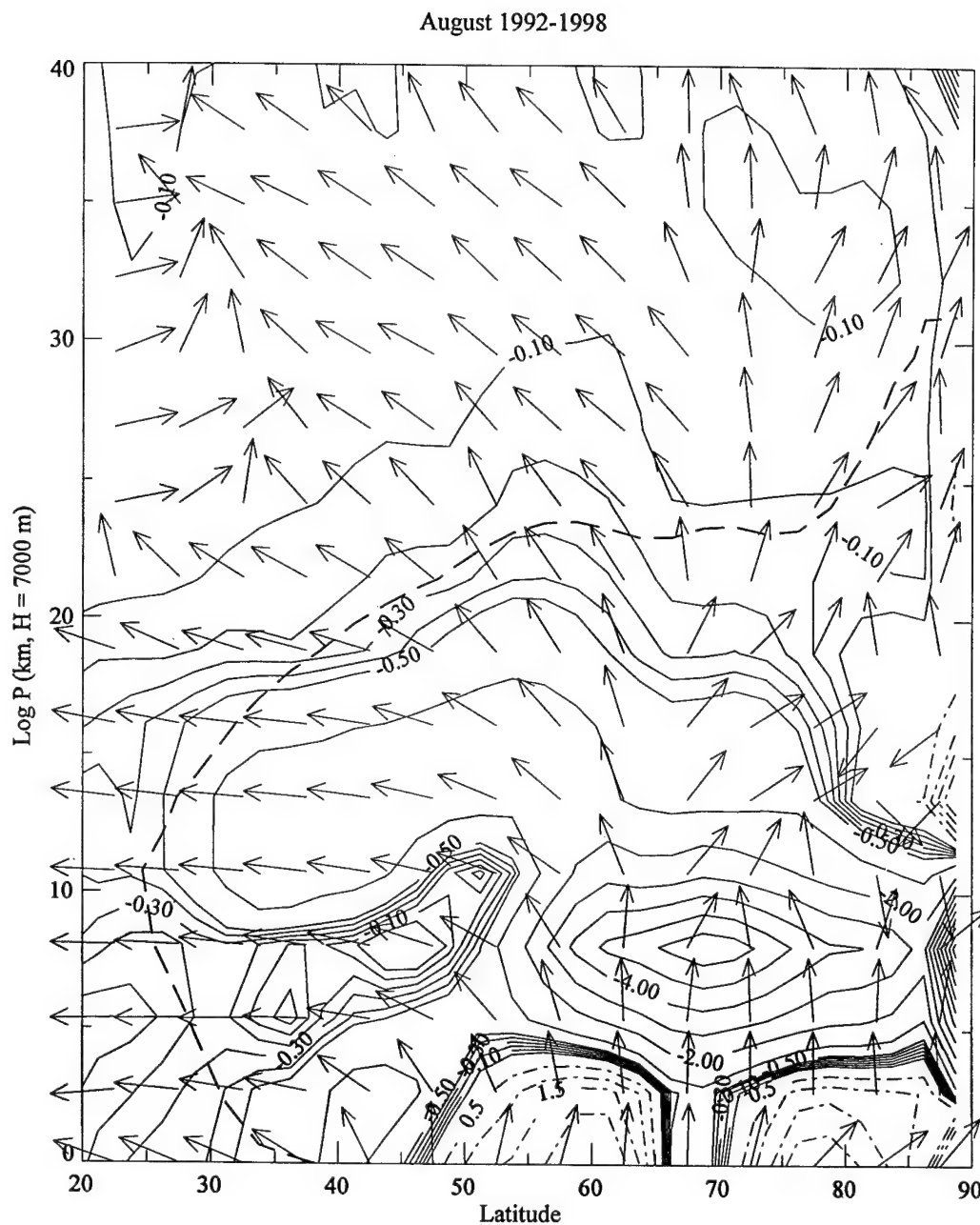


Figure 21. Climatological monthly-mean scaled EP-flux (arrows) and flux divergence (D , contours) for August 1992-1998 in the extratropical NH. Solid contours represent negative D and dashed contours represent positive D . Units of D are 10^{-5} m s^{-2} .

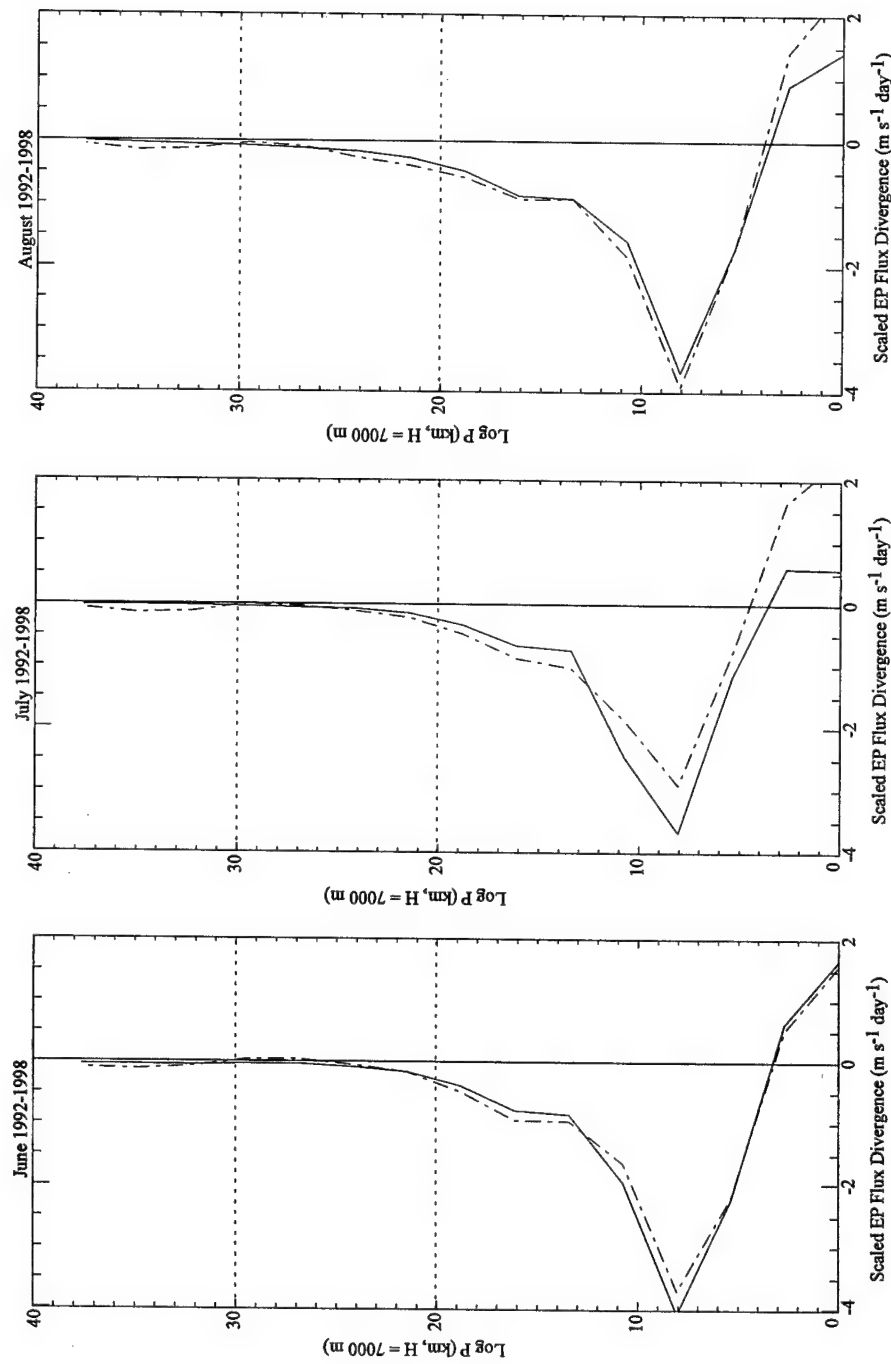


Figure 22. Climatological monthly-mean total scaled EP-flux divergence meridionally averaged over the latitudinal width of the RMV for June, July, and August 1992-1998. Dashed curves represent the original unmodified UKMO data and solid curves represent the modified UKMO data. Horizontal dotted lines represent lower and upper boundaries of the RMV.

stationary waves were removed from that region when seasonal time-means were removed.

Concentrating on the modified (solid-line) plots in Figure 22, the most notable similarities between all three months are a positive (divergent) maximum in the lower troposphere up to ~3.5 km and a negative (convergent) maximum at approximately 8 km in the upper troposphere. Above this convergent maximum, convergent values of D decrease approximately exponentially into the upper stratosphere. D is clearly nonzero in the RMV, meaning that the zonal-mean flow is still being forced by waves in this region.

4.4.3. EP-Flux Divergence by Wavenumber in the RMV

The total EP-flux divergence can be written as the sum of the EP-flux divergence for each wavenumber. To illustrate this, the total scaled climatological monthly-mean EP-flux divergence (D) for June 1992-1998, meridionally averaged over the latitudinal width of the RMV, is plotted as a dashed curve in Figure 23. Solid curves (from right to left above 35km) denote

$$\hat{D}_n = \sum_{k=1}^n D_k, \quad (24)$$

where D_k is the scaled EP-flux divergence for wavenumber k and \hat{D}_n is the sum of D_k for the first n wavenumbers. The distance between curve n and $n-1$ is the EP-flux divergence contributed by wavenumber n . Figures 24 and 25 are configured in the same manner for July and August 1992-1998. Wavenumbers higher than 8 contribute a positive EP-flux divergence at some levels, so the total EP-flux divergence is occasionally larger (less negative) than the sum of waves 1-8.

In the RMV during each NH summer month (Figures 23-25), D appears to consist almost entirely of the forcing contributions by waves 1-8. Table 3 clearly shows this to be true. The cumulative percent contribution by wavenumbers 1-8 to the total D is well over 90% at all levels of the RMV throughout the NH summer except at 26.9 km and 29.6 km in June (89.1% and 86.4% respectively). Within waves 1-8, the percent contributions at each level by each individual wavenumber are not equally distributed.

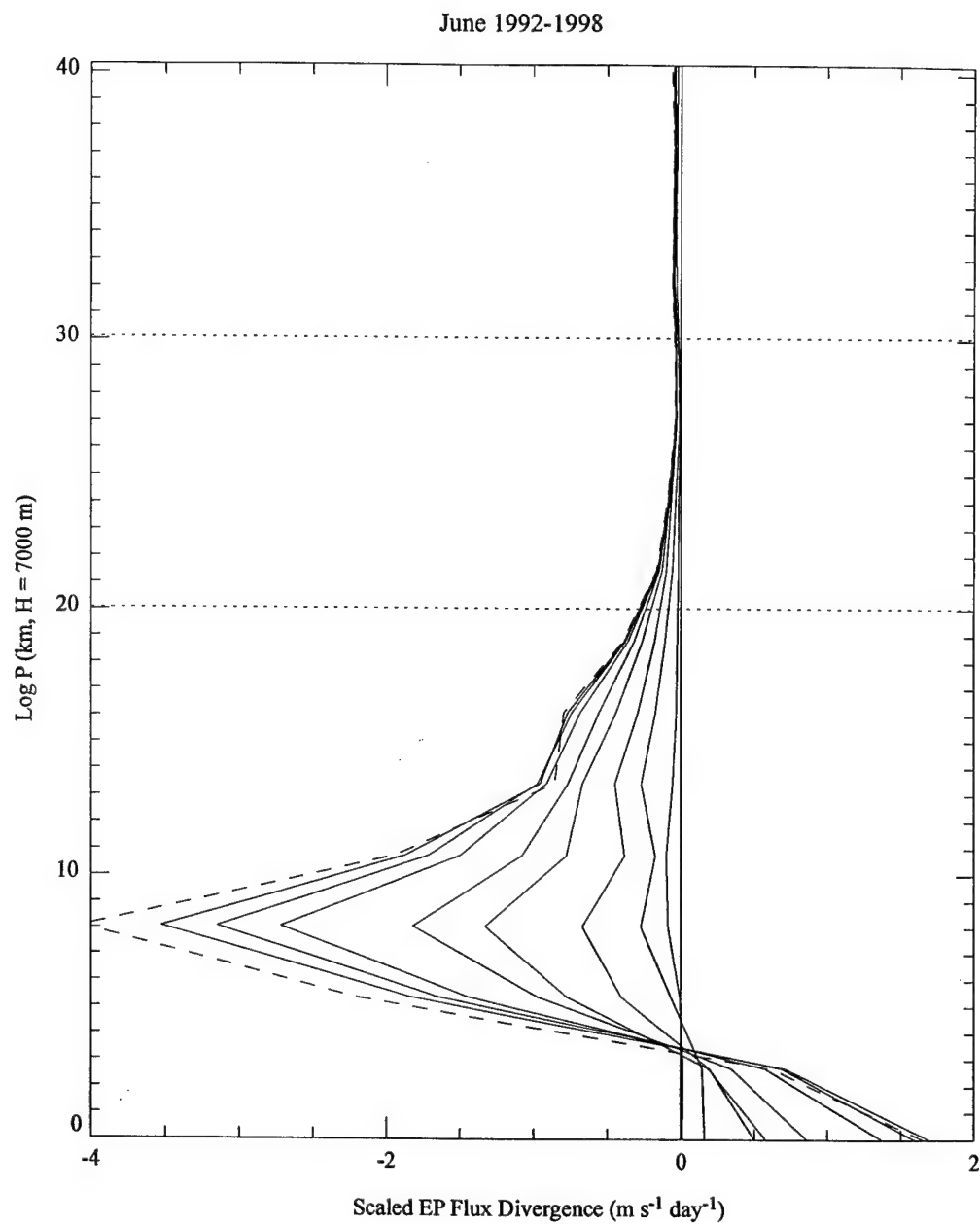


Figure 23. Climatological monthly-mean scaled EP-flux divergence meridionally averaged over the latitudinal width of the RMV for June 1992-1998. Horizontal dotted lines represent the lower and upper boundaries of the RMV. Dashed curve represents the total scaled EP-flux divergence (includes all waves).

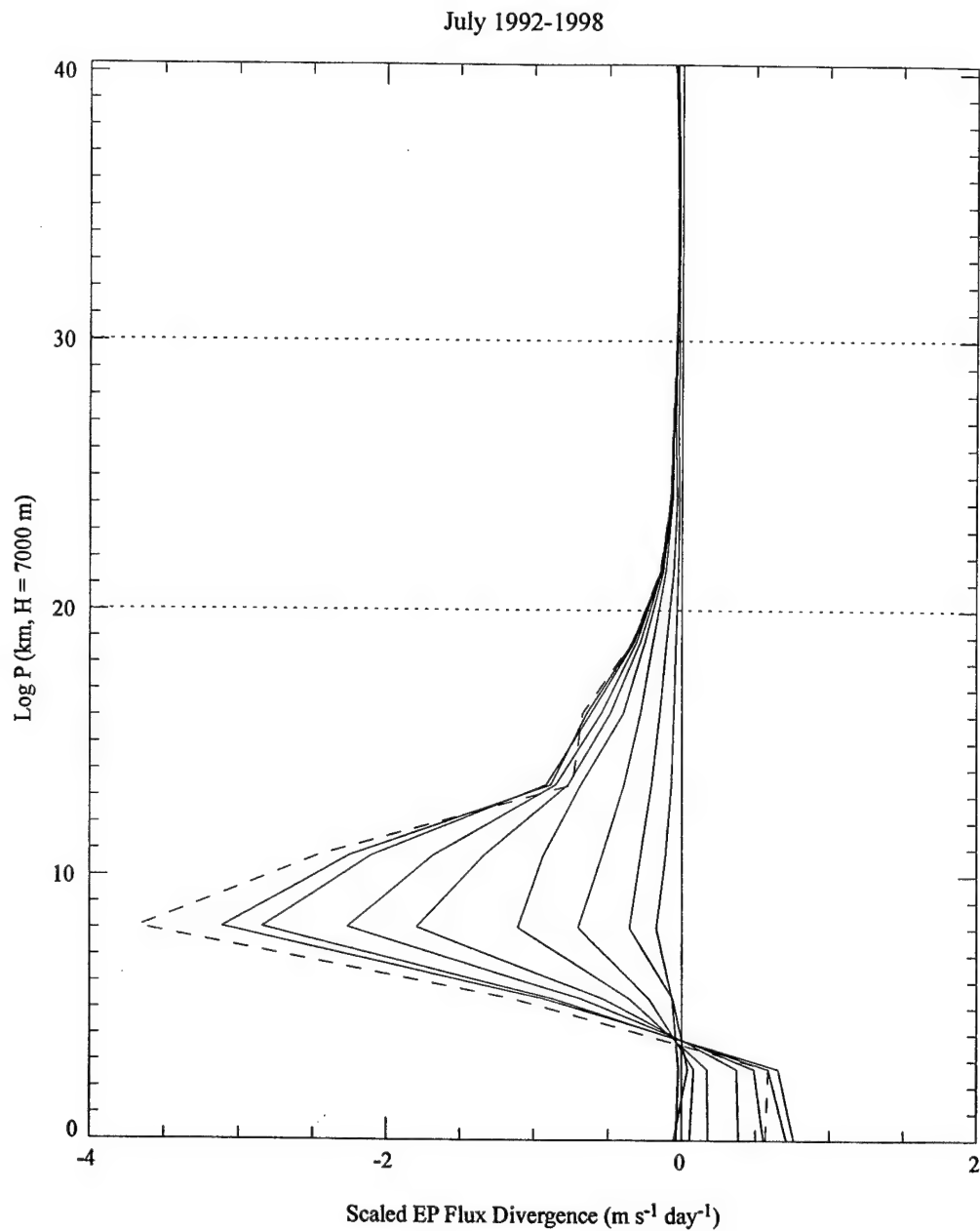


Figure 24. Climatological monthly-mean scaled EP-flux divergence meridionally averaged over the latitudinal width of the RMV for July 1992-1998. Horizontal dotted lines represent the lower and upper boundaries of the RMV. Dashed curve represents the total scaled EP-flux divergence (includes all waves).

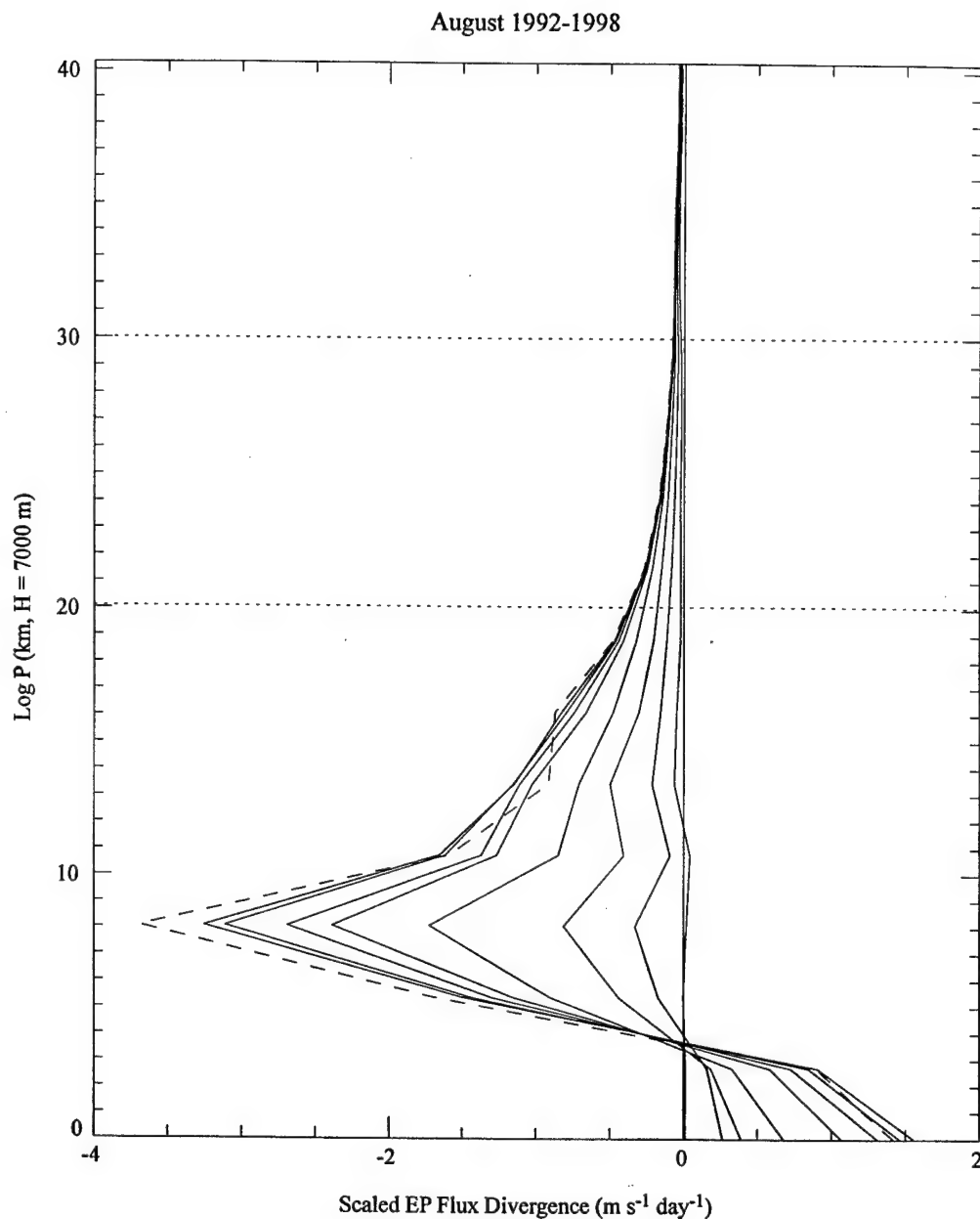


Figure 25. Climatological monthly-mean scaled EP-flux divergence meridionally averaged over the latitudinal width of the RMV for August 1992-1998. Horizontal dotted lines represent the lower and upper boundaries of the RMV. Dashed curve represents the total scaled EP-flux divergence (includes all waves).

Table 4. Percent contribution by wavenumber to the total climatological monthly-mean scaled EP-flux divergence for June, July, and August 1992-1998. Shaded boxes represent individual wavenumber percent contributions less than 4% of the total.

Month	June				July				August			
Log p (km)	21.5	24.2	26.9	29.6	21.5	24.2	26.9	29.6	21.5	24.2	26.9	29.6
Wavenumber												
1	10.0	15.8	7.8	25.5	16.6	22.1	40.2	43.5	8.0	14.7	15.1	26.5
2	24.2	23.5	13.0	17.3	21.0	19.1	29.8	34.1	22.6	23.1	26.4	23.7
3	24.9	33.1	46.5	30.7	36.1	37.8	19.1	14.5	25.0	26.9	27.5	25.8
4	17.7	13.1	14.9	2.1	11.8	6.8	1.2	-0.4	23.7	20.3	17.6	13.6
5	11.4	4.7	2.6	2.5	7.1	7.7	3.3	0.7	12.1	9.0	6.4	5.0
6	3.1	0.1	-0.6	3.1	3.6	2.9	1.7	0.9	3.7	2.2	1.4	-0.2
7	2.0	0.4	1.0	3.2	0.8	-0.8	-0.5	0.7	1.4	0.4	0.8	0.80
8	1.9	2.6	3.9	2.0	0.7	0.7	1.2	0.6	0.7	-0.16	0.8	1.3
Cumulative												
% of Total	95.2	93.3	89.1	86.4	97.7	96.3	96.0	94.6	97.2	96.4	96.0	96.5
Contribution	1-5	1-5	1-4	1-3	1-5	1-5	1-3	1-3	1-5	1-5	1-5	1-5
by Waves	88.2	90.2	82.2	73.5	92.6	93.5	89.1	92.1	91.4	94.0	93.0	94.6

Table 5. Climatological monthly-mean scaled EP-flux divergence by zonal wavenumber for June, July and August 1992-1998.

Climatological Monthly-Mean Scaled EP Flux Divergence ($10^{(-2)}$ m/s per day) by Zonal Wavenumber												
Month	June				July				August			
Log p (km)	21.5	24.2	26.9	29.6	21.5	24.2	26.9	29.6	21.5	24.2	26.9	29.6
Wavenumber												
1	-1.66	-1.38	-0.32	-1.02	-2.46	-1.70	-2.45	-1.86	-2.14	-2.44	-1.76	-2.10
2	-4.00	-2.06	-0.53	-0.69	-3.11	-1.47	-1.82	-1.46	-6.08	-3.84	-3.07	-1.88
3	-4.11	-2.91	-1.87	-1.22	-5.33	-2.90	-1.17	-0.62	-6.74	-4.46	-3.21	-2.05
4	-2.93	-1.15	-0.60	-0.08	-1.74	-0.52	-0.08	+0.02	-6.39	-3.38	-2.05	-1.08
5	-1.89	-0.42	-0.11	-0.10	-1.05	-0.59	-0.20	-0.03	-3.27	-1.49	-0.75	-0.40
6	-0.52	-0.01	+0.02	-0.12	-0.53	-0.22	-0.11	-0.04	-1.01	-0.37	-0.16	+0.01
7	-0.33	-0.04	-0.04	-0.13	-0.12	+0.06	+0.03	-0.03	-0.38	-0.06	-0.09	-0.07
8	-0.31	-0.23	-0.16	-0.08	-0.10	-0.06	-0.07	-0.03	-0.19	+0.03	-0.09	-0.10
Total Contribution by Wavenumbers 1-8 to Climatological Monthly-Mean Scaled EP Flux Divergence ($10^{(-2)}$ m/s per day)												
	-15.75	-8.20	-3.61	-3.44	-14.44	-7.40	-5.87	-4.05	-26.20	-16.01	-11.18	-7.67
Total Contribution by Wavenumbers 1-8 to Climatological Monthly-Mean Scaled EP Flux Divergence (m/s per month)												
	-4.73	-2.46	-1.08	-1.03	-4.33	-2.22	-1.76	-1.22	-7.86	-4.80	-3.35	-2.30
Sum of Unshaded Wavenumber Contributions to Climatological Monthly-Mean Scaled EP Flux Divergence ($10^{(-2)}$ m/s per day)												
	-14.59	-7.92	-3.32	-2.93	-13.69	-7.18	-5.44	-3.94	-24.62	-15.61	-10.84	-7.51
Sum of Unshaded Wavenumber Contributions to Climatological Monthly-Mean Scaled EP Flux Divergence (m/s per month)												
	-4.38	-2.37	-0.995	-0.88	-4.11	-2.15	-1.63	-1.18	-7.39	-4.68	-3.25	-2.25

To highlight the waves responsible for the largest forcing of the zonal-mean flow at each RMV level, individual wave contributions less than 4% of the total D are shaded gray (the 4% cutoff was chosen arbitrarily).

In June, near the lower boundary of the RMV (21.5 km), waves 1-5 are responsible for 88.2% of the total forcing of the zonal-mean flow. At 24.2 km, waves 1-5 are responsible for more than 90% of the total forcing. At 26.9 km, wave 5 has been effectively filtered out by the stratospheric easterlies, and waves 1-4 contribute most to the total forcing. At the top of the RMV, wave 4 has been mostly filtered out and waves 1-3 contribute the majority of the forcing.

July shows an increase in scale with height similar to June. In August, on the other hand, when winds are only weakly easterly, waves 1-5 contribute more than 91% to the total forcing at every level.

Wavenumbers 1-5 are clearly the dominant waves in the lower levels of the RMV during the NH summer. In the upper levels of the RMV, waves 1-5 also dominate the forcing in August, but only waves 1-3 dominate the forcing in June and July. Table 4 shows the discrete values of climatological monthly-mean D by wavenumber at each level in the RMV. Wavenumber contributions that were less than 4% of the total D in Table 3 are again shaded out in this table. Total contributions to D by waves 1-8 and the unshaded wavenumbers are summed up at the bottom of the table for each month at each RMV level.

In June and July, forcing by waves 1-8 equate to easterly accelerations of the zonal mean flow that range from almost -5 m s^{-1} per month to around -1 m s^{-1} per month throughout the depth of the RMV. In August, forcing by these waves is significantly greater, ranging from approximately -8 m s^{-1} per month to about -2 m s^{-1} per month throughout the depth of the RMV.

The wave forcing in the lower half of the RMV in June and July and throughout the RMV in August is large enough to noticeably accelerate the stratospheric easterlies over the course of the NH summer were it the only force acting. This is not generally observed, however, \bar{u} actually decreases in the RMV from June to August, indicating

that the advection, frictional dissipation, and Coriolis terms in the zonal-mean momentum equation (12) effectively offset the negative forcing imparted by D .

Figure 26 shows the meridionally averaged total D in the lower and middle stratosphere (including the RMV) for each NH summer month plotted on a logarithmic scale. To determine the rate of decrease in the magnitude of D in the lower stratosphere and RMV, e -folding depths are calculated for each month by assuming an exponential decay rate of the form

$$D = D_0 e^{-\frac{z}{H_e}} \quad (25)$$

and fitting it to the equation of a line in the same manner as performed for the meridional mixing (K_{yy}) e -folding depths. The e -folding depths for negative D in June, July, and August are 4.5 km, 5.3 km, and 6.5 km respectively. Like the meridional mixing calculations, the e -folding depth increases from June to August.

Figure 27 shows that, in the lower half of the RMV (below ~25 km), D decreases in magnitude in July and increases in August. This is a consistent trend also visible in the climatological monthly-mean v amplitudes (Figure 15) and K_{yy} profiles (Figure 18).

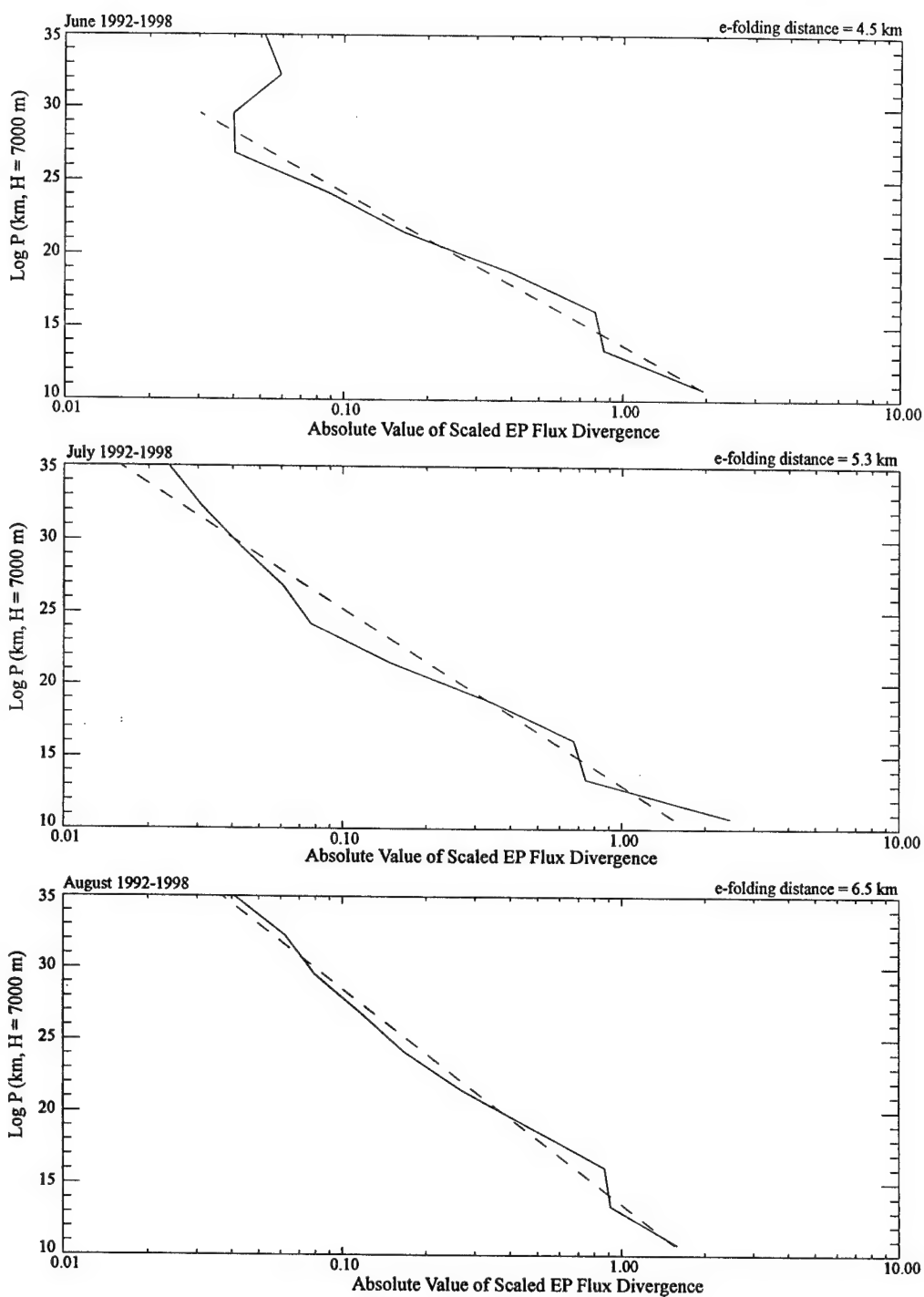


Figure 26. Absolute value of scaled EP-flux divergence (meridionally averaged over the width of the RMV) in the middle stratosphere plotted on a \log_{10} scale with a linear fit for June, July, and August 1992-1998.

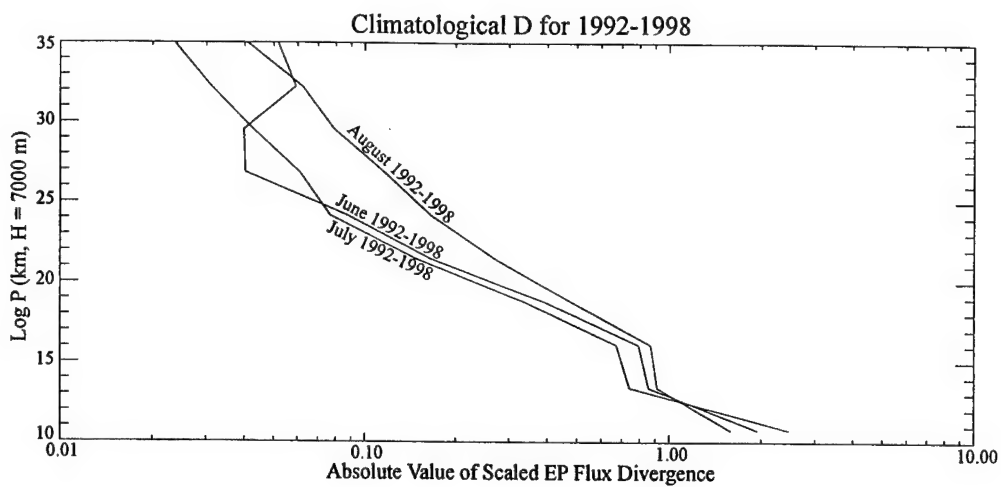


Figure 27. Composite of Figure 26 highlighting the decrease in negative D from June to July and subsequent increase in August in the lower half of the RMV (below ~ 25 km).

CHAPTER V

SUMMARY AND CONCLUSIONS

In the NH summer stratosphere, \bar{u} is easterly and increases with height. In the midlatitude stratosphere between 55°-65°N and ~20-30 km (RMV), the easterlies gradually weaken from June to August. *Charney and Drazin* [1961] showed that it is possible for westward-propagating waves to propagate vertically into stratospheric easterlies as long as the phase speeds of the waves are faster than \bar{u} as indicated in (1). Otherwise, the waves are trapped at their critical levels ($\bar{u} = c$) and become evanescent above. Power spectra (Figure 16) actually show this in the RMV; maximum power is greater in the westward propagating waves (mostly waves 1-5), indicating filtering of eastward propagating waves as they propagate vertically into the stratospheric easterlies in accordance with (1). Further filtering of the spectrum is evident at successively higher levels as wave power shifts toward faster negative phase speeds.

Despite the fact that summertime waves are substantially weaker than their wintertime counterparts, significant meridional transport and mixing occur. This is indicated by a region of enhanced zonal variance of ozone observed in POAM II data and Lagrangian trajectory calculations [*Hoppel et al.*, 1999]. The ozone variance decreases from June to July and increases to a maximum in August. Climatological monthly-mean meridional mixing (K_{yy}) calculations for June, July, and August 1992-1998 (Figure 17) show the same June-to-July decrease and subsequent increase in August as the ozone variance observed by POAM II. Meridional mixing (transport) is on the order of $3.4 \cdot 10^5 - 1.5 \cdot 10^5 \text{ m}^2 \text{ s}^{-2}$ from the base to the top of the RMV in June and July, increasing to $\sim 4 \cdot 10^5 - 2 \cdot 10^5 \text{ m}^2 \text{ s}^{-2}$ (from RMV base to top) in August.

EP-flux vectors calculated from the UKMO data set (modified by removal of time-mean waves) show that during the NH summer months wave activity propagates vertically from source regions in the lower midlatitude troposphere into the stratosphere and RMV (Figures 19-21). Throughout the NH summer, the total scaled EP-flux divergence (D) has a convergent maximum in the upper troposphere and lower stratosphere that decreases approximately exponentially into the upper stratosphere. In

the RMV, however, D is clearly nonzero [D is shown to be negative (convergent) throughout the summer in Figure 22], which means that the zonal-mean zonal flow is forced by waves in this region.

Close examination of the individual zonal wavenumber contributions to D (Figures 23-25 and Table 3) shows that contributions by wavenumbers 1-5 generally account for over 90% of the forcing of the zonal-mean flow in the lower half of the RMV from June to August. In the upper half of the RMV, planetary waves 1-3 dominate the forcing in June and July, but waves 1-5 appear to be able to penetrate to all RMV levels in August. The forcing in August is substantially greater than either June or July. This lends credibility to the accuracy of the somewhat noisy power spectra.

In the RMV, D decreases over e -folding distances of 4.5 km, 5.3 km, and 6.5 km for June, July, and August respectively. The larger e -folding depth and larger negative D in August is due to the weakness of the stratospheric easterlies (Figure 11, bottom left panel) which, by *Charney and Drazin* [1961], allows more waves (in this case waves 4 and 5 as well as 1-3) with easterly zonal phase speeds to propagate higher into the stratospheric easterlies and contribute more forcing to the zonal-mean zonal flow.

The wave forcing in the lower half of the RMV in June and July and throughout the RMV in August is large enough to noticeably accelerate the stratospheric easterlies over the course of the NH summer (were it the only force acting). This is not generally observed, however; \bar{u} actually decreases in the RMV from June to August, indicating that advection, frictional dissipation, and the Coriolis term in the zonal-mean momentum equation (12) effectively offset the negative forcing imparted by D .

The generalized Eliassen-Palm theorem [*Andrews et al.*, 1987] defines the EP flux divergence ($\nabla \cdot \bar{\mathbf{F}}$) as

$$\nabla \cdot \bar{\mathbf{F}} = R + O(\alpha^3) - \frac{\partial A}{\partial t} \quad (26)$$

where R represents dissipation and diabatic effects, $\partial A / \partial t$ represents wave-transience effects, and $O(\alpha^3)$ represents nonlinear effects (e.g., wave breaking). Since all values of $\nabla \cdot \bar{\mathbf{F}}$ calculated in this study are climatological monthly-means, effects of wave-transience have been effectively removed, which means the term $\partial A / \partial t$ can be neglected.

Figure 28 depicts 6 hemispheric particle tracer maps spanning July 1996. Tracer positions were computed on the 550 K isentropic surface (bottom level of RMV) from trajectories using the modified UKMO winds. Tracer positions are initialized on 1 July 1996 at 1200 UTC (Figure 28, top left panel). Each subsequent panel represents tracer positions 5 days later. The parcels that initially reside within the POAM II observation band (55° - 65° N) are colored yellow. By 6 July, waves can already be seen to deform to the point just prior to breaking in the upper right quadrant of the hemisphere (Figure 28, top right panel), and by 11 July, wave breaking is clearly evident (middle left panel). In subsequent panels, wave breaking continues but dissipation is also taking place. The time-scale for wave breaking is estimated from Figure 28 to be on the order of 10-15 days, which is comparable to radiative time scales in the RMV which are on the order of 10-20 days [Goody and Yung, 1989]. From this, we conclude that wave breaking, dissipation, and diabatic effects all play a role in forcing the zonal-mean zonal flow in the RMV. However, the meridional transport of tracers (e.g., ozone) is clearly driven primarily by wave breaking in Figure 28. This can be seen by the considerable meridional dispersion of the yellow tracers during the wave breaking event. Thus, it is safe to assume that, in the RMV, forcing of the zonal-mean zonal flow by D is largely (though not solely) due to dissipation of waves that are breaking near their respective critical levels in the region.

Since waves break at their critical levels ($\bar{u} = c$), and power spectra show power in westward-propagating waves 1-5 with phase speeds equal to the zonal-mean zonal flow at most levels in the RMV during all 3 NH summer months, it is clear that the waves breaking in the RMV are westward-propagating waves 1-5.

The decrease in the RMV meridional mixing (K_{yy}) and zonal eddy ozone variance (observed by POAM II) from June to July as well as the significant increase in both quantities in August closely mirror the June-August trend in D . This trend appears to be a function of the amplitudes of the waves interacting with the zonal-mean flow in the RMV. Figure 15 shows a similar decrease in the amplitudes of waves 1-5 from June to July and subsequent increase in August. Therefore, it is reasonable to conclude that breaking of westward propagating waves 1-5 is the primary mechanism driving the

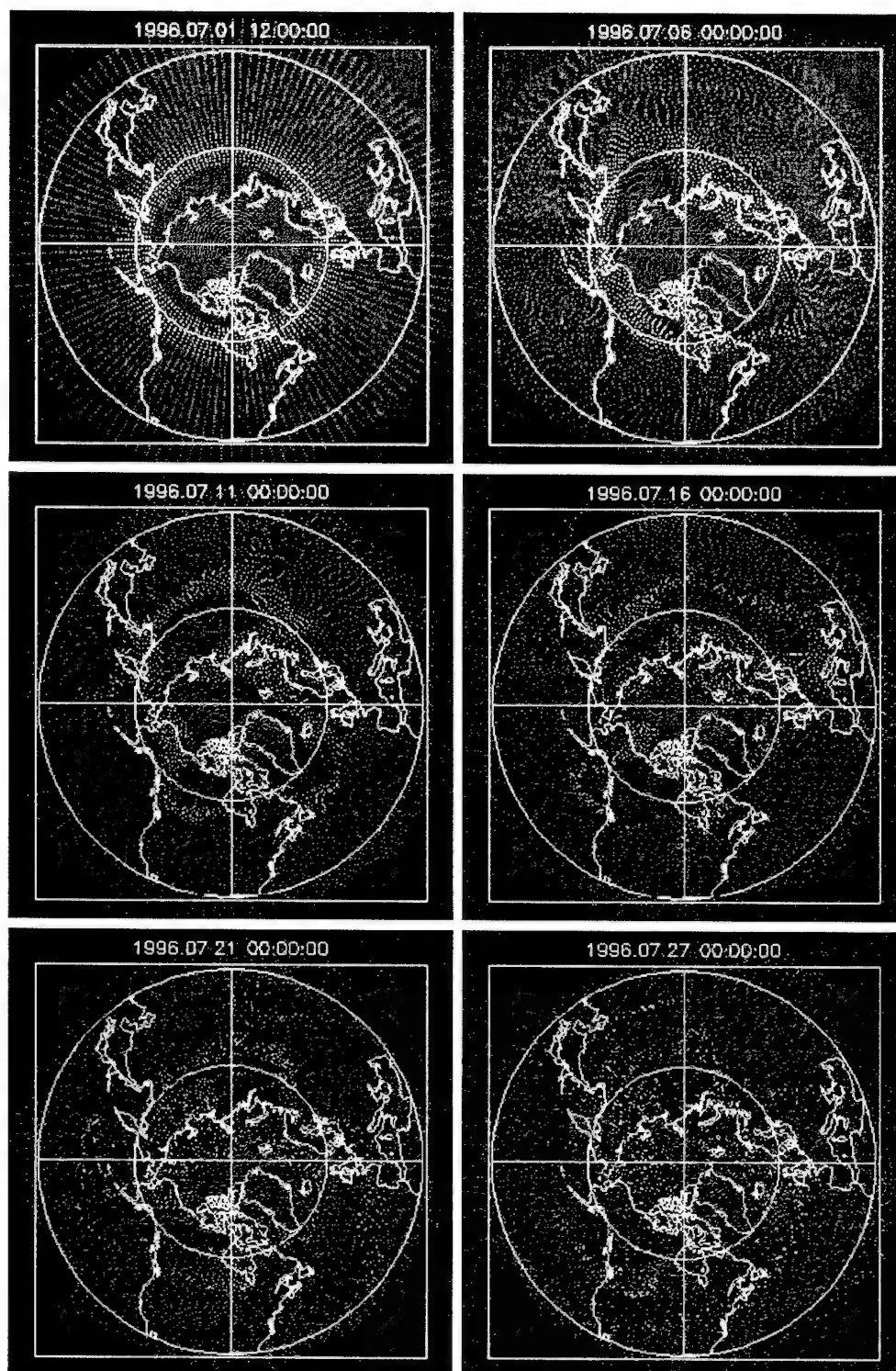


Figure 28. Location of particle tracers (initialized on 1 July 1996) around latitude circle at 5-day intervals in NH. Particle positions are calculated on the 550 K isentropic surface from trajectories computed using the modified UKMO winds.

meridional transport which is causing the observed zonal eddy ozone variance in the RMV.

Because both the meridional mixing (transport) and D decrease approximately exponentially with height, it seems reasonable to assume that the zonal eddy variance in ozone in the RMV (Figure 3) would do the same. But this does not happen. *Hoppel et al.* [1999] concluded that the zonal ozone variance maxima in the RMV in June, July, and especially August (where the variance is the largest) is due to the presence of a significant meridional ozone gradient above ~21 km. Below 21 km (~550 K) the gradient is almost negligible as shown in Figure 29, rendering meridional transport ineffective in producing ozone variations. Above the upper boundary of the RMV (~800 K), photochemical time scales are so rapid (on the order of a day [*Garcia and Solomon*, 1985]) compared to meridional mixing and transport time scales that ozone gradients cannot be maintained (transport cannot keep up with the photochemistry), so above and below the RMV the ozone variance is much smaller.

There is compelling evidence from calculating EP flux divergence in the NH summer stratosphere that breaking of westward propagating planetary-scale waves 1-3 and medium-scale waves 4 and 5 in the RMV is largely responsible for inducing the meridional transport that causes the maximum zonal eddy variance of ozone observed in the POAM II data by *Hoppel et al* [1999].

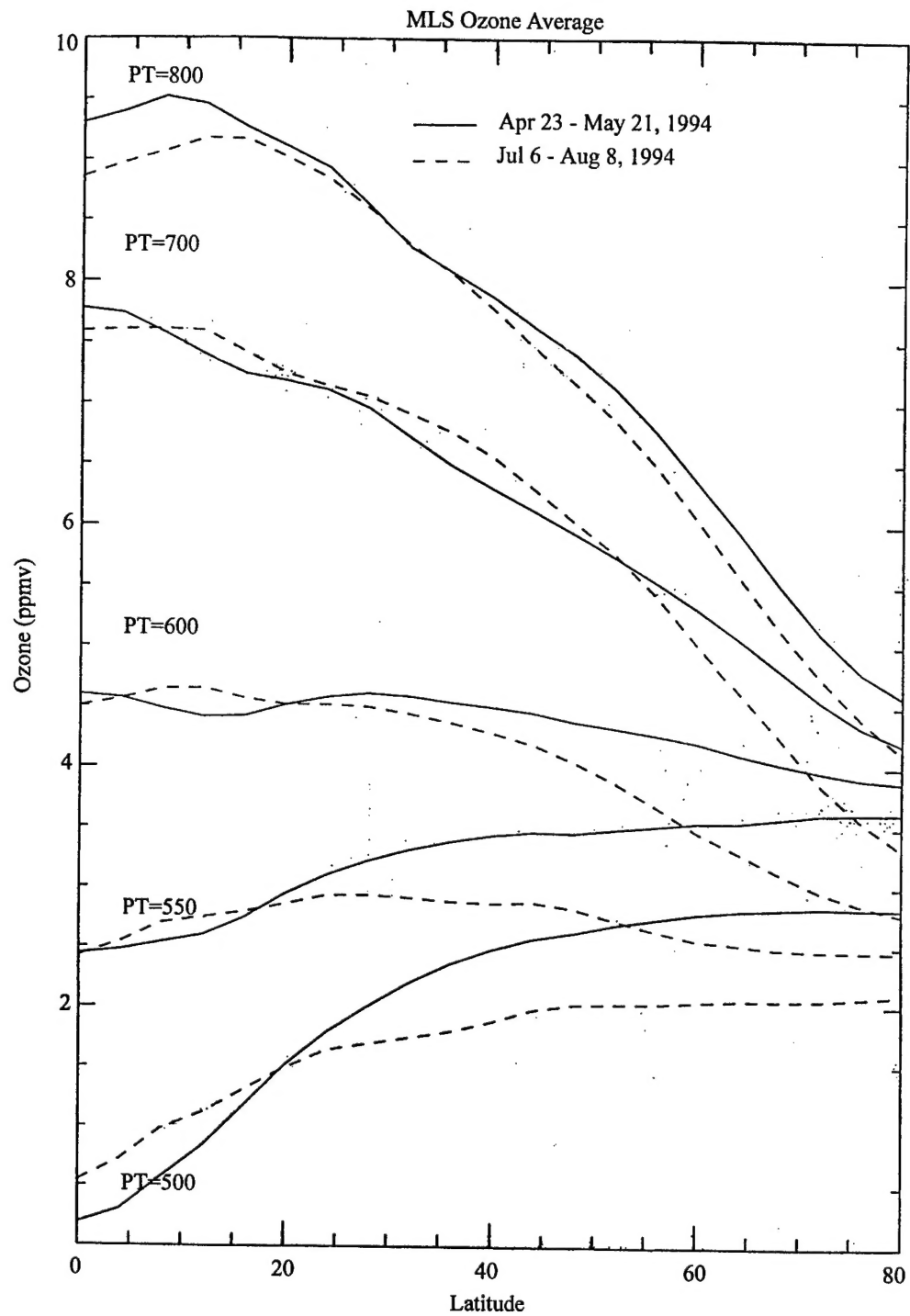


Figure 29. Plot of MLS ozone vs. latitude on potential temperature levels for NH summer 1994.

REFERENCES

- Andrews, D. G., J. D. Mahlman, and R. W. Sinclair, Eliassen-Palm diagnostics of wave-mean flow interaction in the GFDL "SKYHI" general circulation model, *J. Atmos. Sci.*, 40, 2768-2784, 1983.
- Andrews, D. G., J. R. Holton, and C. B. Leovy, *Middle Atmosphere Dynamics*, Academic Press, Orlando, Florida, 1987.
- Bowman, K. P., Large-scale isentropic mixing properties of the Antarctic polar vortex from analyzed winds, *J. Geophys. Res.*, 98, 23,013-23,027, 1993.
- Bowman, K. P., Diffusive transport by breaking waves, *J. Atmos. Sci.*, 52, 2416-2427, 1995.
- Bowman, K. P., Rossby wave phase speeds and mixing barriers in the stratosphere. Part I: Observations, *J. Atmos. Sci.*, 53, 905-916, 1996.
- Bowman, K. P., K. W. Hoppel, and R. Swinbank, Stationary anomalies in stratospheric meteorological data sets, *Geophys. Res. Lett.*, 25, No. 13, 2429-2432, 1998.
- Charney, J. G., and P. G. Drazin, Propagation of planetary-scale disturbances from the lower into the upper atmosphere, *J. Geophys. Res.*, 66, No. 1, 83-108, 1961.
- Edmon Jr., H. J., B. J. Hoskins, and M. E. McIntyre, Eliassen-Palm cross sections for the troposphere, *J. Atmos. Sci.*, 37, 2600-2616, 1980.
- Elson, L. S., G. L. Manney, L. Froidevaux, and J. W. Waters, Large-scale variations in ozone from the first two years of UARS MLS data, *J. Atmos. Sci.*, 51, 2867-2876, 1994.
- Garcia, R. R., and S. Solomon, The effect of breaking gravity waves on the dynamics and chemical composition of the mesosphere and lower thermosphere, *J. Geophys. Res.*, 90, 3850-3868, 1985.
- Goody, R. M., and J. L. Yung, *Atmospheric Radiation, Theoretical Basis*, Oxford University Press, New York, 1989.
- Hartmann, D. L., and R. R. Garcia, A mechanistic model of ozone transport by planetary waves in the stratosphere, *J. Atmos. Sci.*, 36, 350-364, 1979.
- Hess, P. G., J. R. Holton, The origin of temporal variance in long-lived trace constituents in the summer stratosphere, *J. Atmos. Sci.*, 42, 1455-1463, 1985.

- Holton, J. R., *The Dynamic Meteorology of the Stratosphere and Mesosphere*, Lancaster Press, Lancaster, Pennsylvania, 1975.
- Hoppel, K. W., K. P. Bowman, and R. M. Bevilacqua: Northern Hemisphere summer ozone variability observed by POAM II, *Geophys. Res. Lett.*, **26**, 827-830, 1999.
- James, I. N., *Introduction to Circulating Atmospheres*, Cambridge Univ. Press, Cambridge, England, 1994.
- Lorenc, A.C., R.S. Bell, and B. Macpherson, The Meteorological Office analysis correction data assimilation scheme, *Quart. J. Roy. Meteor. Soc.*, **117**, 59-89, 1991.
- Luo, M., J. H. Park, K. M. Lee, J. M. Ressel, and C. Bruehl, An analysis of HALOE observations in summer high latitudes using air mass trajectory and photochemical model calculations, *J. Geophys. Res.*, **102**, 16145-16156, 1997.
- Miles, T., W. L. Grose, E. E. Remsberg, and G. Lingenfelter, Evolution of the southern hemisphere subpolar middle atmosphere during summer and autumn, *J. Atmos. Sci.*, **51**, 677-693, 1994.
- Muench, H. S., Large-scale disturbances in the summertime stratosphere, *J. Atmos. Sci.*, **25**, 1108-1115, 1968.
- Natarajan, M., and L.V. Callis, Ozone variability in the high latitude summer stratosphere, *Geophys. Res. Lett.*, **24**, 1191-1194, 1997.
- Park, J. H., and J. M. Russell, Summer polar chemistry observations in the stratosphere made by HALOE, *J. Atmos. Sci.*, **51**, 2903-2913, 1994.
- Randel, W. J., Global normal-mode Rossby waves observed in stratospheric ozone data, *J. Atmos. Sci.*, **50**, 406-420, 1993.
- Schoeberl, M. R., L. R. Lait, P. A. Newman, J. E. Rosenfield, The structure of the polar vortex, *J. Geophys. Res.*, **97**, 7859-7882, 1992.
- Swinbank, R., and A. O'Neill, A stratosphere-troposphere data assimilation system, *Mon. Wea. Rev.*, **122**, 686-702, 1994.

VITA

Richard Emmett Wagner was born in Seattle, Washington, on March 18, 1967, to Richard and Kathleen Wagner. His father's duties as an Air Force officer took Richard and his brothers and sister all across the U.S. and Germany, where they attended a number of parochial and Department of Defense Dependents schools. Richard graduated from Fort Vancouver High School, Vancouver, Washington, in 1985. In 1991, he earned a B.S. in Mathematics from Oregon State University and his commission as a Second Lieutenant in the United States Air Force through the Reserve Officer Training Corps.

Lieutenant Wagner's first assignment, in 1992, was to attend the Air Force Institute of Technology (AFIT) Basic Meteorology Program at Florida State University where he was inducted into the Chi Epsilon Pi National Meteorology Honor Society. In 1993, he was assigned to Royal Air Force Mildenhall, United Kingdom. While a Lieutenant, he served as Base Weather Station Forecaster and Squadron Operations Weather Officer for the 100th Air Refueling Wing as well as Officer-in-Charge of the 352d Special Operations Weather Team. After his promotion to Captain in 1995, he served as Chief of Group Weather Operations for the 352d Special Operations Group and Weather Functional Manager for all Air Force Special Operations Command weather units in Europe. Captain Wagner gained extensive field experience deploying across Europe and Africa in support of numerous U.S. Air Force, Army, Navy, and NATO Special Forces missions. He has forecasted for aerial refueling, airlift, reconnaissance, air strike, close air support, air drop, night low-level, infiltration/exfiltration, and combat search and rescue missions from the Arctic Circle to the Equator.

Soon after completion of Squadron Officer's School in 1997, Captain Wagner was accepted into the AFIT Advanced Degree Program at Texas A&M University. He will receive his M.S. in Meteorology in August 1999.

In March of 1993, Richard married the former Miss Karen Elizabeth Alexander of Stonehaven, Scotland. Richard is stationed with Karen and their two cats, Cally and Jeffrey, at Eglin Air Force Base, Florida, until 2002. His permanent address is 5106 N.E. 46th Street, Vancouver, WA 98661.